

## RESTRICTED



FP7-ICT Future Networks  
SPECIFIC TARGETTED RESEARCH PROJECT  
Project Deliverable

<b>PHYDYAS Doc. Number</b>	PHYDYAS_ 012
<b>Project Number</b>	ICT – 211887
<b>Project Acronym+Title</b>	PHYDYAS – PHYsical layer for DYnamic AccesS and cognitive radio
<b>Deliverable Nature</b>	Report
<b>Deliverable Number</b>	D3.2
<b>Contractual Delivery Date</b>	July 1 <sup>st</sup> , 2009
<b>Actual Delivery Date</b>	July 29 <sup>th</sup> , 2009
<b>Title of Deliverable</b>	Optimization of transmitter and receiver
<b>Contributing Workpackage</b>	WP3
<b>Project starting date; Duration</b>	01/01/2008; 30 months
<b>Dissemination Level</b>	CO
<b>Author(s)</b>	Jérôme Louveaux (UCL – WP3 leader), Mario Tanda (UNINA), Markku Renfors (TUT), Leonardo Baltar (TUM), Aissa Ikhlef (UCL), Tobias Hidalgo-Stitz (TUT), Maurice Bellanger (CNAM), Carlos Bader (CTTC).

### Abstract

This document is a follow-up to deliverable D3.1. It provides complements on joint estimation techniques, equalization structures and channel estimation methods. In addition, it covers new topics, such as the joint transmitter-receiver design and the possible connection between equalization and decoding. To conclude, a set of recommendations is given for system design and the main achievements of the workpackage WP3 are listed.

## Table of Contents

<b>1</b>	<b>Introduction.....</b>	<b>10</b>
<b>2</b>	<b>Synchronization.....</b>	<b>12</b>
2.1	Joint symbol timing and CFO estimation for FBMC systems in multipath channels.....	12
2.1.1	System Model .....	12
2.1.2	Joint symbol timing and CFO estimator .....	13
2.1.3	Performance evaluation of the proposed joint estimator .....	16
2.2	Joint FTD and Channel Estimation based on Iterative Interference Cancellation (IIC) .....	23
2.2.1	Signal Model.....	23
2.2.2	Iterative Interference Cancellation.....	26
2.2.3	Simulation setup and results .....	28
2.2.4	Conclusion .....	35
2.3	Uplink multi-user synchronization.....	35
2.3.1	Effects of intracell interference in the uplink .....	35
<b>3</b>	<b>Equalization structures .....</b>	<b>40</b>
3.1	Review of the system model and MMSE equalizer .....	40
3.2	Two-stage interference cancellation equalizer (TS-IC) .....	43
3.3	MMSE Decision-feedback equalizer .....	46
3.4	Frequency domain equalization .....	50
<b>4</b>	<b>Channel estimation .....</b>	<b>53</b>
4.1	Pilot-based channel estimation.....	53
4.1.1	Simulation Setup and Results .....	53
4.1.2	Conclusion .....	59
4.2	Adaptive MMSE-DFE.....	60
<b>5</b>	<b>Joint Transmitter-receiver design .....</b>	<b>64</b>
5.1	Subchannel and power allocation and rate adaptation for FBMC systems.....	64
5.1.1	Calculating the $ H_{eff,n} $ : OFDM case.....	65
5.1.2	Calculating the $ H_{eff,n} $ : FBMC case .....	66
5.1.3	Demodulation and ZF equalization:.....	67
5.1.4	Radio resource unit capacity .....	69
5.1.5	Improved Joint RU Allocation and bit loading (JRAB) by Scheduling .....	70
<b>6</b>	<b>Equalization and coding.....</b>	<b>75</b>
6.1	Unitary precoding.....	75
6.1.1	Precoded FBMC/OQAM .....	76
6.1.2	Discussion .....	77
6.1.3	Simulations .....	78
6.1.4	Conclusion .....	80
6.2	Influence of noise correlation on decoding.....	80
<b>7</b>	<b>Recommendations.....</b>	<b>83</b>
<b>8</b>	<b>Conclusion and achievements .....</b>	<b>85</b>
<b>9</b>	<b>References.....</b>	<b>86</b>



### List of Acronyms:

A/D	Analog-to-Digital
AFB	Analysis Filter Bank
AMC	Adaptive Modulation and Coding
AWGN	Additive White Gaussian Noise
BER	Bit Error Rate
CFO	Carrier Frequency Offset
CP-OFDM	Orthogonal Frequency Division Multiplexing with Cyclic Prefix
D/A	Digital-to-Analog
DAC	Digital-to-Analog Conversion
DFT	Discrete Fourier Transform
DL	Downlink
EMFB	Exponentially Modulated Filter Bank
FB	Filter Bank
FBMC	Filter Bank based MultiCarrier
FDD	Frequency Division Duplexing
FDMA	Frequency Division Multiple Access
FFT	Fast Fourier Transform
FIR	Finite Impulse Response
FTD	Fractional Time Delay
IDFT	Inverse Discrete Fourier Transform
IFFT	Inverse Fast Fourier Transform
ICI	Inter-carrier Interference
ISI	Intersymbol Interference
LS	Least Squares
MAI	Multiple Access Interference
MDFT	Modified Discrete Fourier Transform
MIMO	Multiple-Input Multiple-Output
ML	Maximum Likelihood
MMSE	Minimum Mean Squared Error
MS	Mobile Station
NPR	Nearly Perfect Reconstruction
OFDM	Orthogonal Frequency Division Multiplexing
OFDMA	OFDM Access
OQAM	Offset Quadrature Amplitude Modulation
PAPR	Peak-to-Average Power Ratio
PR	Perfect Reconstruction
PSD	Power Spectrum Density
PUSC	Partial Usage of Subchannels
QAM	Quadrature Amplitude Modulation
QPSK	Quadrature Phase Shift Keying
QoS	Quality-of-Service
RC	Raised Cosine
RHS	Right hand side

RMSE	Root Mean Squared Error
SFB	Synthesis Filter Bank
SNR	Signal-to-Noise Ratio
TDD	Time Division Duplexing
TDMA	Time Division Multiple Access
TED	Timing Error Detector
UL	Uplink
WiMAX	Worldwide Interoperability for Microwave Access

## Notations

$\angle\{x\}$	the argument of a complex number $x$ in $[0, 2\pi)$ ,
$\text{Re}\{\cdot\}$	real part
$\text{Im}\{\cdot\}$	imaginary part
$(\cdot)^*$	complex conjugation
$ \cdot $	absolute value
$M$	overall number of subcarriers, FFT size
$M_u^i$	number of used subcarriers of the $i$ th user (in single-user case, index $i$ is dropped)
$\mathbf{M}_u^i$	set of used subcarriers of the $i$ th user
$M_v$	number of virtual (unused) subcarriers
$K$	overlapping factor in prototype filter design
$\alpha$	roll-off factor in prototype filter design
$L_p$	prototype filter length
$L_{eq}$	subcarrier equalizer length
$T_s$	sampling interval (at SFB output and AFB input)
$f_s$	sampling rate (at SFB output and AFB input) $f_s = 1/T_s$
$T$	OQAM symbol duration; $T = MT_s$
$\Delta f$	subcarrier spacing, $\Delta f = 1/T = f_s/M$
$k$	subcarrier index ( $k=0, \dots, M-1$ ; $k=0$ corresponds to center subcarrier)
$l$	time index at OQAM symbol rate ( $\rightarrow T$ )
$n$	time index at OQAM subsymbol rate ( $\rightarrow T/2$ )
$m$	time index at SFB output/AFB input ( $\rightarrow T/M$ )
$i$	user index in multiuser cases
$U$	number of users
$v^R[n]$	real part of (arbitrary) complex sequence $v[n]$
$v^I[n]$	imaginary part of (arbitrary) complex sequence $v[n]$
$p(t)$	prototype filter impulse response, continuous-time model
$p[m]$	prototype filter impulse response, discrete-time <sup>(1)</sup> $p[m] = \sqrt{T_s} p(mT_s)$
$P(z)$	prototype filter transfer function
$f_k[m]$	analysis filter impulse response for subchannel $k$
$F_k(z)$	analysis filter transfer function for subchannel $k$
$G_k(z)$	synthesis filter transfer function for subchannel $k$
$g_k[m]$	synthesis filter impulse response for subchannel $k$ $g_k[m] = p[m] e^{j \frac{2\pi}{M} k \left( m - \frac{L_p-1}{2} \right)}$

$p_{k,n}[m]$  SFB impulse response for real symbol  $d_{k,n}$  (see also definition of  $s[m]$ )

$$p_{k,n}[m] = \theta_{k,n} \beta_{k,n} g_k[m - nM/2]$$

$$= \theta_{k,n} \beta_{k,n} p[m - nM/2] e^{j \frac{2\pi}{M} km}$$

$\theta_{k,n}$  phase mapping between real data sequence and complex samples at the SFB input

In general,

$$\theta_{k,n} = \begin{cases} \pm 1 & \text{for } k+n \text{ even} \\ \pm j & \text{for } k+n \text{ odd} \end{cases}$$

The recommended choice (following Siohan's papers) is <sup>(2)</sup>:

$$\theta_{k,n} = j^{k+n}$$

$$\beta_{k,n} = e^{j 2\pi k \left( -\frac{n}{2} - \frac{L_p - 1}{2M} \right)}$$

$d_{k,n}^i$  transmitted sequence of the  $i$ th user (data & pilots) (real)

$x_{k,n}$  observed ideal (without channel) complex sample sequence at AFB output,

$$\theta_{k,n}^* x_{k,n} = d_{k,n} + j u_{k,n}$$

Here  $u_{k,n}$  is the un-interesting part of the received complex samples.

$$\tilde{x}_{k,n} = \theta_{k,n}^* x_{k,n}$$

$y_{k,n}$  observed channel-distorted complex sample sequence at AFB output

$\tilde{d}_{k,n}$  real part of the subcarrier sequence after equalization and multiplication by  $\theta_{k,n}^*$

$\hat{d}_{k,n}$  detected sequence (real)

$s[m]$  transmitted sequence at SFB output, single user case

$$\begin{aligned} s[m] &= \sum_{k \in \mathbb{M}_u} \sum_{n=-\infty}^{\infty} d_{k,n} \theta_{k,n} g_k[m - nM/2] \\ &= \sum_{k \in \mathbb{M}_u} \sum_{n=-\infty}^{\infty} d_{k,n} \theta_{k,n} p[m - nM/2] e^{j \frac{2\pi}{M} k \left( m - n \frac{M}{2} - \frac{L_p - 1}{2} \right)} \\ &= \sum_{k \in \mathbb{M}_u} \sum_{n=-\infty}^{\infty} d_{k,n} \theta_{k,n} (-1)^{kn} p[m - nM/2] e^{j \frac{2\pi}{M} k \left( m - \frac{L_p - 1}{2} \right)} \\ &= \sum_{k \in \mathbb{M}_u} \sum_{n=-\infty}^{\infty} d_{k,n} \theta_{k,n} \beta_{k,n} p[m - nM/2] e^{j \frac{2\pi}{M} km} \\ &= \sum_{k \in \mathbb{M}_u} \sum_{n=-\infty}^{\infty} d_{k,n} p_{k,n}[m] \end{aligned}$$

$s_i[m]$  transmitted sequence at SFB output in the uplink multiuser FBMC system, e.g.,

$$s_i[m] = \sum_{k \in \mathbb{M}_u^i} \sum_{n=-\infty}^{\infty} d_{k,n} p_{k,n}[m]$$

$s(t)$  transmitted continuous-time signal ( $s_i(t)$  correspondingly for user  $i$  in multiuser case)

$$s(t) = \sum_{k \in \mathbb{M}_u} \sum_{n=-\infty}^{\infty} d_{k,n} \theta_{k,n} (-1)^{kn} p\left(t - n\frac{T}{2}\right) e^{j2\pi k\left(\Delta f t - \frac{L_p-1}{2M}\right)}$$

$r(t)$  received continuous-time signal in the uplink multiuser FBMC system

$$r(t) = \sum_{i=1}^U e^{j2\pi\left(\frac{\varepsilon_i}{T}t\right)} h_i(t, \tau) * s_i(t) + \eta(t) \quad \text{general case}$$

$$r(t) = \sum_{i=1}^U e^{j2\pi\left(\frac{\varepsilon_i}{T}t\right)} \sum_{p=0}^{P_i-1} c_{i,p} s_i(t - \tau_{i,p}) + \eta(t) \quad \text{discrete multipath case}$$

$$r(t) = \sum_{i=1}^U e^{j2\pi\left(\frac{\varepsilon_i}{T}t\right)} c_i s_i(t - \tau_i) + \eta(t) \quad \text{AWGN case}$$

$$= \sum_{i=1}^U e^{j2\pi\left(\frac{\varepsilon_i}{T}t + \phi_i\right)} |c_i| s_i(t - \tau_i) + \eta(t)$$

$\varepsilon_i$  carrier frequency offset of the  $i$ th user, normalized to subcarrier spacing

$\phi_i$  carrier phase offset (radians) of the  $i$ th user in the AWGN model

$h_i(t, \tau)$  time-variant channel impulse response of  $i$ th user

$P_i$  number of paths in the multipath channel model of user  $i$

$c_{i,p}$  complex gain of the  $p$ th path of the channel of user  $i$

$\tau_{i,p}$  delay of the  $p$ th path of the channel of user  $i$

$\tau_i$  timing offset of the  $i$ th user in the AWGN model

$\eta(t)$  complex envelope of white (Gaussian) noise whose real and imaginary parts are statistically independent and have a power spectral density level of  $N_0$

$\sigma_\eta^2$  channel noise variance

$N_0$  one-sided noise power spectral density of white channel noise

$r[m]$  received complex sequence at AFB input

$\eta[m]$  channel noise

$h_i[m]$  discrete-time channel impulse response for user  $i$  in block-fading model

$H_i(e^{j\omega})$  channel frequency response for user  $i$

$H_k$  channel response of subcarrier  $k$  (assuming flat-fading and time invariant/block-fading case)

$H_{k,n}$  channel response for subcarrier  $k$  and symbol  $n$  (assuming flat-fading and time variant case)

$H_{k,n}^{p,q}$  channel response for subcarrier  $k$  and symbol  $n$  from TX antenna  $p$  to RX antenna  $q$

$w_k[n]$  subcarrier-wise channel equalizer impulse response for subchannel  $k$

**Notes:**

<sup>(1)</sup> This assumes causal continuous-time prototype filter impulse response, which is different from Siohan's continuous-time model.

<sup>(2)</sup> The choice of  $\theta_{k,n}$ , i.e., the signs in mapping real data sequence to complex samples at the SFB input is an internal choice of the filter bank module (i.e., the definition of  $x_{k,n}$  above can be assumed to be valid in any case). However, it has an effect on the signal models at the SFB output and for the complex sequences at the AFB output. In the receiver side,  $\beta_{k,n}^*$  is implemented before the subband processing, and  $\theta_{k,n}^*$  after it. With this choice, all the subchannels are centered at DC at the subchannel processing stage.

# 1 Introduction

The first objective of WP3 is to define the processing functions for equalization and demodulation at the receiver, best suited for the FBMC system investigated in the PHYDYAS project, in the case of a single antenna communication<sup>1</sup>. The main focus has been put on studying the questions of *channel estimation* and *equalization* for which specific solutions need to be designed in the FBMC case, due to the particular structure of the filter banks. Several results for these issues have already been presented in deliverable D3.1. Additional work has been performed on these two topics taking into account several important aspects:

- Synchronization is another important issue of any receiver, and has been extensively covered within WP2. However, there is a strong interaction between the synchronization, the channel estimation and the equalization. The accuracy of the synchronization operation greatly impacts the performance of the channel estimator which further affects the performance of the equalizer. Besides, as already mentioned in D3.1, some synchronization effects can be partially compensated by the equalizers. For instance, the fractional time delay can be taken care of by a multiple taps equalizer inside each subchannel<sup>2</sup>. It is thus natural to try considering these different effects jointly instead of having a separate synchronization component and a separate channel estimation process. This question is investigated in section 2.
- Prior results have shown that simple equalizers perform well on reasonably selective channels. Even one tap is sufficient in some situations, especially when using a large number of subchannels. All of these equalizers however exhibit some performance floor at high signal-to-noise ratio and high frequency selectivity. This is due to the fact that some intersymbol and/or intercarrier interference is remaining and cannot be completely removed. In order to try to further improve the performance in these cases, other solutions are investigated in section 3.
- In order to cope with mobility, which is inherent to most wireless systems, the receiver needs to be able to track variations in the channel. The two common ways to deal with this issue are:
  - Use regular pilots embedded in the data bursts to perform frequent channel estimations. Some pilot schemes, specific to the FBMC system, have been presented in D3.1. and are further evaluated here taking mobility into account.
  - Use adaptive equalizers that can follow these variations in a decision-directed fashion. This is also further studied in this deliverable.
- Finally, error-correcting codes are another important component of any communication system. One particular role of error-correcting code is to capture diversity. In multicarrier systems, frequency diversity can be obtained by applying coding across the different subchannels. The same diversity can however be obtained without error correcting code by a simple linear precoding operation. The application of this precoding to FBMC systems is investigated in section 6.1. Still on the topic of error-correcting codes, the particular structure of the FBMC scheme and of the receivers considered here may generate decision variables which are

---

<sup>1</sup> The multiple antenna case is investigated in WP4 and the associated deliverables.

<sup>2</sup> This is particularly useful for an uplink multiuser scenario where the time delays may be different among the users, and thus different among subchannels.

correlated. This could potentially have an impact on the decoding process of the error-correcting code which typically assumes uncorrelated symbol errors. This issue is investigated in section 6.2.

The second objective of WP3 is to study the joint optimization of transmitter and receiver when channel information is available at the transmitter. In practice, the knowledge of the channel at the transmitter can be used to perform adaptive modulation and coding as well as resource allocation. This can considerably improve the performance with respect to a non adaptive scheme and is studied in section 5. Further optimizations of the transmitter could include an optimization of the filter bank based on the channel knowledge, but this is not very practical and is not considered here.

In summary, this document is organized as follows. In section 2, joint synchronization and channel estimation is investigated. Two particular channel models are considered to make this joint estimation possible. The last part of section 2 is devoted to the study of synchronization effects in multiuser scenarios. In section 3, two additional equalization structures are proposed to cope with highly selective channels with high SNRs, namely the two stage interference cancellation, and the decision feedback MMSE equalizer. In addition, a frequency domain equalizer is presented in section 3.4 that has the advantage of reducing the overall latency of the equalization process. In section 4, the channel estimation methods based on pilot schemes are further evaluated in the presence of mobility. Then, the adaptive decision feedback equalizer is derived. In section 5, resource allocation and adaptive modulation are considered for situations where channel information is available at the transmitter. Section 6 is devoted to the issues related to coding. The use of linear unitary precoding is first investigated in order to capture frequency diversity. Then, the question of correlation between equalizer is considered, as well as its impact on decoding.

The final objective of WP3 is to provide, for other WPs, some recommendation regarding the processing functions to use in a typical FBMC receiver in practical scenarios. This is summarized in section 7.

## 2 Synchronization

In this section, two joint synchronization and channel estimation methods are presented, for the preamble case (section 2.1) and the pilot case (section 2.2) respectively. Finally, the influence of synchronization mismatches between different users in the uplink case is studied in the last section.

### 2.1 Joint symbol timing and CFO estimation for FBMC systems in multipath channels

In this section, we deal with the problem of data-aided synchronization for FBMC system in multipath channels. In particular, the joint maximum-likelihood (ML) estimator for carrier-frequency offset (CFO), amplitudes, phases and delays, exploiting a short known preamble is derived. The ML estimators for phases and amplitudes are obtained in closed form. Moreover, under the assumption that the CFO is sufficiently small, a closed form approximate ML (AML) CFO estimator is obtained. By exploiting the obtained closed form solutions, a cost function whose peaks provide an estimate of the delays, is derived. In particular, the symbol timing (i.e., the delay of the first multipath component) is obtained by considering the smallest estimated delay.

#### 2.1.1 System Model

Let us consider a FBMC system with  $M$  subcarriers in a multipath channel. The received signal in the presence of a CFO normalized to subcarrier spacing  $\varepsilon = \Delta f T$ , can be written as

$$r(t) = e^{j\frac{2\pi}{T}\varepsilon t} \sum_{p=0}^{P-1} |c_p| e^{j\phi_p} s(t - \tau_p) + n(t) \quad (2.1)$$

where  $s(t)$  is the information-bearing signal,  $P$  is the number of multipath components and,  $|c_p|$ ,  $\phi_p$  and  $\tau_p$  denote amplitude, phase and delay, respectively, of the  $p$ -th path. Moreover, in (2.1)  $n(t)$  denotes zero-mean circular complex white Gaussian noise with independent real and imaginary parts, each with two-sided power spectral density  $N_0/2$ . The received signal  $r(t)$  is filtered with an ideal low-pass filter with a bandwidth of  $1/T_s$ , where  $T_s$  denotes the sampling period. The sampled signal  $s(mT_s)$  is equal to

$$s(mT_s) = \sum_{k \in \mathcal{K}_u} \sum_{n=0}^{S-1} d_{k,n} \theta_{k,n} \beta_{k,n} p[(m - nM/2)T_s] e^{j\frac{2\pi}{M}km} \quad (2.2)$$

### 2.1.2 Joint symbol timing and CFO estimator

In this section we derive the joint ML estimator for CFO, amplitudes, phases and delays, exploiting a short known preamble embedded in the received burst. Specifically, the known preamble is given by

$$z(mT_s) = \sum_{k \in \mathcal{M}_u} \sum_{n=0}^L d_{k,n} \theta_{k,n} \beta_{k,n} p\left[(m - nM/2)T_s\right] e^{j\frac{2\pi}{M}km} \quad (2.3)$$

where  $d_{k,n}$ ,  $0 \leq n \leq L$ ,  $k \in \mathcal{M}_u$  denote the known pilot symbols. By considering an observation window of total length  $\eta M$  containing the non-zero support of the received preamble, the log-likelihood function for the unknown parameters  $\varepsilon$ , and  $|c_p|$ ,  $\phi_p$  and  $\tau_p$ ,  $p = 0, \dots, P-1$ , is given by (up to irrelevant factors)

$$\ln \Lambda(\underline{\widetilde{c}}, \underline{\widetilde{\phi}}, \underline{\widetilde{\tau}}, \underline{\widetilde{\varepsilon}}) = - \sum_{k=0}^{\eta M-1} \left| \sum_{p=0}^{P-1} \widetilde{c}_p e^{j\widetilde{\phi}_p} z^{\widetilde{\tau}_p, \widetilde{\varepsilon}}(kT_s) \right|^2 + 2\Re \left[ \sum_{k=0}^{\eta M-1} r(kT_s) \sum_{p=0}^{P-1} \widetilde{c}_p e^{-j\widetilde{\phi}_p} z^{\widetilde{\tau}_p, \widetilde{\varepsilon}}(kT_s)^* \right] \quad (2.4)$$

where  $\underline{\widetilde{c}} = [\widetilde{c}_0, \widetilde{c}_1, \dots, \widetilde{c}_{P-1}]^T$ ,  $\underline{\widetilde{\phi}} = [\widetilde{\phi}_0, \widetilde{\phi}_1, \dots, \widetilde{\phi}_{P-1}]^T$ ,  $\underline{\widetilde{\tau}} = [\widetilde{\tau}_0, \widetilde{\tau}_1, \dots, \widetilde{\tau}_{P-1}]^T$ ,

$$z^{\tau, \varepsilon}(kT_s) \triangleq z(kT_s - \tau) e^{j\frac{2\pi}{M}\varepsilon k} \quad (2.5)$$

and the notation of type  $\widetilde{x}$  indicates trial value of  $x$ . The first term in the right hand side (RHS) of (2.4) for  $M \gg 1$  can be approximated as

$$\sum_{k=0}^{\eta M-1} \left| \sum_{p=0}^{P-1} \widetilde{c}_p e^{j\widetilde{\phi}_p} z^{\widetilde{\tau}_p, \widetilde{\varepsilon}}(kT_s) \right|^2 \approx \sum_{p=0}^{P-1} \widetilde{c}_p^2 \sum_{k=0}^{\eta M-1} |z(kT_s - \widetilde{\tau}_p)|^2. \quad (2.6)$$

Therefore, for sufficiently high values of  $M$  the log-likelihood function can be written as

$$\ln \Lambda(\underline{\widetilde{c}}, \underline{\widetilde{\phi}}, \underline{\widetilde{\tau}}, \underline{\widetilde{\varepsilon}}) = \sum_{p=0}^{P-1} \left\{ 2\widetilde{c}_p \Re \left[ e^{-j\widetilde{\phi}_p} g(\widetilde{\tau}_p, \widetilde{\varepsilon}) \right] - \widetilde{c}_p^2 d(\widetilde{\tau}_p) \right\} \quad (2.7)$$

where

$$d(\widetilde{\tau}) = \sum_{k=0}^{\eta M-1} |z(kT_s - \widetilde{\tau})|^2 \quad (2.8)$$

and

$$g(\widetilde{\tau}, \widetilde{\varepsilon}) \triangleq \sum_{k \in \mathcal{M}_u} \sum_{n=0}^L d_{k,n} [\theta_{k,n} \beta_{k,n}]^* w_n^{(k)}(\widetilde{\tau}, \widetilde{\varepsilon}) \quad (2.9)$$

with

$$w_n^{(k)}(\widetilde{\tau}, \widetilde{\varepsilon}) = \sum_{m=0}^{\eta M-1} r(mT_s) p\left(mT_s - n\frac{M}{2}T_s - \widetilde{\tau}\right) e^{-j\frac{2\pi}{M}km} e^{-j\frac{2\pi}{M}\widetilde{\varepsilon}m}. \quad (2.10)$$

From (2.7), it immediately follows that the ML estimator for phase and amplitude of the  $p$ -th path is given by

$$\hat{\phi}_{p_{ML}}(\tilde{\tau}_p, \tilde{\epsilon}) = \arg \max_{\tilde{\phi}_p} \left\{ \ln \Lambda(\underline{\tilde{c}}, \underline{\tilde{\phi}}, \underline{\tilde{\tau}}, \underline{\tilde{\epsilon}}) \right\} = \angle g(\tilde{\tau}_p, \tilde{\epsilon}) \quad (2.11)$$

$$\hat{c}_{p_{ML}}(\tilde{\tau}_p, \tilde{\epsilon}) = \arg \max_{\tilde{c}_p} \left\{ \ln \Lambda(\underline{\tilde{c}}, \underline{\tilde{\phi}}, \underline{\tilde{\tau}}, \underline{\tilde{\epsilon}}) \right\} = \frac{|g(\tilde{\tau}_p, \tilde{\epsilon})|}{d(\tilde{\tau}_p)}. \quad (2.12)$$

Moreover, by replacing the estimate of the phase and the amplitude of each path in (2.7) we get

$$\ln \Lambda(\underline{\hat{c}}(\underline{\tilde{\tau}}, \underline{\tilde{\epsilon}}), \underline{\hat{\phi}}(\underline{\tilde{\tau}}, \underline{\tilde{\epsilon}}), \underline{\tilde{\tau}}, \underline{\tilde{\epsilon}}) = \sum_{p=0}^{P-1} \frac{|g(\tilde{\tau}_p, \tilde{\epsilon})|^2}{d(\tilde{\tau}_p)}. \quad (2.13)$$

Therefore, the joint estimator for CFO and delays is given by

$$(\hat{\underline{\tau}}_{ML}, \hat{\underline{\epsilon}}_{ML}) = \arg \max_{(\underline{\tilde{\tau}}, \underline{\tilde{\epsilon}})} \left\{ \sum_{p=0}^{P-1} \frac{|g(\tilde{\tau}_p, \tilde{\epsilon})|^2}{d(\tilde{\tau}_p)} \right\}. \quad (2.14)$$

The derived joint ML estimator evaluates, for each trial value of each delay and for each trial value of the CFO, the response of the filter matched to the pulse shaping  $p(\cdot)$  to the CFO compensated and down-converted signal. Specifically, the down-conversion is performed by considering all the frequencies of the used subcarriers. Then, exploiting the known pilot symbols, these quantities are combined according to (2.10), (2.9) and (2.14). The joint ML estimate for delays and CFO is obtained by considering the value of  $(\underline{\tilde{\tau}}, \underline{\tilde{\epsilon}})$  that maximizes the statistic in (2.13). The  $(P+1)$ -dimensional maximization required by the joint ML estimator in (2.14) undertakes heavy computational burden. Therefore, in the following it is derived a more feasible synchronization scheme by exploiting the assumption that the CFO is sufficiently small. Specifically, taking into account that the observations window contains the non-zero support of the received preamble and that the prototype filter  $p(mT_s)$  is different from zero for  $m \in \{0, KM-1\}$ , where  $K$  is the overlap parameter, from (2.10) it follows that

$$w_n^{(k)}(\tilde{\tau}, \tilde{\epsilon}) \simeq e^{-j\frac{2\pi}{M}k\left(n\frac{M}{2}+\tilde{\theta}\right)} e^{-j\frac{2\pi}{M}\tilde{\epsilon}\left(n\frac{M}{2}+\tilde{\theta}\right)} u_k\left(n\frac{M}{2}+\tilde{\theta}\right) \quad (2.15)$$

where

$$u_k(l) = \sum_{m=0}^{KM-1} r[(m+l)T_s] p(mT_s) e^{-j\frac{2\pi}{M}mk} \quad (2.16)$$

and  $\tilde{\tau} = \tilde{\theta}T_s$ . In particular, into the case of a training sequence composed of one FBMC symbol, (2.9) taking into account (2.15) and (2.16), becomes

$$g(\tilde{\tau}, \tilde{\epsilon}) \approx e^{-j\frac{2\pi}{M}\tilde{\theta}(k+\tilde{\epsilon})} \left[ \underbrace{\sum_{k \in \mathcal{M}_u} [\theta_{k,0} \beta_{k,0}]^* u_k(\tilde{\theta})}_{A(\tilde{\tau})} + e^{-j\pi\tilde{\epsilon}} \underbrace{\sum_{k \in \mathcal{M}_u} e^{-j\pi k} d_{k,1} [\theta_{k,1} \beta_{k,1}]^* u_k(\tilde{\theta} + M/2)}_{B(\tilde{\tau})} \right]. \quad (2.17)$$

Therefore, the AML estimator for the CFO, taking into account (2.14) is given by

$$\tilde{\varepsilon}_{AML}(\tilde{\tau}) = \arg \max_{\tilde{\varepsilon}} \left\{ \sum_{p=0}^{P-1} \frac{|A(\tilde{\tau}_p) + e^{-j\pi\tilde{\varepsilon}} B(\tilde{\tau}_p)|^2}{d(\tilde{\tau}_p)} \right\} = \frac{1}{\pi} \angle \left\{ \sum_{p=0}^{P-1} \frac{A^*(\tilde{\tau}_p) B(\tilde{\tau}_p)}{d(\tilde{\tau}_p)} \right\}. \quad (2.18)$$

Moreover, from (2.14)-(2.18), it follows that

$$\hat{\tau}_{AML} = \arg \max_{\tilde{\tau}} \left\{ \sum_{p=0}^{P-1} \left[ \frac{|A(\tilde{\tau}_p)|^2 + |B(\tilde{\tau}_p)|^2}{d(\tilde{\tau}_p)} \right] + 2 \left| \sum_{p=0}^{P-1} \frac{A^*(\tilde{\tau}_p) B(\tilde{\tau}_p)}{d(\tilde{\tau}_p)} \right| \right\}. \quad (2.19)$$

Thus, although under the assumption of small CFO values a closed form approximate estimator can be obtained, the estimation of delays remains a  $P$ -dimensional problem. To simplify the estimation of the delays the last term in the RHS of (2.19) can be neglected and then we obtain

$$\hat{\tau}_{AML_1} = \arg \max_{\tilde{\tau}} \left\{ \sum_{p=0}^{P-1} \left[ \frac{|A(\tilde{\tau}_p)|^2 + |B(\tilde{\tau}_p)|^2}{d(\tilde{\tau}_p)} \right] \right\}. \quad (2.20)$$

In this case, if the number of paths  $P$  is known, it immediately follows that the  $P$ -dimensional vector of delays that maximizes (2.20) can be obtained by considering the  $P$  points where the cost function

$$MD(\tilde{\tau}) = \frac{|A(\tilde{\tau})|^2 + |B(\tilde{\tau})|^2}{d(\tilde{\tau})} \quad (2.21)$$

presents the highest  $P$  peaks. Moreover, the lowest among the obtained delays represents an estimate of the ST. If the number of paths  $P$  is not known in advance, a sufficiently high number of paths should be considered to avoid to lose a strong path and, moreover, to avoid to consider very weak paths. The obtained delays can be substituted in (2.18) to obtain the CFO estimate and, finally, phases and amplitudes can be obtained from (2.11) and (2.12), respectively. It can be shown that if  $P=1$  and  $\tau_0=0$  in (2.1) also if the interference from the data burst following the training symbol is neglected the CFO estimator is expected to exhibit a performance floor [2]. This performance floor can be substantially reduced if the training symbol satisfies the condition [2]

$$\sum_{k \in \mathcal{M}_t} d_{k,0} [\theta_{k,0} \beta_{k,0}]^* d_{k,1} \theta_{k,1} \beta_{k,1} = 0. \quad (2.22)$$

In the case of a single path channel and of perfect ST synchronization, the mean square error (MSE) of the AML CFO estimator in (2.18) can be approximated by [2]

$$E[(\hat{\varepsilon} - \varepsilon)^2] = \frac{2}{\pi^2 MSNR} \frac{1}{\left| \sum_{k=0}^{KM-1} \bar{p}(k)^2 e^{j \frac{2\pi}{M} \varepsilon k} \right|^2} \quad (2.23)$$

where  $SNR \triangleq \frac{|c_0|^2 \sum_{l=0}^{KM-1} p^2(l)}{N_0}$  and  $\bar{p}(k) \triangleq p(kT_s) / \sqrt{\sum_{l=0}^{KM-1} p^2(lT_s)}$ . It is worthwhile to emphasize that the MSE in (2.23) has been derived by neglecting the interference at the output of each matched filter due to

adjacent subcarriers. Therefore, the actual performance of the proposed AML CFO estimator presents a floor that is not predicted by (2.23).

### 2.1.3 Performance evaluation of the proposed joint estimator

The performance of the proposed joint AML estimator is assessed via computer simulations. A number of 5000 Monte Carlo trials has been performed under the following conditions (unless otherwise stated)

- The considered FBMC system has a bandwidth  $B = 1/T_s = 11.2\text{MHz}$ .
- The data symbols belong to a QPSK constellation.
- The overlap parameter of the prototype filter is fixed at  $K=4$ .
- The considered multipath fading channel model is the ITU Vehicular A.
- The channel is fixed in each run but it is independent from one run to another.

In the first set of simulations we have tested the sensitivity of the performance of the derived CFO estimators to the condition (2.22) and to the interference due to the data burst sent after the training symbol. Specifically, four operating conditions have been considered:

1. in the first case, denoted as OC1, condition (2.22) is satisfied and, moreover, to reduce the interference due to the data symbols, the data burst is delayed by one FBMC symbol interval;
2. in the second case, denoted as OC2, condition (2.22) is not satisfied and the data burst is not delayed;
3. in the third case, termed OC3, condition (2.22) is not satisfied and the data burst is delayed;
4. in the fourth case, termed OC4, condition (2.22) is satisfied and the data burst is not delayed.

Figure 2-1 and Figure 2-2 display the root mean square error (RMSE) of the considered CFO estimators as a function of SNR in the previously described operating conditions and, in the case where the number of subcarriers is  $N = 256$  and the actual value of the normalized CFO is  $\varepsilon = 0.2$ . Specifically, the AML CFO estimator for multipath channel reported in (2.18) is denoted as AML1 while the label AML2 indicates the AML estimator for AWGN channel, i.e., that based on the choice  $P = 1$ . In the case of the AML1 CFO estimator two paths have been considered to avoid to lose a strong path and, moreover, to avoid to consider very weak paths. As one would expect, the performance of both AML1 and AML2 estimators is coincident in AWGN channel (see Figure 2-1) while the AML1 outperforms the AML2 estimator in multipath channel (see Figure 2-2). Moreover, only when condition (2.22) is satisfied (curves labeled as OC1 and OC4), the insertion of the considered delay in the data burst can lead to a performance improvement both in AWGN and multipath channel. In particular, when condition (2.22) is satisfied and the data burst is delayed (curves labeled as OC1) a floor is observed only around  $\text{SNR} = 30\text{dB}$ . In Figure 2-1 and Figure 2-2 is also reported the theoretical RMSE (TRMSE) predicted by (2.23). The results show that the derived expression can be exploited in AWGN channel for  $\text{SNR} \leq 15\text{dB}$ . As regards the performance of the AML1 and AML2 ST estimators, no errors were observed in AWGN channel while in multipath channel A an RMSE (normalized to the FBMC symbol interval  $T$ ) less then  $3 \cdot 10^{-3}$  was obtained in all operating conditions for  $\text{SNR} \geq 5\text{dB}$ . Taking into account the previous results in the following experiments only the operating condition OC1 is considered since it assures the best performance. In particular, in Figure 2-3 and Figure 2-4, the normalized RMSE of the AML CFO

estimators is compared with that of the SC estimator proposed in [1], both in AWGN (Figure 2-3) and in multipath channel A (Figure 2-4). Specifically, the number of subcarriers is  $M = 256$  and the actual value of the normalized CFO is  $\varepsilon = 0.2$ . The results show that in multipath channel A the performance of both estimators presents a floor, but for different reasons. In the case of the SC estimator the floor is due to the inaccuracy in the ST estimate (normalized RMSE nearly equal to  $2 \cdot 10^{-1}$  (see Figure 2-5)), while in the case of the AML estimator the floor is due (as well as in the AWGN channel (see Figure 2-3)) to the interference from adjacent subcarriers. To gain some insight about the acquisition range of the considered estimators, the normalized RMSE of the AML CFO estimators are reported in Figure 2-6 as a function of the actual value of the normalized CFO  $\varepsilon$  in AWGN (solid lines) and multipath channel A (dashed lines) for SNR = 10dB. In Figure 2-6 the RMSE of the SC estimator is also reported. Note that in this case a number of 10000 Monte Carlo trials has been performed. The results show that although the AML estimators have been derived under the assumption of small values of CFO they assure a satisfactory performance in the range  $\varepsilon \in [-0.8, 0.8]$ . Figure 2-7 and Figure 2-8 show the normalized RMSE of the considered CFO estimators as a function of the number of subcarriers  $M$  in AWGN (Figure 2-7) and in multipath channel A (Figure 2-8), and for two SNR conditions. The results show that in AWGN the performance of both AML1 and AML2 estimators is coincident with that predicted by (2.23) for SNR = 10dB while it is slightly different for SNR = 20dB. Moreover, Figure 2-8 shows that in multipath channel A the AML1 CFO estimator outperforms the AML2 estimator and assures estimates whose accuracy is quite similar to that provided by the SC estimator. As regards the performance of the ST estimators results, not reported here for the sake of brevity, have shown that the SC ST estimator assures a normalized RMSE nearly equal to  $10^{-1}$  both in AWGN and multipath channel due to the presence of the plateau (see [2]). On the other hand, as regards the AML ST estimators no errors were observed in AWGN while a normalized RMSE less than  $10^{-2}$  was obtained for  $M \geq 64$ . Finally, Figure 2-9 and Figure 2-10 show, for  $M = 256$  and  $\varepsilon = 0.2$ , the bit error rate (BER) obtained with the adoption of the AML and SC estimators followed by a one-tap equalizer with perfect knowledge of the channel and of the residual synchronization errors. The performance is compared with that of the perfectly synchronized FBMC system (PS-FBMC) and with that of the perfectly synchronized OFDM system (PS-OFDM) with cyclic prefix (CP) fixed at  $CP = M/4$ . Note that the slight difference between the performance of the PS-FBMC systems and that of the PS-OFDM systems is due to the fact that, to take into account the energy loss due to the CP, the amplitude of the OFDM signal has been reduced by  $\sqrt{1/(1+CP/M)}$  where  $CP = M/4$ . The results show that both in AWGN and multipath channel A the AML estimators assure a negligible degradation with respect to the perfectly synchronized system while the adoption of the SC synchronization scheme leads to an error floor due essentially to the inaccuracy of the ST estimates.

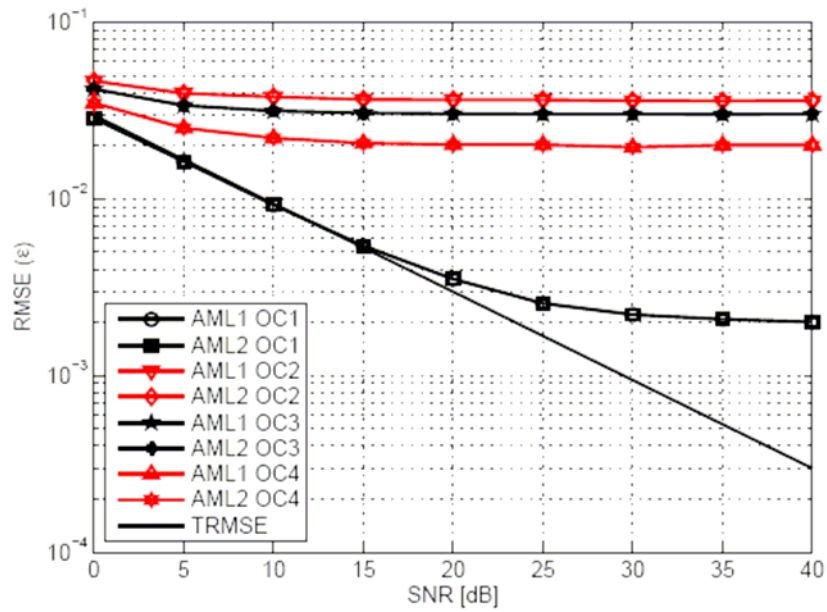


Figure 2-1: Performance of the proposed SML CFO estimators in AWGN channel

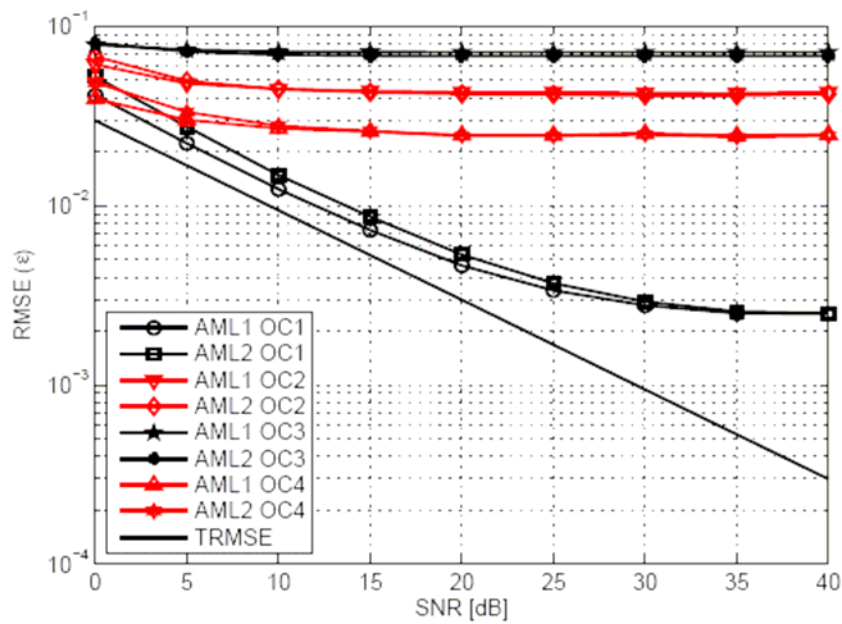


Figure 2-2: Performance of the proposed AML CFO estimators in ITU Vehicular A multipath channel

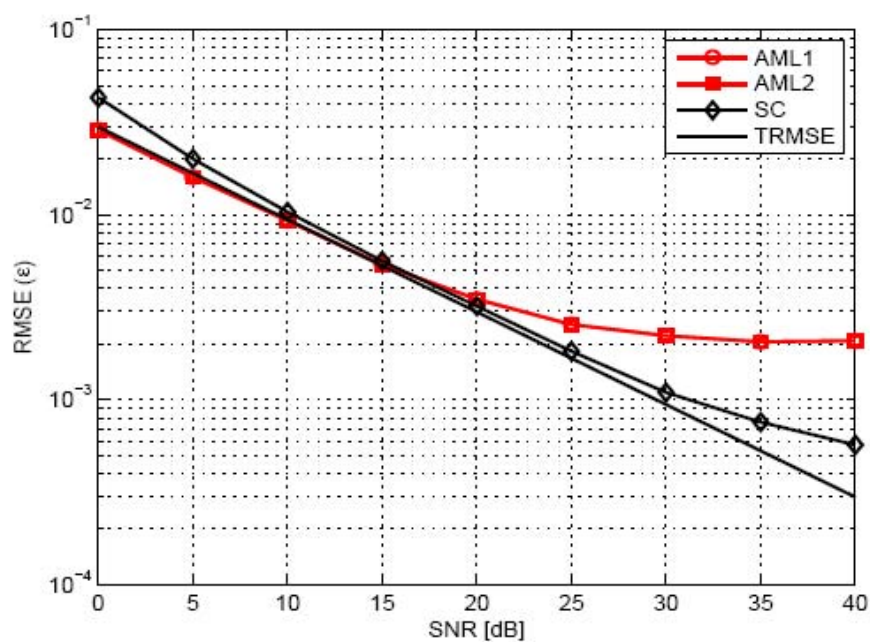


Figure 2-3: Performance of the considered CFO estimators in AWGN channel

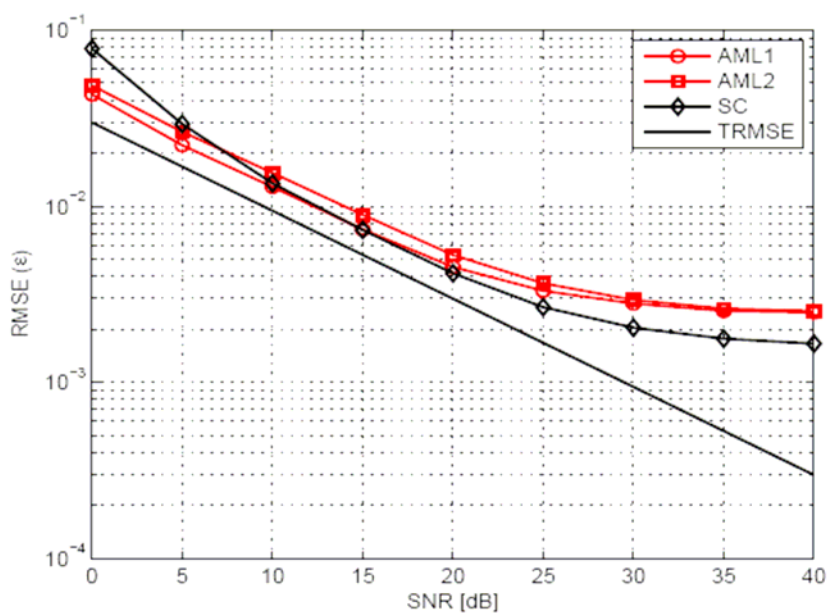


Figure 2-4: Performance of the considered CFO estimators in ITU Vehicular A multipath channel

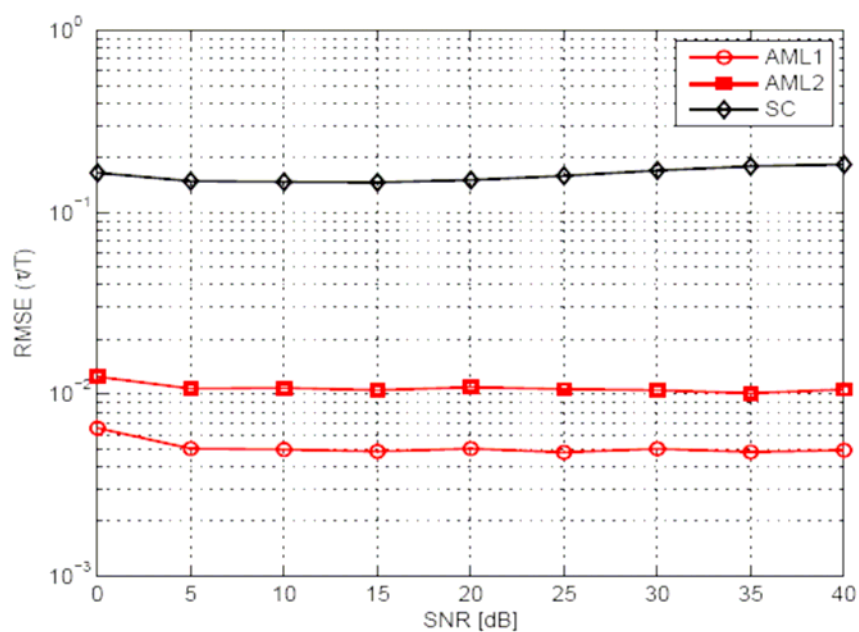


Figure 2-5: Performance of the considered ST estimators in ITU Vehicular A multipath channel

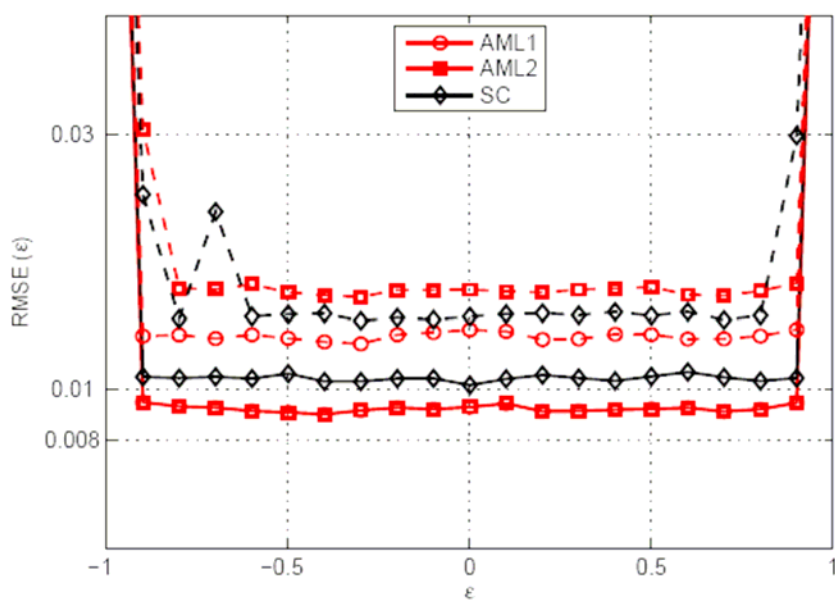


Figure 2-6: Performance of the considered CFO estimators as a function of the actual value of the normalized CFO

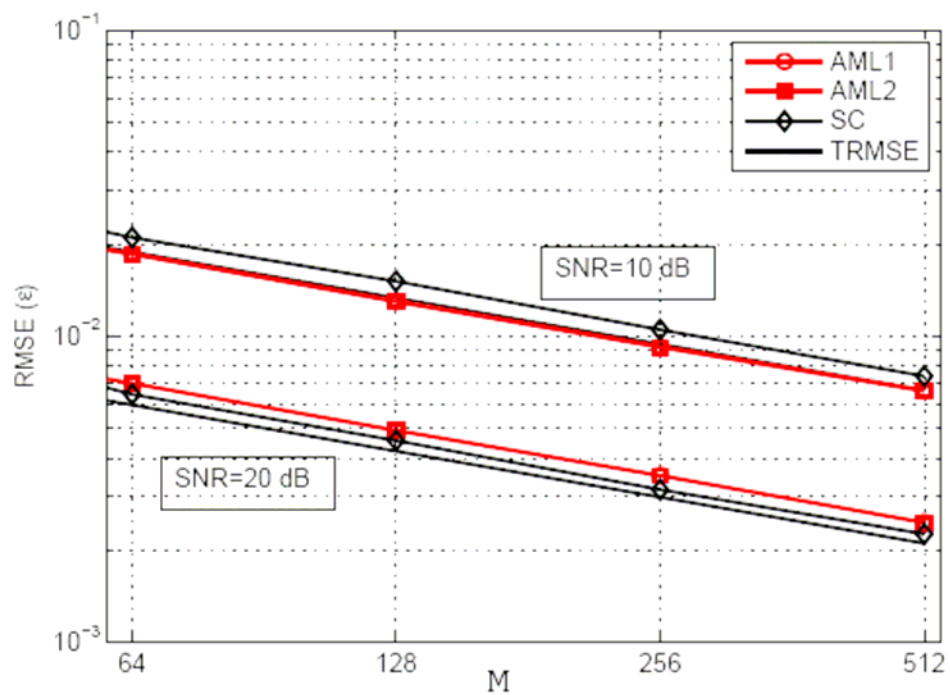


Figure 2-7: Performance of the considered CFO estimators as a function of the number of subcarriers in AWGN channel

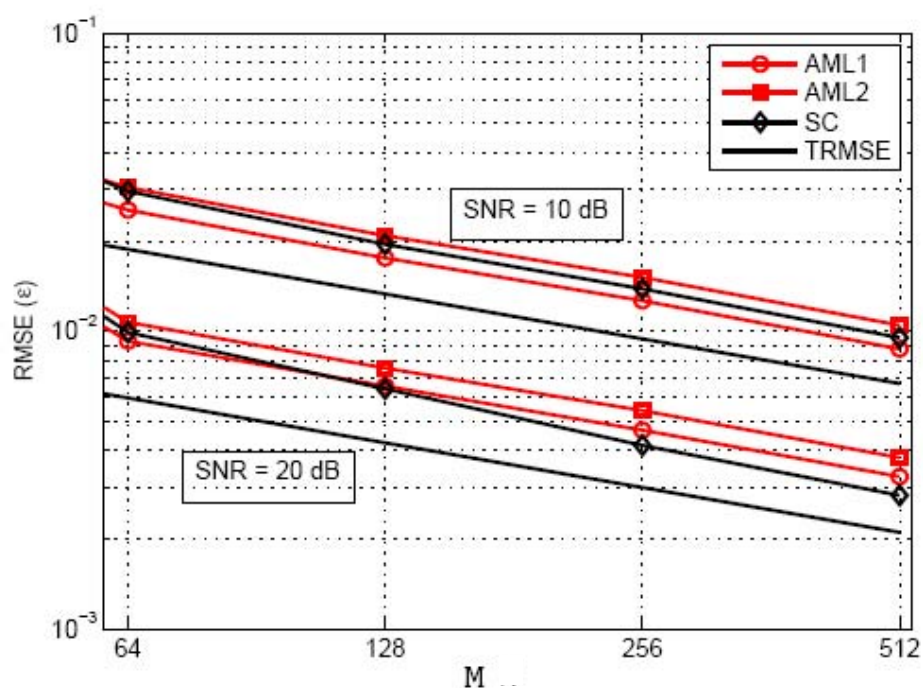


Figure 2-8: Performance of the considered CFO estimators as a function of the number of subcarriers in ITU Vehicular A multipath channel

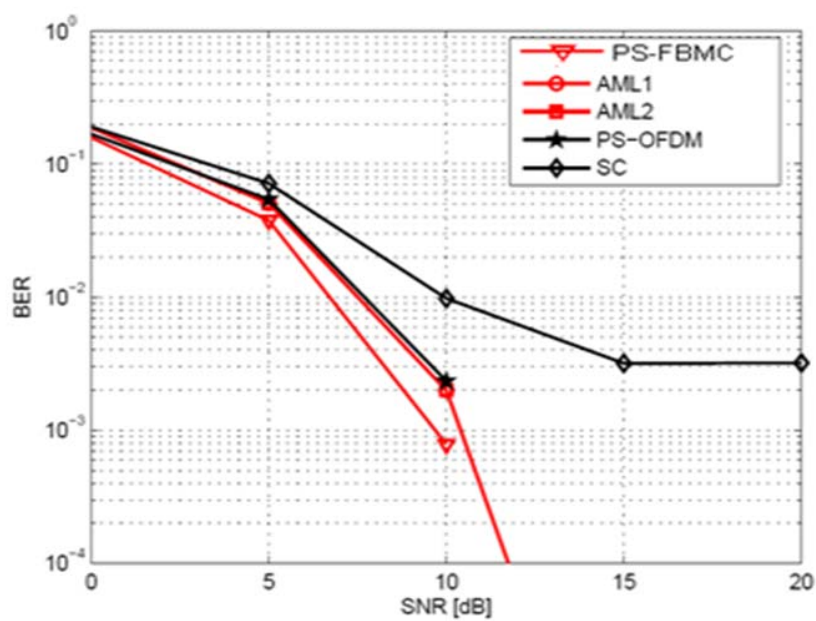


Figure 2-9: BER of the considered joint estimators in AWGN channel

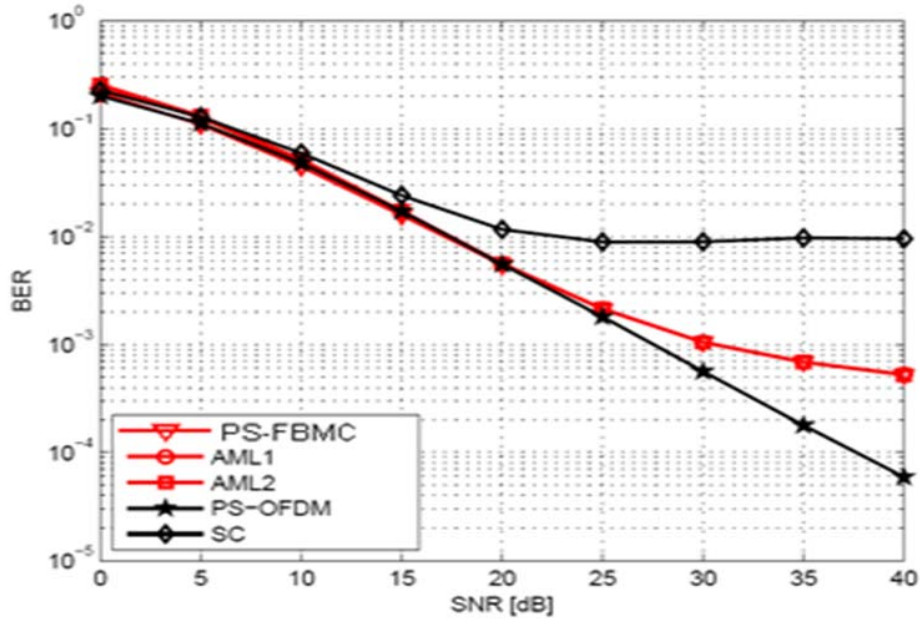


Figure 2-10: BER of the considered joint estimators in ITU-Vehicular A multipath channel

## 2.2 Joint FTD and Channel Estimation based on Iterative Interference Cancellation (IIC)

### 2.2.1 Signal Model

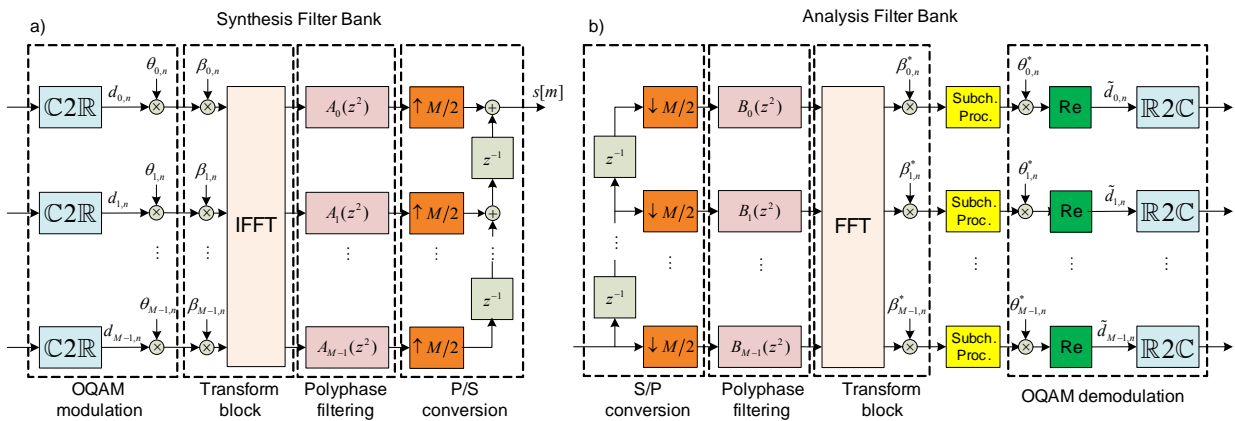


Figure 2-11: FBMC/OQAM transmultiplexer model. Transmitter (a) and receiver (b).

The PHYDYAS reference FBMC/OQAM communication system presented in Section 1.2 of deliverable D3.1 and depicted again in

Figure 2-11 produces the following baseband continuous time signal at the receiver, after passing through a time-varying multipath channel  $h(t, \tau)$ , with a carrier frequency offset (CFO)  $\varepsilon$  relative to the subcarrier spacing and a fractional time delay (FTD)  $\tau_{FTD}$  relative to the FBMC/OQAM symbol period  $T$ :

$$r(t) = (s(t) \star h(t, \tau) \star \delta(t - \tau_{FTD}T))e^{j2\pi\frac{\varepsilon}{T}t} + \eta(t). \quad (2.24)$$

Here  $s(t)$  is the continuous-time waveform generated by the transmitter synthesis filter bank,  $\eta(t)$  is additive white Gaussian noise and  $\star$  is the convolution operator. At the receiver,  $r(t)$  is sampled and filtered by the analysis bank filters  $f_k[m]$ , so that the signal in subchannel  $k$  is expressed by

$$y_{k,n} = r[m] \star f_k[m] \downarrow_{\frac{M}{2}} = \sum_{i=k-1}^{k+1} v_{i,n} \star q_{i,k,n} + \eta_{k,n}, \quad (2.25)$$

where

$$q_{i,k,n} = ((g_i[m] \star h[n, m] \star \delta[m - \tau_{FTD}\frac{T}{T_s}])e^{j2\pi\frac{\varepsilon}{M}m}) \star f_k[m] \downarrow_{\frac{M}{2}}. \quad (2.26)$$

Above,  $q_{i,k,n}$  is the subchannel-dependant 2-dimensional impulse response, including the channel effects, from subchannel  $i$  to subchannel  $k$ , and  $v_{i,n} = \theta_{k,n}^* d_{i,n}$  (see Figure 1-4 in D3.1). The notation  $\downarrow_{\frac{M}{2}}$  represents the downsampling by a factor of  $M/2$  of the overall expression. The sampled and filtered noise is  $\eta_{k,n}$ . Note that the summation in equation (2.25) assumes that the selectivity of the prototype filter is sufficiently high and only the transmitted subchannels  $i=k-1$  to  $i=k+1$  contribute interference to the received signal in subchannel  $k$ . The transform of the subchannel-dependant 2-dimensional impulse response (2.26) shows the effects of the channel distortions in the frequency domain:

$$\begin{aligned} Q_{i,k}(e^{j\omega}) &= \left( (G_i(e^{j\omega}) H_n(e^{j\omega}) e^{-j\omega\tau_{FTD}M}) \star \delta(\omega - 2\pi\varepsilon) \right) F_k(e^{j\omega}) \downarrow_{\frac{M}{2}} \\ &= \left( G_i(e^{j(\omega-2\pi\varepsilon)}) H_n(e^{j(\omega-2\pi\varepsilon)}) e^{-j(\omega-2\pi\varepsilon)\tau_{FTD}M} \right) F_k(e^{j\omega}) \downarrow_{\frac{M}{2}} \\ &= G_i(e^{j(\omega-2\pi\varepsilon)}) H_n(e^{j(\omega-2\pi\varepsilon)}) F_k(e^{j\omega}) e^{-j(\omega-2\pi\varepsilon)\tau_{FTD}M} \downarrow_{\frac{M}{2}}. \end{aligned} \quad (2.27)$$

The main effects of synchronization errors on the received subchannel signals can be analyzed with equations (2.26) and (2.27): The fractional time delay introduces a subchannel-dependant phase shift and the main effects of the CFO is a constantly varying phase rotation of the received symbols and the misalignment of the transmit and receive subchannel filters.

Equation (2.25) can further be developed into

$$\begin{aligned} y_{k,n} &= \sum_{i=k-1}^{k+1} \sum_{l=-\infty}^{\infty} v_{i,l} q_{i,k,n-l} + \eta_{k,n} \\ &= v_{k,n} q_{i,k,0} + \sum_{i=k-1}^{k+1} \sum_{\substack{l=-\infty \\ (i,l) \neq (k,n)}}^{\infty} v_{i,l} q_{i,k,n-l} + \eta_{k,n}, \end{aligned} \quad (2.28)$$

or, equivalently, into the equations that relate the signals before and after the real/imaginary mapping performed by the multiplications by  $\theta_{k,n}$  ( $=j^{k+n}$ ) and  $\theta_{k,n}^*$ :

$$\begin{aligned}\tilde{y}_{k,n} &= \theta_{k,n}^* y_{k,n} \\ &= \theta_{k,n}^* v_{k,n} q_{i,k,0} + \theta_{k,n}^* \sum_{i=k-1}^{k+1} \sum_{\substack{l=-\infty \\ (i,l) \neq (k,n)}}^{\infty} v_{i,l} q_{i,k,n-l} + \theta_{k,n}^* \eta_{k,n} \\ &= d_{k,n} q_{i,k,0} + \sum_{i=k-1}^{k+1} \sum_{\substack{l=-\infty \\ (i,l) \neq (k,n)}}^{\infty} j^{i-k} d_{i,l} q_{i,k,n-l} + \theta_{k,n}^* \eta_{k,n}.\end{aligned}\quad (2.29)$$

The auxiliary pilot scheme thoroughly introduced in deliverables D2.1, D2.2 and D3.1 can be derived by simplifying (2.29) with a 2-D impulse response that is free of any channel effects, i.e.,  $q_{i,k,n}$  becomes the transmultiplexer response. In this case,

$$\tilde{y}_{k,n} = d_{k,n} + (\eta_{k,n}^{NPR} + ju_{k,n}) + \theta_{k,n}^* \eta_{k,n}, \quad (2.30)$$

where  $\eta_{k,n}^{NPR}$  is the (usually neglectable) residual intersymbol and intercarrier interference (ISI and ICI) from the filter bank prototype design, and  $ju_{k,n}$  is the imaginary valued interference that is eliminated at the receiver by taking the real part of the received, distortion-free signal. The auxiliary pilot that nulls the imaginary valued interference  $ju_{k,n}$  on a pilot  $d_{k_p,n_p}$  is calculated as

$$d_{k_a,n_a} = - \frac{\sum_{\substack{(k,n) \in \Omega_{k_p,n_p} \\ (k,n) \neq (k_p,n_p) \\ (k,n) \neq (k_a,n_a)}} d_{k,n} \hat{t}_{k_p-k,n_p-n}}{\hat{t}_{k_p-k_a,n_p-n_a}}, \quad (2.31)$$

where  $\hat{t}_{k,n}$  is obtained from the transmultiplexer response  $t_{k,n}$  as  $\hat{t}_{k,n} = \text{Im}[\theta_{k,n}^* t_{k,n}]$ . Without channel distortions,  $t$  and  $q$  are related as  $q_{i,k,n} = t_{k,i,n}$ . The working principle of the auxiliary pilot technique is sketched in Figure 2-12.

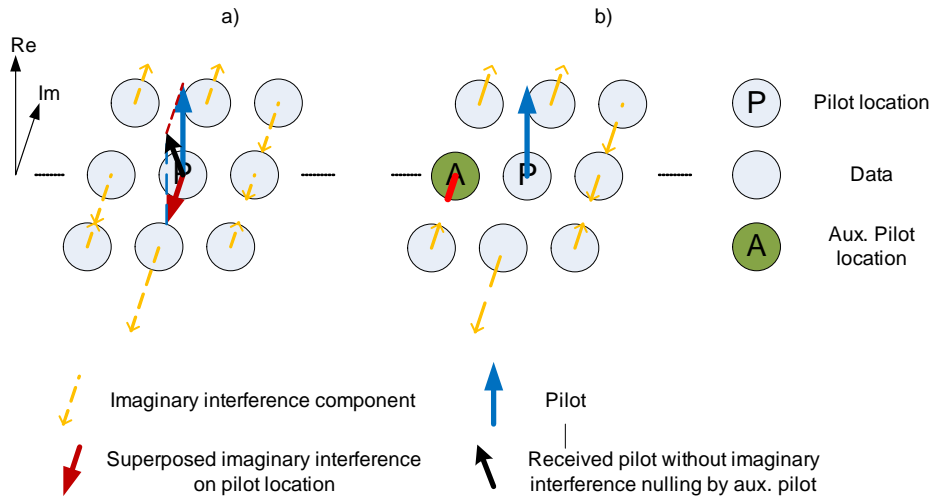


**Figure 2-12: Auxiliary pilot technique. Imaginary interference without auxiliary pilot (a). Auxiliary pilot nulls imaginary interference (b).**

Applying the auxiliary pilot approach, the received pilot estimate can be written as

$$\tilde{y}_{k_p, n_p} \simeq d_{k_p, n_p} q_{i, k_p, 0} + \theta_{k, n}^* \eta_{k, n}. \quad (2.32)$$

It should be mentioned that the auxiliary pilot scheme has the drawback of somewhat increased latency and memory requirements on the transmitter side.

### 2.2.2 Iterative Interference Cancellation

The analysis above shows a clear interplay between the quality of the estimates and the channel distortion, including the FTD and CFO. Therefore, it is desirable to apply the information of the estimated synchronization parameters to the estimated pilots in order to improve the quality of all the estimates. One way to achieve this is by jointly estimating the subcarrier-wise channel coefficients and the phase slope. Here, we present an approach that utilizes the FTD-induced linear phase slope within each pilot subcarrier. We assume a simplified signal model, where the amplitude response is assumed to be constant within each subchannel and the phase is assumed to be a linear function of frequency within each subchannel. This is motivated by the observation that, in many cases, a 1-tap equalizer is able to equalize the channel quite well in the absence of timing offsets. The joint channel-FTD estimation includes two parts: estimation of the complex channel coefficient for each pilot, and estimation of the phase slope jointly for all pilots participating in the estimation window  $\Omega_{JE}$ .

If the 1-tap equalizer coefficient at  $k, n$  is obtained as  $w_{k, n}$ , the FTD-compensating target response of the 3-tap subcarrier equalizer presented in subsection 4.1 of deliverable D3.1 can be written as

$$\begin{aligned} W_{k, n} \left( e^{-j\frac{\pi}{2}} \right) &= w_{k, n} e^{j\psi} \\ W_{k, n} \left( e^{j0} \right) &= w_{k, n} \\ W_{k, n} \left( e^{j\frac{\pi}{2}} \right) &= w_{k, n} e^{-j\psi}, \end{aligned} \quad (2.33)$$

where the equalizer phase difference correction between the subchannel center frequency and the edge is

$$\psi = -\pi \tau_{FTD} \quad (2.34)$$

The subcarrier equalizer impulse response in the frequency sampling design can now be written as:

$$W_{k, n}(z) = \left[ 0.5(1 - \cos(\psi) - \sin(\psi))z + \cos(\psi) + 0.5(1 - \cos(\psi) + \sin(\psi))z^{-1} \right] w_{k, n}, \quad (2.35)$$

resulting in the following signal model for the subcarrier equalizer output:

$$\bar{y}_{k, n}(\psi) = \cos(\psi) w_{k, n} y_{k, n} + 0.5(1 - \cos(\psi) + \sin(\psi)) w_{k, n} y_{k, n-1} + 0.5(1 - \cos(\psi) - \sin(\psi)) w_{k, n} y_{k, n+1}. \quad (2.36)$$

If  $\psi$  is assumed to be small, we can approximate (2.36) as

$$\bar{y}_{k, n}(\psi) \simeq w_{k, n} y_{k, n} + \frac{\psi}{2} w_{k, n} (y_{k, n-1} - y_{k, n+1}). \quad (2.37)$$

This can be rewritten as

$$\begin{aligned}
 \tilde{d}_{k,n} + j\tilde{u}_{k,n} &= \theta_{k,n}^* \bar{y}_{k,n}(\psi) \\
 &\simeq w_{k,n} \theta_{k,n}^* y_{k,n} + \frac{\psi}{2} w_{k,n} \theta_{k,n}^* (y_{k,n-1} - y_{k,n+1}) \\
 &= w_{k,n} \tilde{y}_{k,n} + \psi w_{k,n} \tilde{\Delta y}_{k,n},
 \end{aligned} \tag{2.38}$$

where we define

$$\tilde{\Delta y}_{k,n} = \theta_{k,n}^* (y_{k,n-1} - y_{k,n+1}) / 2. \tag{2.39}$$

The ideal output corresponding to the pilot symbols is  $d_{k,n}$  (the subindices  $(\cdot)_p$  are ignored here for readability). Now, the channel equalization problem can be formulated as:

$$\{\hat{\psi}, \hat{w}_{k,n}\} = \arg \min_{\psi, w_{k,n}} \left\{ \sum_{k,n \in \Omega_{JE}} \left| d_{k,n} - (w_{k,n} \tilde{y}_{k,n} + \psi w_{k,n} \tilde{\Delta y}_{k,n}) \right|^2 \right\}, \tag{2.40}$$

where  $\Omega_{JE}$  is the set of subcarrier symbols used in the joint estimation. The idea is to adjust  $\psi$  and  $w_{k,n}$  in such a way that difference between the equalizer output and the known pilot  $d_{k,n}$  is minimized in the least-squares sense. This is a nonlinear optimization problem, which can be solved for example by iterating the following two steps:

1) Assuming that the phase slope is known from the previous iteration (slope is initialized to 0 in the beginning),  $\{w_{k,n}^i\}$  are solved from pilots  $\tilde{y}_{k,n} + \psi(i-1)\tilde{\Delta y}_{k,n}$ . Note that here  $i$  is the iteration index.

2) Assuming that  $\{w_{k,n}^i\}$  are known, the observation is a linear function of  $\psi$  and the optimum  $\hat{\psi}$  can easily be calculated with the derivative of the expression in brackets in Equation (2.40) with respect to  $\psi$  and setting the result to 0, yielding

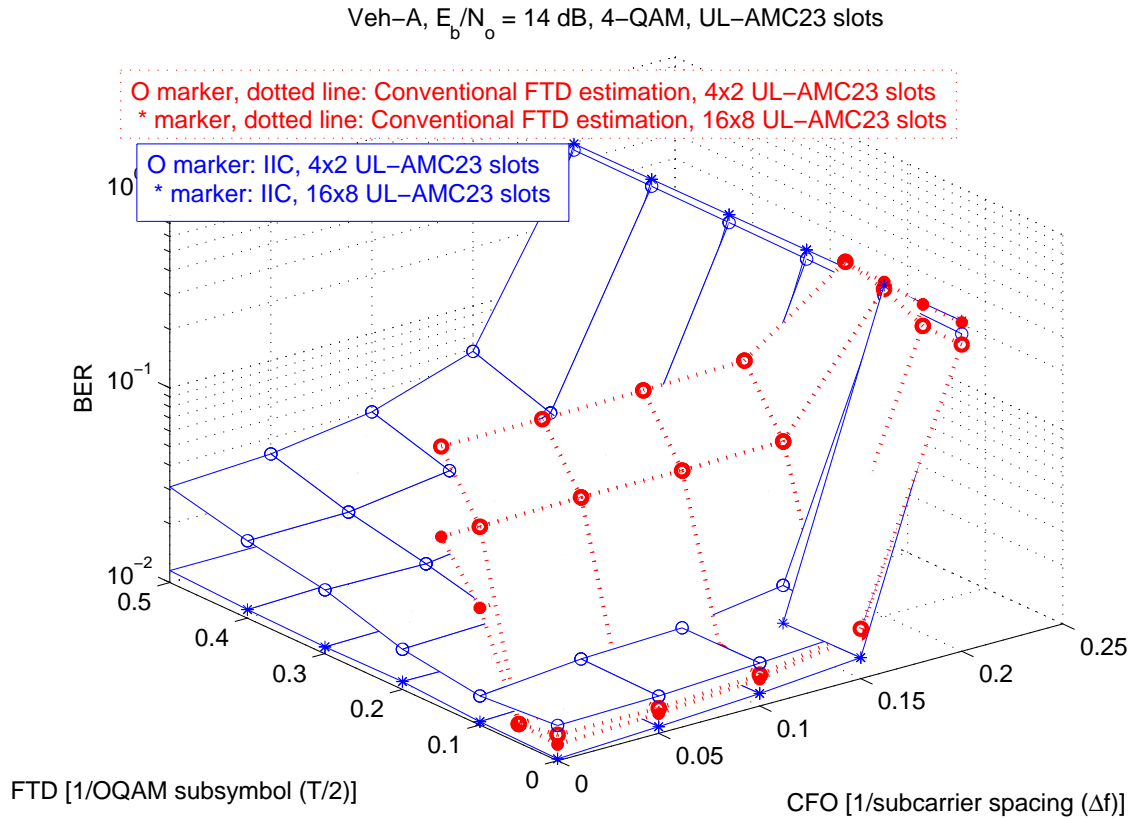
$$\hat{\psi} = \frac{\sum_{k,n \in \Omega_{JE}} d_{k,n} \operatorname{Re}[w_{k,n} \tilde{\Delta y}_{k,n}] - |w_{k,n}|^2 \operatorname{Re}[\tilde{y}_{k,n} \tilde{\Delta y}_{k,n}^*]}{\sum_{k,n \in \Omega_{JE}} |w_{k,n} \tilde{\Delta y}_{k,n}|^2}, \tag{2.41}$$

which, from Equation (2.34), yields  $\hat{\tau}_{FTD} = -\hat{\psi} / \pi$ . This process converges typically in 2-5 iterations. Moreover, the estimates  $\hat{\psi}$  are quite accurate even for higher values of  $\psi$ . With this IIC approach, the FTD estimation range can be extended beyond the limit in which the basic estimation methods presented and evaluated in deliverable D2.2 perform correctly. This limit is imposed by the frequency separation of the pilots.

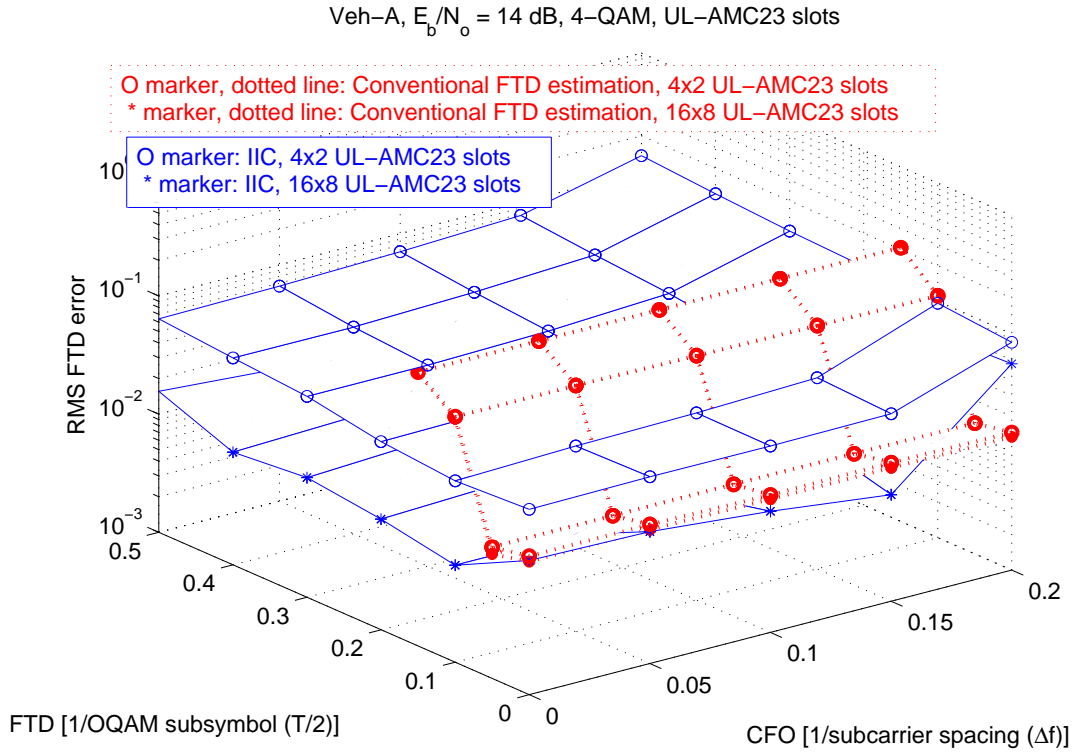
### 2.2.3 Simulation setup and results

Simulation results for the performance of the IIC technique for the WiMAX UL-AMC23 transmission configuration are presented next. For the simulations, the standard WiMAX-like FBMC/OQAM system of previous simulations has been used: The filter bank is of size  $M = 1024$  and the prototype filter is the NPR optimized design with  $K = 4$ . The FBMC signal is sent through a quasi-static ITU-R Vehicular-A channel, if not indicated otherwise. For each simulation, 3000 independent burst transmissions with independent channel realizations are performed. The estimation of the synchronization parameters and the channel state relies on scattered pilots obtained with the auxiliary pilot technique. The combined pilot/auxiliary pilot symbol is boosted on average by 4.5 dB with respect to the data. The overall channel response is obtained from the scattered channel estimates by triangulation based linear interpolation between the pilots. If not stated otherwise, the novel IIC method iterates 10 times.

Figure 2-13 presents the BER results of the IIC and conventional FTD and channel estimation method with respect to the CFO and FTD at  $E_b/N_0 = 14$  dB and for different burst sizes. The bursts are composed of AMC23 slots, where each slot consists of 18 consecutive subcarriers and 3 MC symbols. Within each slot there are 6 pilot/auxiliary pilot pairs, according to the AMC23 configuration. Figure 2-14 presents the FTD estimation RMS error under the same conditions.

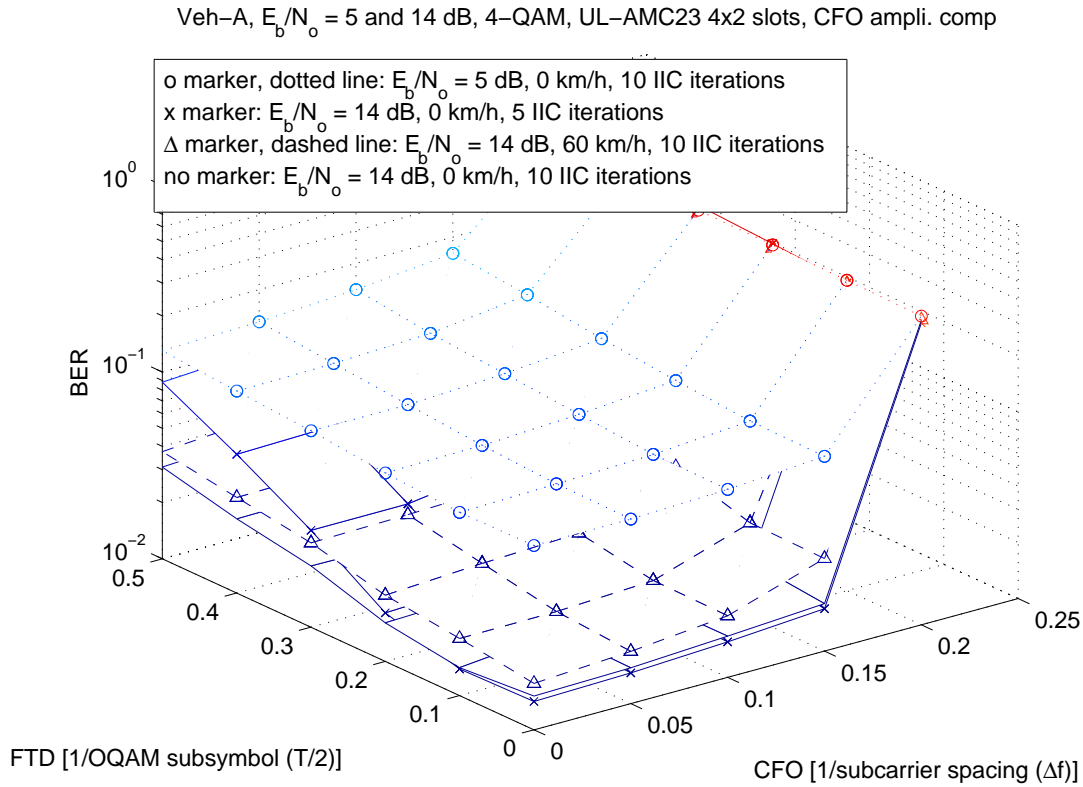


**Figure 2-13: BER performance vs. CFO and FTD of the IIC joint FTD and channel estimation method compared to classical FTD estimation. 4-QAM transmission of 4x2 and 16x8 UL-AMC23 slots in Vehicular-A channel at  $E_b/N_0 = 14$  dB. Static user.**



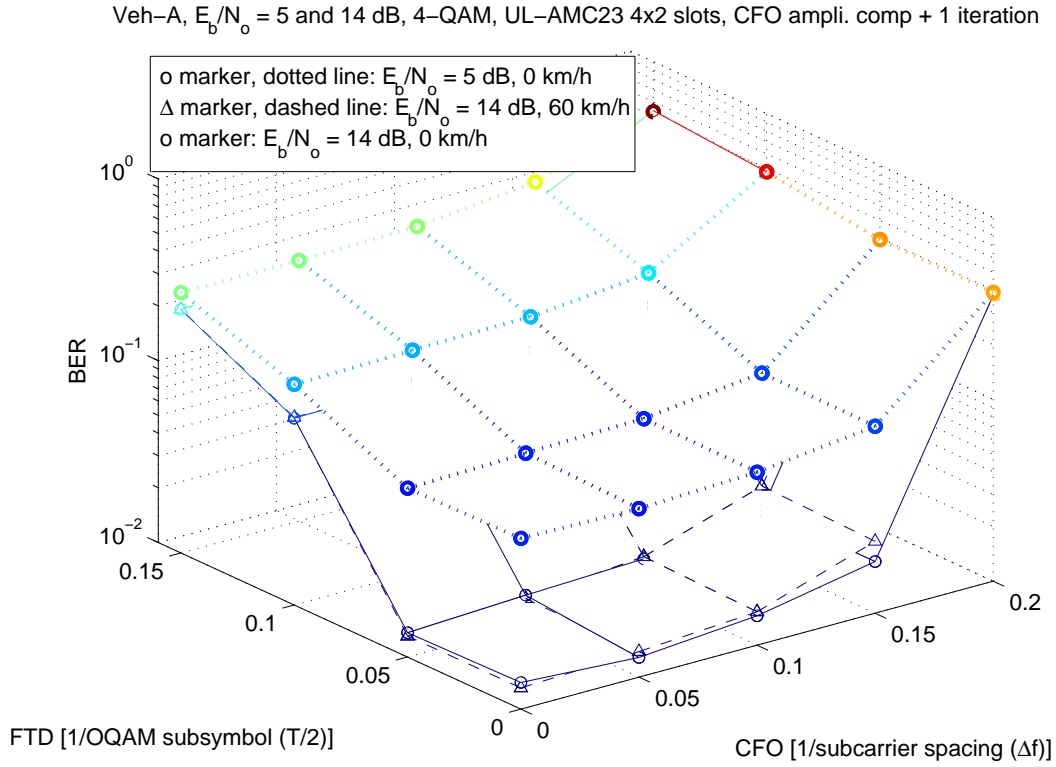
**Figure 2-14: RMS error in FTD estimation vs. CFO and FTD of the IIC FTD estimation method compared to classical FTD estimation. 4-QAM transmission of 4x2 and 16x8 UL-AMC23 slots in Vehicular-A channel at  $E_b/N_0 = 14$  dB. Static user.**

The extension into longer delay operating ranges is evident, and the BER performance for this  $E_b/N_0$  is better than for the conventional technique when the larger bursts are compared. However, when a mobile user transmits using small bursts, and consequently few pilots, the BER and estimation performances of the IIC approach suffer greatly. If the interference cancellation method performs poorly in estimating the FTD because it has not enough pilots, it can, nevertheless, be applied for a coarse estimation within a wide FTD range to pin the delay to a value from where the conventional FTD estimation can take over the task.



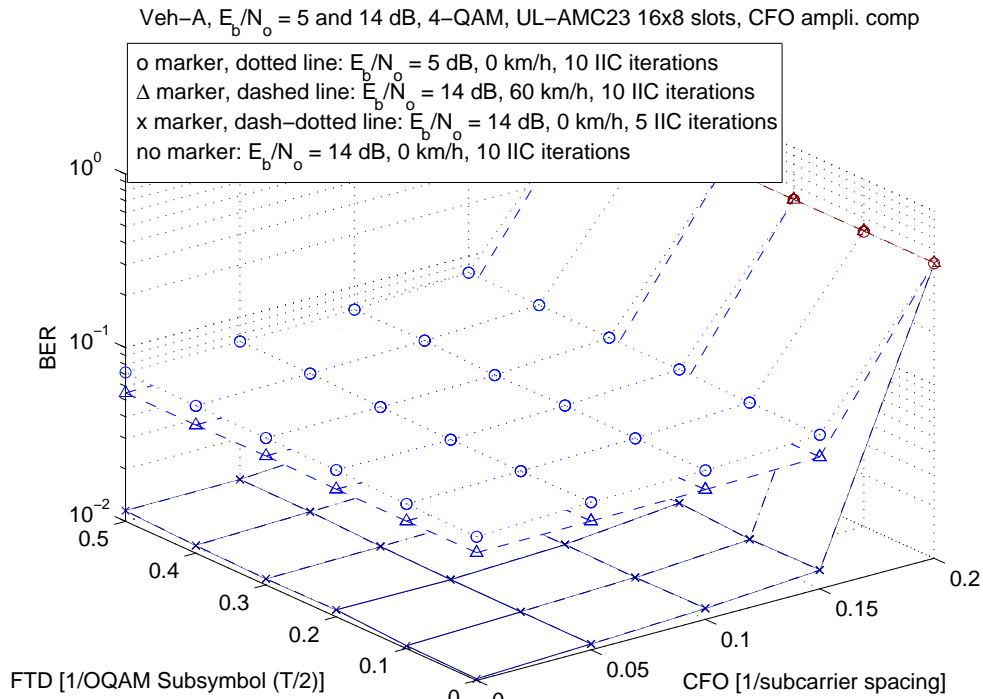
**Figure 2-15: BER performance vs. CFO and FTD of the IIC joint FTD and channel estimation method in different channel scenarios. 4-QAM transmission of 4x2 UL-AMC23 slots in Vehicular-A channel at  $E_b/N_0 = 5$  dB and  $E_b/N_0 = 14$  dB and at different velocities. 5 and 10 iterations in the IIC technique.**

Figure 2-15 presents the performance of the IIC method for UL-AMC23 transmission of 4x2 slots under different channel conditions. We see that this method is more sensitive to the mobility conditions than the conventional FTD and channel estimation method (see Figure 2-16). The BER performance with low SNR is also worse in this small burst case. If only 5 iterations in the IIC are performed, then the BER worsens for longer fractional time delays.

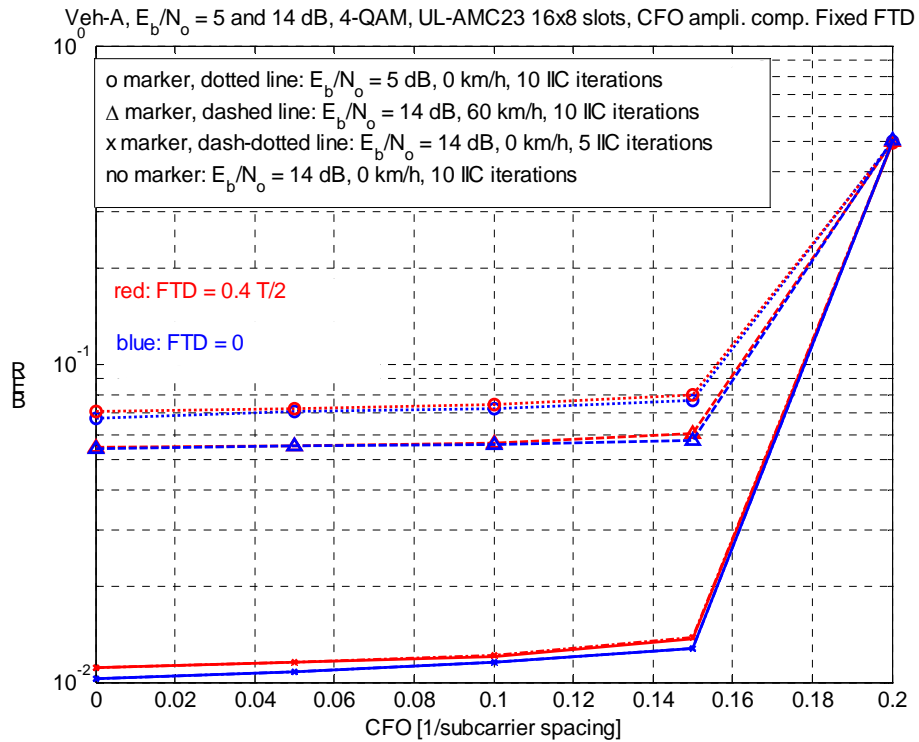


**Figure 2-16: BER performance vs. CFO and FTD with basic FTD and channel estimation as described in D2.2. Uplink transmission of 4x2 AMC23 slots in Vehicular-A channel at  $E_b/N_0 = 5$  dB and  $E_b/N_0 = 14$  dB using 4-QAM. Static user and user with 60 km/h mobility. Synchronization with CFO amplitude distortion correction and one iteration.**

In a scenario, in which larger bursts are sent, the performance in the quasi-static channel is much better and, additionally, the number of iterations in the IIC approach can be reduced. The following figures show BER and FTD estimation RMS error performance with a transmission burst consisting of 16x8 AMC23 slots. Figure 2-17 presents the BER performance under different channel conditions and different number of iterations. In this case, the BER performance for 5 and 10 IIC iterations is almost exactly the same. The following figure permits a clearer quantitative evaluation, since it shows sections of Figure 2-17 at fixed fractional time delays (a) and carrier frequency offsets (b).



**Figure 2-17: BER performance vs. CFO and FTD of the IIC joint FTD and channel estimation method in different channel scenarios. 4-QAM transmission of 16x8 UL-AMC23 slots in Vehicular-A channel at  $E_b/N_0 = 5$  dB and  $E_b/N_0 = 14$  dB and at different velocities. 5 and 10 iterations in the IIC technique.**



(a)

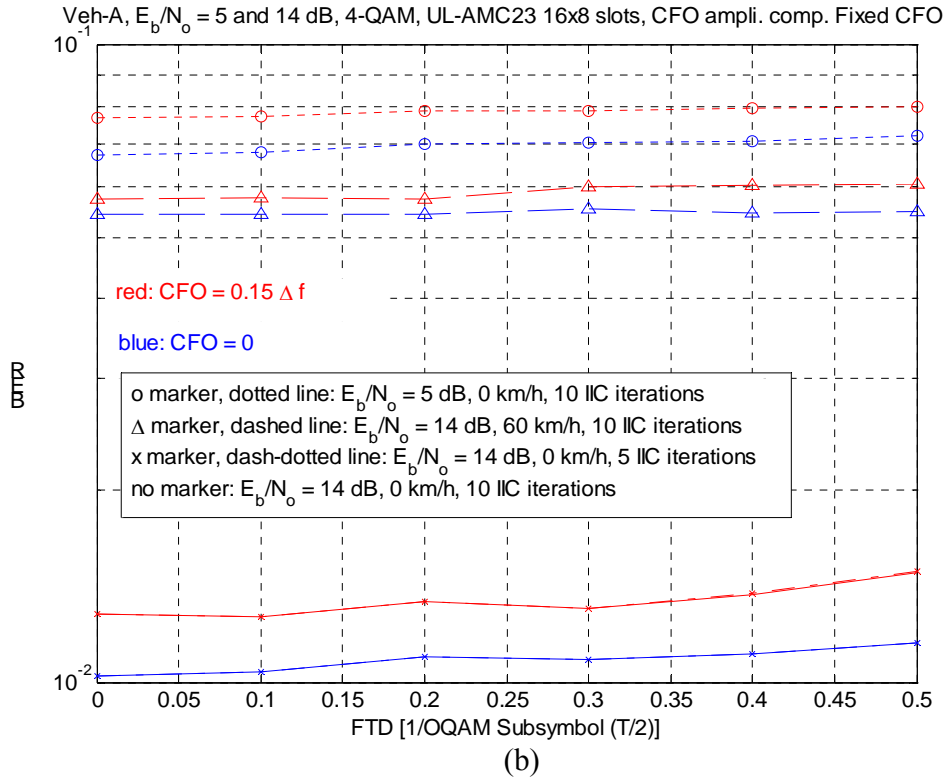


**Figure 2-18: BER performance vs. a) CFO (with fixed FTD = 0 and 0.4 T/2) and b) FTD (with fixed CFO = 0 and 0.15 $\Delta f$ ) of the IIC joint FTD and channel estimation method in different channel scenarios. 4-QAM transmission of 16x8 UL-AMC23 slots in Vehicular-A channel at  $E_b/N_0 = 5$  dB and  $E_b/N_0 = 14$  dB and at different velocities. 5 and 10 iterations in the IIC technique.**

The RMS error in FTD estimation is depicted in Figures 2-19 and 2-20, where the latter is again a cut of the 3-D FTD RMS error graph with fixed CFO of 0 and 15% of subcarrier spacing. These figures seem to indicate that when the user is mobile, the IIC method applied to larger transmission bursts suffers degradation in its performance. Although the degradation can be seen in the FTD estimation, the error is still reasonable, below 2% of half an FBMC/OQAM symbol (T/2), without CFO. The strong BER performance degradation points to a high sensitivity of the IIC channel estimation part to the user mobility when the pilots of a bigger burst are used.

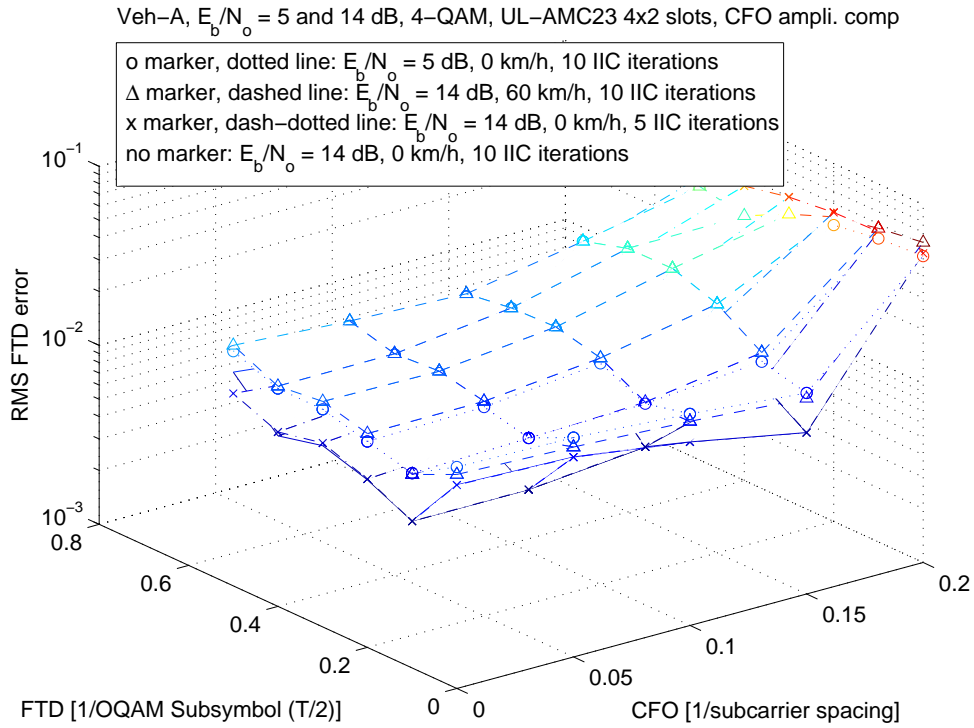


**Figure 2-19: RMS error in FTD estimation vs. CFO and FTD of the IIC joint FTD and channel estimation method. 4-QAM transmission of 16x8 UL-AMC23 slots in Vehicular-A channel at  $E_b/N_0 = 5$  dB and  $E_b/N_0 = 14$  dB and at different velocities. 5 and 10 iterations in the IIC technique.**

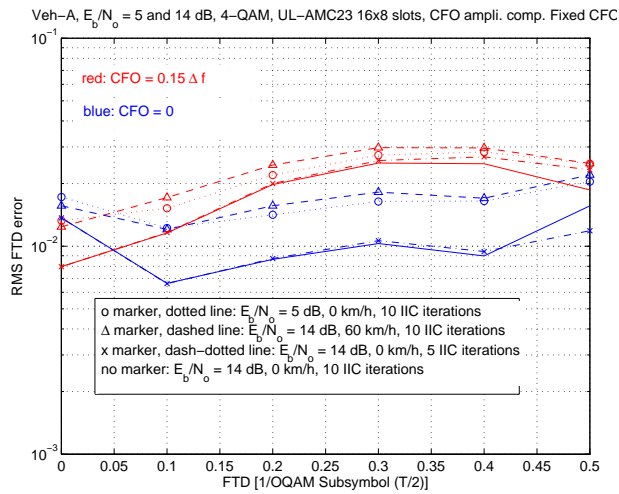


**Figure 2-20: RMS error in FTD estimation vs. FTD for fixed CFO = 0 and 0.15  $\epsilon$ . IIC joint FTD and channel estimation method. 4-QAM transmission of 16x8 UL-AMC23 slots in Vehicular-A channel at  $E_b/N_0 = 5$  dB and  $E_b/N_0 = 14$  dB and at different velocities. 5 and 10 iterations in the IIC technique.**

#### 2.2.4 Conclusion

The presented results show that the introduced joint FTD and channel estimation approach can outperform the conventional method under favorable channel conditions (good SNR and low mobility) allowing acceptable reception under severe FTD. In adverse conditions, it provides sufficiently good estimates for a wide range of FTD, making it suitable for coarse estimation and synchronization of robust data signals. It could be interesting to study what is the optimal number of pilots in time and frequency direction used in the IIC approach at different mobilities. Moreover, when multiple-input multiple-output (MIMO) techniques are used to improve the throughput, the scattered pilot locations have to be shared by the different transmit antenna - receive antenna streams, thus making the pilot grid for a certain antenna link more sparse. This reduces the FTD estimation range with classical estimation methods. In this scenario, the new FTD estimation can prove itself as very practical.

### 2.3 Uplink multi-user synchronization

The multiple access technique used in a multicarrier system naturally is Frequency Division Multiple Access (FDMA). In the downlink, there is no carrier frequency offset (CFO) and no timing offset (TO) between the different users. Therefore, orthogonality between users is not destroyed. In the uplink the situation is quite different. Between users, there is CFO and TO and the BS cannot synchronize to all users simultaneously. The performance degradation due to these offsets in multipath channels is investigated for two allocation schemes. FBMC and CP-OFDM are compared in the basis of the same bandwidth and the same symbol rate on the channel. Therefore, the data rate of the FBMC system is higher, because there is no CP and more subcarriers can be loaded because of the much better reduction of the out-of-band emissions. The FBMC needs an equalizer per sub-carrier to mitigate multipath induced inter-symbol interference (ISI) and inter-carrier interference (ICI).

#### 2.3.1 Effects of intracell interference in the uplink

In this section, the performance degradation of a FDMA FBMC system due to the presence of multiple access interference in the uplink is analyzed in the case where the user of interest is perfectly synchronized while the signals of the other users present a CFO and a TO. Moreover, a performance comparison with a FDMA CP-OFDM system with the same bandwidth and the same symbol rate is presented. Two different allocations schemes are considered: block-wise and interleaved schemes. In particular, as illustrated in Figure 2-21, in the block-wise scheme group of adjacent subcarriers are allocated to the same user while in the case of interleaved scheme group of adjacent subcarriers are allocated to different users. Note that in the block-wise allocation scheme an empty subcarrier is introduced between group of subcarriers assigned to different users.

## Subcarrier allocation schemes:

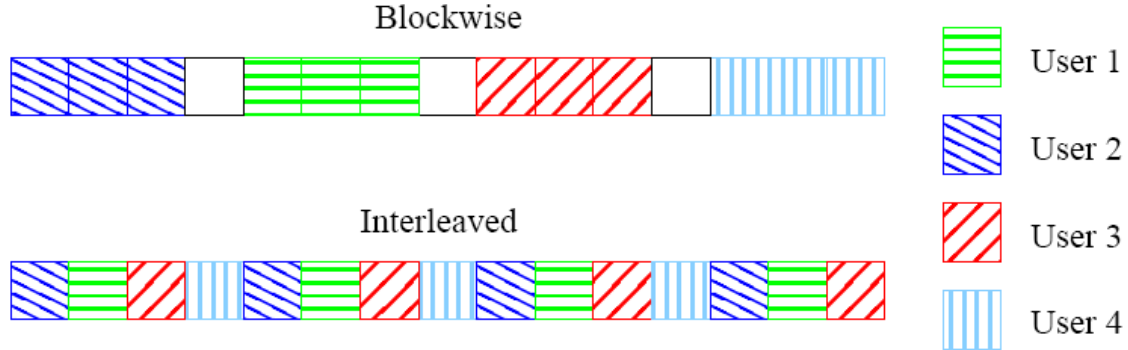


Figure 2-21: sub-carriers allocation schemes

The performance has been assessed via computer simulation by considering a certain subcarrier and exploiting a number of 10000 Monte Carlo trials. The modulation format is QPSK. The number of subcarriers is  $M = 256$  and the number of users is  $U=4$ . In the FBMC case a prototype filter of length  $K = 4$  with a roll-off factor of one has been used. The used subcarriers are evenly split between the 4 users. In particular, the number of used subcarriers is 228 for the FBMC system and 208 for the OFDM system. In the block-wise allocation scheme the considered subcarrier is the last of the block of subcarriers assigned to the first user which is perfectly synchronized. The other users are completely asynchronous with a timing offset uniformly distributed in the set  $\{-(M/2)T_s, (M/2-1)T_s\}$ , a carrier frequency offset normalized to the subcarrier spacing uniformly distributed in the range  $[-0.125, 0.125]$  and a carrier phase offset uniformly distributed in the interval  $[-\pi, \pi]$ . The multipath fading ITU-Vehicular A channel model has been considered. In particular, for each user the channel is fixed in each run but is independent from one run to another. A perfect knowledge of the multipath channel of the user of interest is assumed. In the case of the FBMC systems a 1-tap equalizer is exploited while in the CP-OFDM case the CP has been fixed at  $CP = 1/4$ , and, moreover, the energy wasted in the cyclic prefix has been taken into account. Figure 2-22 shows the bit error rate (BER) of the first user as a function of  $E_b/N_0$  for both systems for the block-wise allocation scheme. Two values of  $E_b/N_0$  for the other users have been considered, specifically,  $E_b/N_0 = 4\text{dB}$  (dashed lines) and  $E_b/N_0 = 14\text{dB}$  (solid lines). The results show that in the OFDM system the presence of asynchronous users and, then, of the consequent multiple-access interference leads to a performance degradation that is more pronounced when the value of  $E_b/N_0$  for the other users is higher. On the other hand, the performance of the FBMC system is quite similar in the two considered operating conditions, thus, the FBMC system can assure a significant performance gain with respect to the OFDM system due to its robustness to the multiple access interference. The robustness of the FBMC system to the multiple-access interference when the block-wise allocation scheme is adopted is confirmed by the results presented in Figure 2-23 where the BER of the first user is reported, with a value of  $E_b/N_0$  fixed at  $E_b/N_0 = 14\text{dB}$ , as a function of the value of  $E_b/N_0$  for the other users. The results show that as the value of  $E_b/N_0$  for the other users increases the performance of the user of interest in the FBMC case does not change while that of the first user in the OFDM case presents a severe degradation. In Figure 2-24 and Figure 2-25,

the same operating conditions are considered as the ones used in Figure 2-22 and Figure 2-23 with reference to the interleaved allocation scheme. The results show that, in this case both systems assure nearly the same BER and presents a performance degradation due to the increased multiple access interference as the value of  $E_b/N_0$  for the other users increases. Future work will focus on the performance analysis in the up-link of a multi-tap equalizer and on the sensitivity to a residual synchronization error in the signal of interest.

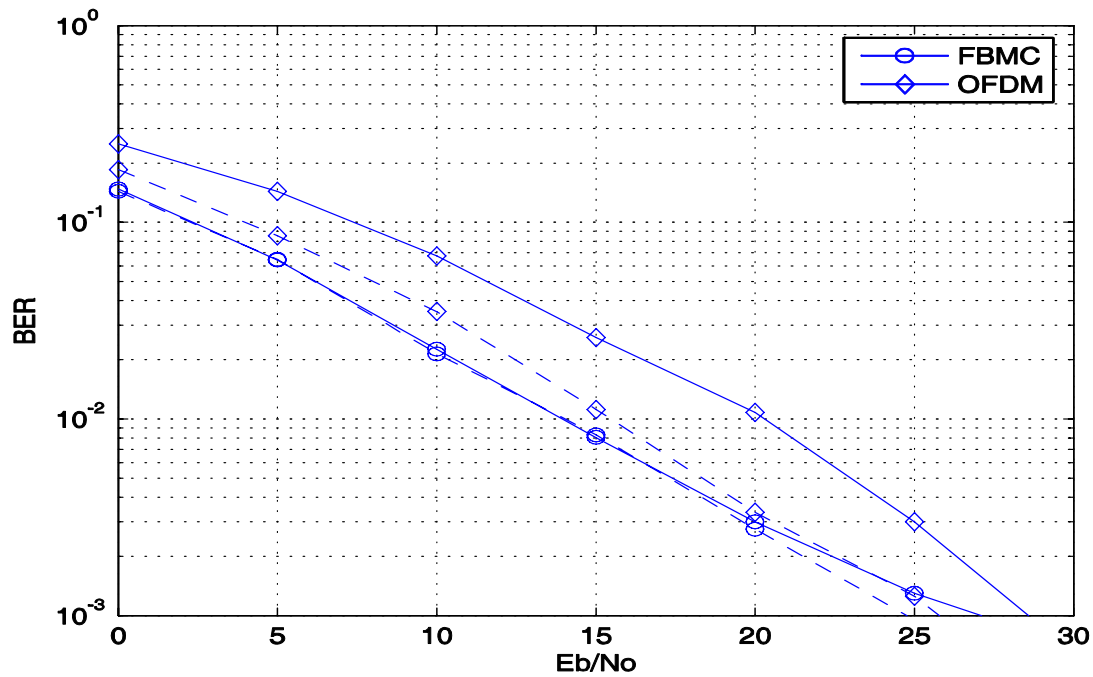


Figure 2-22 : BER of the first user for the blockwise allocation scheme.

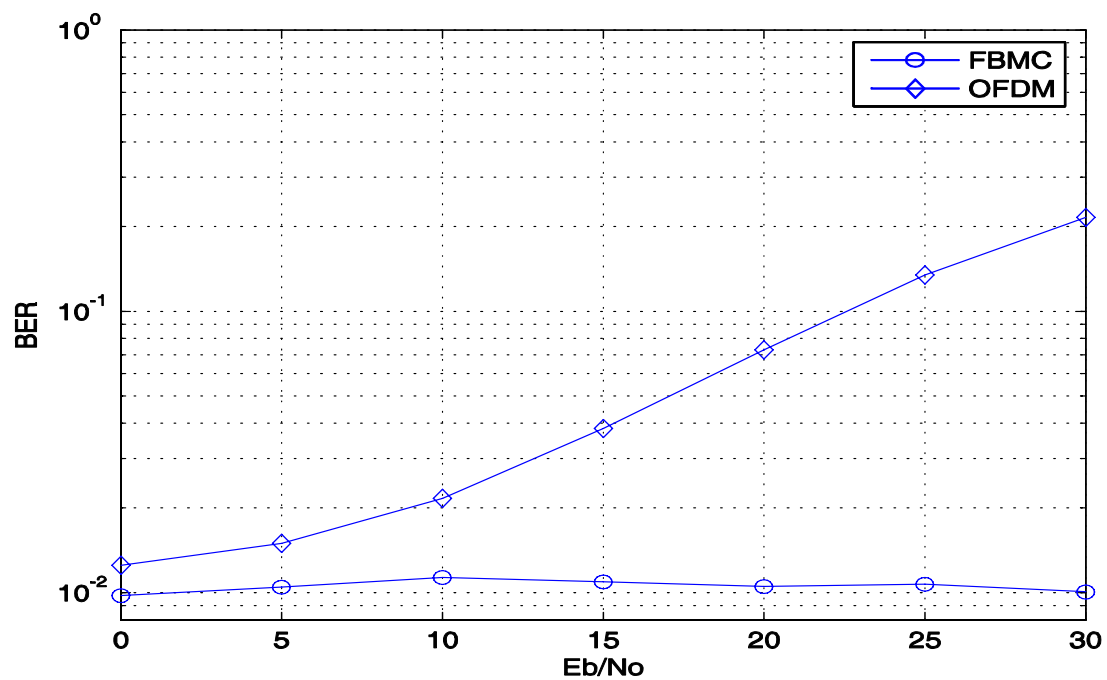


Figure 2-23: BER of the first user for the blockwise allocation scheme.

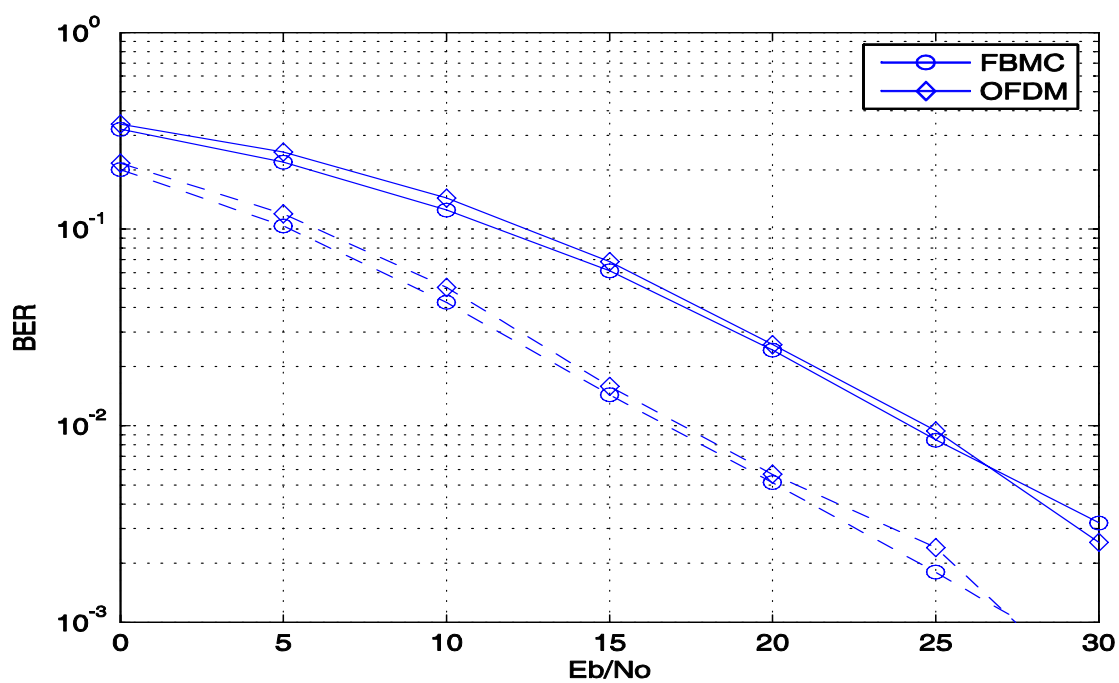


Figure 2-24: BER of the first user for the interleaved allocation scheme.

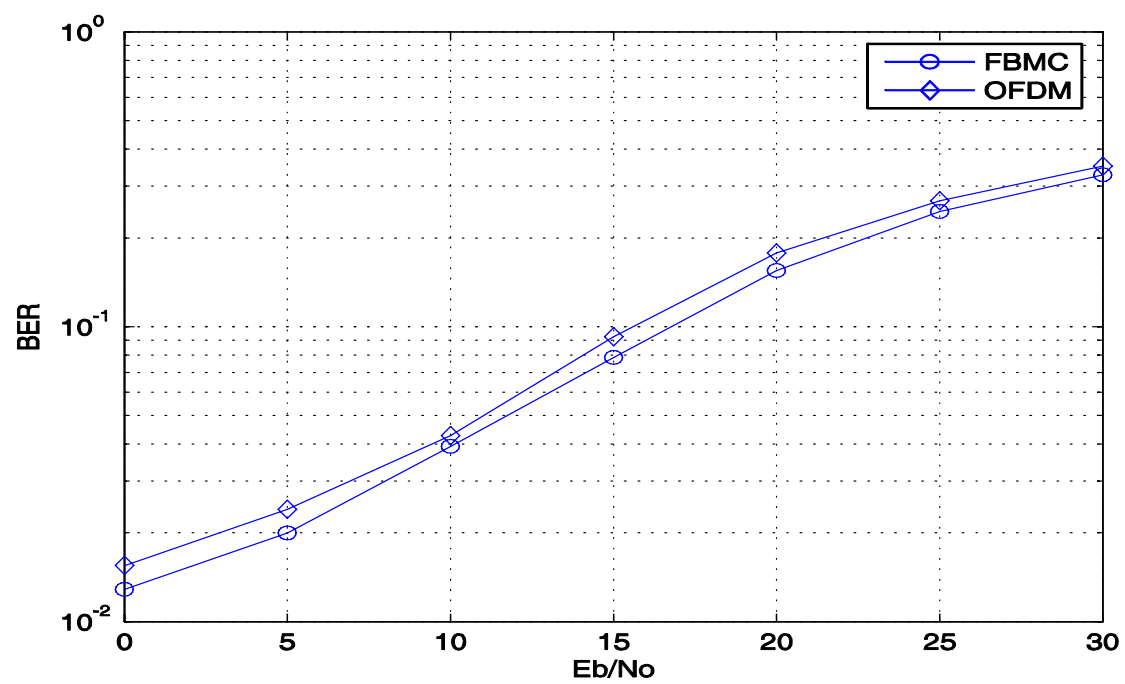


Figure 2-25: BER of the first user for the interleaved allocation scheme.

### 3 Equalization structures

In Deliverable 3.1, it was seen that, even though the MMSE equalizer takes into account interferences coming from the adjacent subchannels, it is not able to remove them completely and some ICI and ISI still remain. For the purpose of compensating for this remaining interference more efficiently we consider two additional equalizer structures derived below. The system model is first reviewed, then the two stage interference cancellation equalizer and the MMSE decision feedback equalizer are presented. The first one focuses on decreasing the intercarrier interference in a two step procedure, while the second one focuses on lowering the intersymbol interference by using a decision-feedback structure. Finally, the last section is devoted to a frequency domain equalization structure that aims at reducing the overall delay of the equalization process.

#### 3.1 Review of the system model and MMSE equalizer

Figure 3-1 depicts the model of the considered FBMC system. The received signal at the output of the analysis filter of the  $k$ -th subchannel can thus be written as

$$y_k[n] = \sum_{i=0}^{M-1} \sum_{\ell=-\infty}^{\infty} q_{ki}[\ell] v_i[n-\ell] + \eta_k[n] \quad (3.1)$$

Where  $q_{ki}[n] = (g_i * h * f_j)[m]_{\downarrow M/2}$  is the impulse response resulting from the convolution between the  $i$ -th synthesis filter, the channel  $h$  and the  $j$ -th analysis filter, then downsampled by a factor of  $M/2$ ,  $v_k[n] = d_k[n]\theta_k[n]$  with  $\theta_k[n] = j^{k+n}$ , and  $\eta_k[n]$  is the additive noise at the output of the analysis filter of the  $k$ -th subchannel.

In FBMC systems, thanks to the higher frequency selectivity of the prototype filter, the interference in each subchannel comes mainly from the adjacent subchannels and the interference from the other subchannels can be neglected. The received signal at the output of the  $k$ -th analysis filter can therefore be approximated by

$$y_k[n] \approx \sum_{i=k-1}^{k+1} \sum_{\ell=-\infty}^{\infty} q_{ki}[\ell] v_i[n-\ell] + \eta_k[n] \quad (3.2)$$

Stacking  $N$  observations, where  $L_{eq}$  represents the equalizer length, (3.2) can be written in matrix notation as follows

$$\mathbf{y}_k[n] = \sum_{i=k-1}^{k+1} \mathbf{Q}_{ki} \mathbf{v}_i[n] + \mathbf{B}_k \boldsymbol{\eta}[nM/2] \quad (3.3)$$

where  $\mathbf{y}_k[n] = [y_k[n], y_k[n-1], \dots, y_k[n-L_{eq}+1]]^T$ ,  $\mathbf{v}_i[n] = [v_i[n], v_i[n-1], \dots, v_i[n-L_q-L_{eq}+1]]^T$ , where  $L_q+1$  is the length of filter  $q_{ij}[n]$ ,  $\mathbf{Q}_{ki}$  is the convolution matrix of size  $L_{eq} \times (L_q + L_{eq})$  constructed from the row vector  $\mathbf{q}_{ki} = [q_{ki}[0], q_{ki}[1], \dots, q_{ki}[L_q]]^T$ ,  $\boldsymbol{\eta}[nM/2] = [\eta[nM/2], \eta[nM/2-1], \dots, \eta[nM/2 - ((L_{eq}-1)M/2 + L) + 1]]^T$ , and  $\mathbf{B}_k$  is an

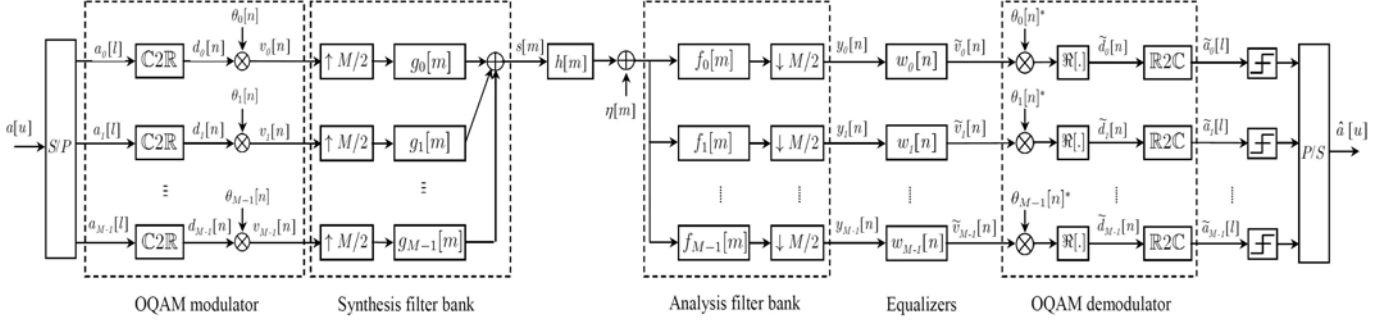


Figure 3-1: FBMC/OQAM model

$N \times (L + (L_{eq} - 1)M / 2)$  convolution matrix constructed from the cascade of  $f_k[m]$  and a downsampler of factor  $M / 2$  (see Figure 3-1), i.e.,

$$\mathbf{B}_k(i, (i-1)M / 2 + 1 : (i-1)M / 2 + L) = f_k(\cdot), \quad \text{for } i = 1, 2, \dots, N \quad (3.4)$$

In order to recover the transmitted symbols, the subchannel output  $\mathbf{y}_k[n]$  is filtered by the equalizer  $\mathbf{w}_k$ . The equalizer output is thus given by

$$\tilde{\mathbf{v}}_k[n] = \mathbf{w}_k^H \mathbf{y}_k[n] \quad (3.5)$$

At the output of the equalizer, due to the OQAM modulation, we are interested only in either the real or the imaginary part of the output depending on the indices  $k$  and  $n$ . We have

$$\begin{aligned} \text{Re}\{\tilde{\mathbf{v}}_k[n]\} &= \text{Re}\{\mathbf{w}_k^H \mathbf{y}_k[n]\} = \text{Re}\{\mathbf{w}_k^T\} \text{Re}\{\mathbf{y}_k[n]\} + \text{Im}\{\mathbf{w}_k^T\} \text{Im}\{\mathbf{y}_k[n]\}, \text{ for } k+n \text{ even} \\ \text{Im}\{\tilde{\mathbf{v}}_k[n]\} &= \text{Im}\{\mathbf{w}_k^H \mathbf{y}_k[n]\} = \text{Re}\{\mathbf{w}_k^T\} \text{Im}\{\mathbf{y}_k[n]\} - \text{Im}\{\mathbf{w}_k^T\} \text{Re}\{\mathbf{y}_k[n]\}, \text{ for } k+n \text{ odd} \end{aligned} \quad (3.6)$$

Where  $\text{Re}\{x\}$  and  $\text{Im}\{x\}$  denotes the real and imaginary part of  $x$ , respectively. The whole system and equalization problem can be rewritten using only real matrices and vectors, by taking into account the structure of the OQAM modulation. In order to obtain this particular formulation, we express  $\text{Re}\{\mathbf{y}_k[n]\}$  and  $\text{Im}\{\mathbf{y}_k[n]\}$  as follows

$$\begin{aligned} \text{Re}\{\mathbf{y}_k[n]\} &= \sum_{i=k-1}^{k+1} \text{Re}\{\bar{\mathbf{Q}}_{ki}\} \bar{\mathbf{v}}_i[n] + \text{Re}\{\bar{\mathbf{B}}_k\} \boldsymbol{\eta}[nM / 2] \\ \text{Im}\{\mathbf{y}_k[n]\} &= \sum_{i=k-1}^{k+1} \text{Im}\{\bar{\mathbf{Q}}_{ki}\} \bar{\mathbf{v}}_i[n] + \text{Im}\{\bar{\mathbf{B}}_k\} \boldsymbol{\eta}[nM / 2] \end{aligned} \quad (3.7)$$

where the matrix  $\bar{\mathbf{Q}}_{ki}$  and vector  $\bar{\mathbf{v}}_i[n]$  are obtained in the following way: consider the product of  $\mathbf{Q}_{ki}$  and  $\mathbf{v}_i[n]$ ; each column of  $\mathbf{Q}_{ki}$  corresponds, in this product, to an entry of  $\mathbf{v}_i[n]$ . The entries of  $\mathbf{v}_i[n]$  are either purely real or purely imaginary. Now the product can be kept identical by removing the factor  $j = \sqrt{-1}$  from the purely imaginary entries of  $\mathbf{v}_i[n]$  and applying it to the corresponding columns of

$\mathbf{Q}_{ki}$ . This is how matrix  $\bar{\mathbf{Q}}_{ki}$  and vector  $\bar{\mathbf{v}}_i[n]$  are obtained. They are such that the product is the same as with the initial matrices, but the new vector  $\bar{\mathbf{v}}_i[n]$  is now purely real. After taking the real and imaginary parts of the output, the above equations are obtained.

The MMSE equalizer is computed by minimizing the mean square error on  $\text{Re}\{\tilde{\mathbf{v}}_k[n]\}$  for  $k+n$  even or  $\text{Im}\{\tilde{\mathbf{v}}_k[n]\}$  for  $k+n$  odd or both of them. It is easily seen that the MMSE equalizer for purely real symbols ( $k+n$  even) and purely imaginary symbols ( $k+n$  odd) are identical, so we only consider the real case. For  $k+n$  even, we get the compact expression

$$\text{Re}\{\tilde{\mathbf{v}}_k[n]\} = \bar{\mathbf{w}}_k^T \bar{\mathbf{y}}_k[n] \quad (3.8)$$

Where  $\bar{\mathbf{w}}_k = \begin{bmatrix} \text{Re}\{\mathbf{w}_k\} \\ \text{Im}\{\mathbf{w}_k\} \end{bmatrix}$  and

$$\bar{\mathbf{y}}_k = \begin{bmatrix} \text{Re}\{\mathbf{y}_k[n]\} \\ \text{Im}\{\mathbf{y}_k[n]\} \end{bmatrix} = \sum_{i=k-1}^{k+1} \bar{\mathbf{Q}}_{ki} \bar{\mathbf{v}}_i[n] + \bar{\mathbf{B}}_k \bar{\boldsymbol{\eta}}[nM/2] \quad (3.9)$$

Where  $\bar{\mathbf{Q}}_{ki} = \begin{bmatrix} \text{Re}\{\bar{\mathbf{Q}}_{ki}\} \\ \text{Im}\{\bar{\mathbf{Q}}_{ki}\} \end{bmatrix}$ ,  $\bar{\boldsymbol{\eta}}[nM/2] = \begin{bmatrix} \text{Re}\{\boldsymbol{\eta}[nM/2]\} \\ \text{Im}\{\boldsymbol{\eta}[nM/2]\} \end{bmatrix}$  and  $\bar{\mathbf{B}}_k = \begin{pmatrix} \text{Re}\{\bar{\mathbf{B}}_k\} & -\text{Im}\{\bar{\mathbf{B}}_k\} \\ \text{Im}\{\bar{\mathbf{B}}_k\} & \text{Re}\{\bar{\mathbf{B}}_k\} \end{pmatrix}$

The MSE criterion to be minimized, for  $k+n$  even, can be expressed as

$$J_{MMSE} = E[|\bar{\mathbf{w}}_k^T \bar{\mathbf{y}}_k[n] - \mathbf{v}_k[n - \Delta]|^2] \quad (3.10)$$

Where  $\Delta$  is the equalizer delay and may be optimized independently for each subchannel to minimize the MSE.

The MMSE equalizer minimizing (3.10) can easily be computed and is given by

$$\bar{\mathbf{w}}_k^T = \mathbf{1}_{k,\Delta}^T \bar{\mathbf{Q}}_{kk}^T \left( \sum_{i=k-1}^{k+1} \bar{\mathbf{Q}}_{ki} \bar{\mathbf{Q}}_{ki}^T + \frac{\sigma_{\bar{\boldsymbol{\eta}}}^2}{\sigma_v^2} \bar{\mathbf{B}}_k \bar{\mathbf{B}}_k^T \right)^{-1} \quad (3.11)$$

Where  $\mathbf{1}_{k,\Delta}$  is an  $(L_q + L_{eq}) \times 1$  vector with  $\mathbf{1}_{k,\Delta}(i) = \delta_{i\Delta}$ , where  $\delta_{i\Delta} = 1$  for  $i = \Delta$  and  $\delta_{i\Delta} = 0$  otherwise. Therefore, by unstacking  $\bar{\mathbf{w}}_k^T$ , we get

$$\mathbf{w}_k = \bar{\mathbf{w}}_k(1:L_{eq}) + j\bar{\mathbf{w}}_k(L_{eq}+1:2L_{eq}) \quad (3.12)$$

Now the output of the equalizer for subchannel  $k$  is given by

$$\tilde{\mathbf{v}}_k[n] = \mathbf{w}_k^H \mathbf{y}_k[n] \quad (3.13)$$

In order to recover the transmitted complex symbol streams from  $\tilde{v}_k[n]$  we perform the OQAM demodulation as follows  $\tilde{d}_k[n] = \text{Re}\{\theta_k[n]^* \tilde{v}_k[n]\}$ . Finally  $\hat{d}_k[n]$  is obtained by taking a hard decision on  $\tilde{d}_k[n]$ .

### 3.2 Two-stage interference cancellation equalizer (TS-IC)

The idea behind the two-stage interference cancellation equalizer is that, for each subchannel, we cancel the interferences coming from the adjacent subchannels more efficiently. Cancellation of the interferences is made possible by first applying the MMSE equalizer and recovering the transmitted symbols. Subsequently we remodulate these symbols so that, for each subchannel, we can cancel the contribution of the adjacent subchannels<sup>3</sup>. After removing ICI from the received signal for each subchannel, only ISI remains. Another MMSE equalizer can then be derived to cope with this remaining ISI. The tentative decisions obtained in the first stage are only used to cancel the interference from adjacent subchannels, and not to cancel the interference inside the subchannel of interest, so that error propagation is limited. The two stage MMSE equalizer is briefly described in the following two paragraphs.

#### Stage 1:

In this stage, initial decisions are obtained on the transmitted symbols to later remove the ICI from each received signal in each subchannel. The equalizer which provides these decisions is the one given by (3.12). Let us suppose that the decisions are correct, i.e.  $\hat{d}_k[n] = d_k[n]$ . Once we have  $d_k[n]$  we remodulate it in order to get  $v_k[n]$  using the OQAM modulation technique. Let  $\mathbf{v}_k[n] = [v_k[n], v_k[n-1], \dots, v_k[n-L_q - L_{eq} + 1]]^T$ , where  $L_q$  and  $L_{eq}$  are the length of cascade synthesis, channel and analysis filters downsampled by factor  $M/2$ , and the equalizer length, respectively. Now we can subtract the contribution of  $v_{k-1}[n]$  and  $v_{k+1}[n]$  from the received signal  $\mathbf{y}_k[n]$  as follows

$$\mathbf{y}_k^-[n] = \mathbf{y}_k[n] - \sum_{\substack{i=k-1 \\ i \neq k}}^{k+1} \mathbf{Q}_{ki} v_i[n] + \mathbf{B}_k \boldsymbol{\eta}[nM/2] = \mathbf{Q}_{kk} v_k[n] + \mathbf{B}_k \boldsymbol{\eta}[nM/2] \quad (3.14)$$

where  $\mathbf{y}_k^-[n]$  is the received vector after removing the contribution of the adjacent subchannels. It is clear that for each subchannel only ISI remains as ICI is already removed (up to decision errors and channel estimation errors).

---

<sup>3</sup> Here we assume that an accurate channel estimation is available to perform this cancellation.

**Stage 2:**

The output of the first stage consists of the received signal corrupted only with ISI and noise as ICI is already removed. Now in order to remove ISI we consider again an equalizer based on minimizing an MSE criterion. Using (3.14) and following a similar reasoning as for the MMSE equalizer above, it can easily be shown that the MMSE equalizer of system in (3.14) is given by

$$\bar{\mathbf{w}}_{k,2^{nd}}^T = \mathbf{1}_{k,\Delta}^T \bar{\mathbf{Q}}_{kk}^T (\bar{\mathbf{Q}}_{kk} \bar{\mathbf{Q}}_{kk}^T + \frac{\sigma_{\eta}^2}{\sigma_v^2} \bar{\mathbf{B}}_k \bar{\mathbf{B}}_k^T)^{-1} \quad (3.15)$$

Now in order to recover the transmitted symbol streams on each subchannel it is sufficient to apply the MMSE equalizer, given by (3.15) which copes only with ISI. Note that this equalizer is the “simplified” equalizer proposed in Deliverable D3.1. In fact, both MMSE equalizer in (3.11) and in (3.15) can be computed at the same time because the terms of the simplified MMSE equalizer are common with those of the MMSE equalizer in (3.11). So the additional computation of the second equalizer is only a small complexity increase.

In order to assess the performance of the two-stage interference cancellation equalizer, we analyze the bit error rate (BER). We consider the following simulation parameters: M=64 carriers, overlapping factor K=4, prototype filter length L=KM, 16-QAM modulation. The CP length for CP-OFDM system is M/4. The FIR channels are chosen randomly with flat power delay profiles. In all simulations, the channel is assumed to be perfectly estimated. All simulation results are averaged over 200 independent realizations. As CP-OFDM uses the cyclic prefix it should be noted that its throughput rate is smaller than that of the FBMC system. The computation of  $E_b/N_0$ , in CP-OFDM, has been taking into account the energy wasted in the cyclic prefix.

Figure 3-2 compares the TS-IC equalizer with the one-tap equalizer, the classical MMSE equalizer and the CP-OFDM in terms of BER as a function of  $E_b/N_0$ . The channel and the MMSE equalizer lengths are 10 taps and 3 taps, respectively. We observe that for low SNR, all the algorithms provide almost the same performance. However for high SNR we can clearly see that the TS-IC equalizer outperforms the others. In this simulation, the channel length is smaller than the cyclic prefix, and the performance of the CP-OFDM is very similar to that of FBMC/OQAM with MMSE equalizer (with smaller throughput however).

In Figure 3-3, we investigate the effect of the channel length on the performance of the equalizers. To that end, we consider different channel lengths: 2, 5, 10, 15, 20 and 25. We consider  $E_b/N_0 = 30dB$ . For short channels, 2 to 5 taps, we observe that all the algorithms approximately have the same performance. Inside each subcarrier, the channel can be considered to be flat and hence the classical one tap equalizer gives a satisfactory performance with a lower complexity. For longer channels (highly frequency selective), TS-IC equalizer provides the best performance thanks to its ability to remove ICI. From these results, it can be seen that the proposed scheme is particularly interesting in the case of highly frequency selective transmission channels. As expected, for CP-OFDM, the performance is good as long as the channel length is smaller than the CP, but then degrades rapidly for longer channels.

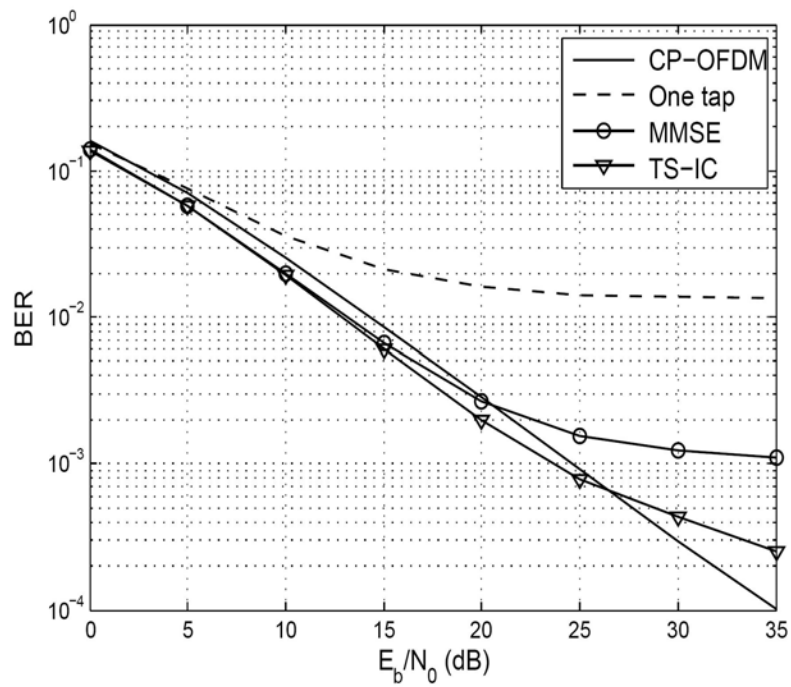


Figure 3-2: Comparison of the equalizers. BER versus  $E_b / N_0$ .  $N=3$ ,  $v+1=10$ .

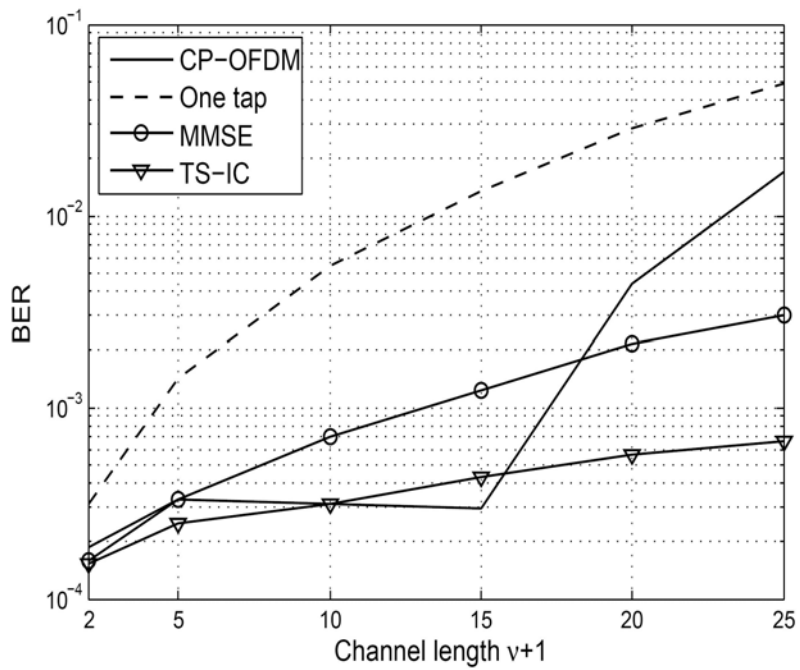


Figure 3-3: Effect of the channel length of the performance of the equalizers. BER versus channel length  $v+1$ .  $E_b / N_0 = 30\text{dB}$ ,  $N=3$ .

### 3.3 MMSE Decision-feedback equalizer

As an extension of the optimum MMSE linear equalizer presented in D3.1, we derive here the optimum MMSE decision feedback equalizer. Let us consider the subcarrier model depicted in Figure 3-4.

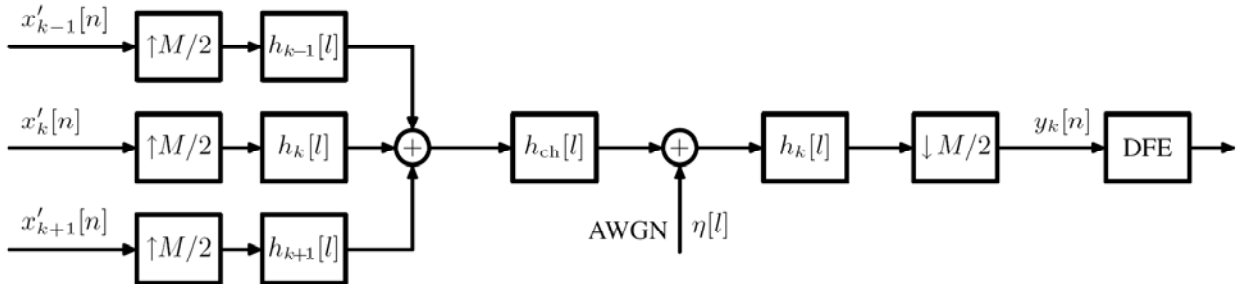


Figure 3-4: Subcarrier model for the FBMC System

The structure of the proposed DFE for even indexed subcarriers is shown in Figure 3-5. The output of the AFB subcarrier filter  $y_k[n]$  is filtered by the subcarrier feedforward filter  $w_k[n]$  of length  $L_{eq}$ . From this signal, the output of the feedback filter  $f_k[n]$  of length  $B+1$  is subtracted. The resulting signal is fed into the de-interleaver and finally the symbols are detected in a decision device. The detected symbols are OQAM staggered and then fed into the feedback filter.

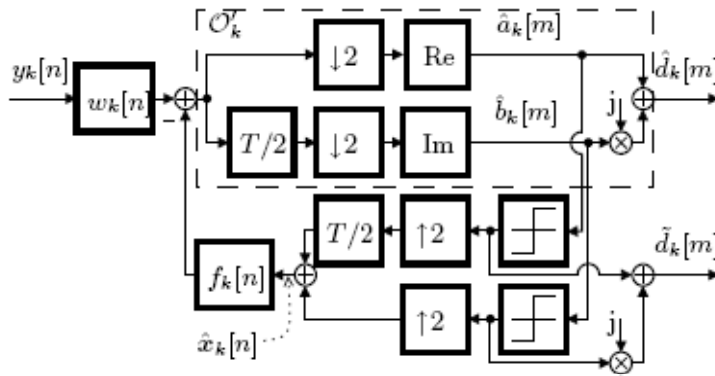


Figure 3-5: Per subchannel DFE OQAM destaggering

Our design criterion is to minimize the mean square error (MSE) between the estimated signal  $\hat{d}_k[n]$  and the input signal  $d_k[n]$ . The received signal at the  $k$ -th subchannel and before the OQAM de-staggering is given by

$$\mathbf{y}_k[n] = \mathbf{Q}_{k,k-1} \mathbf{v}_{k-1}[n] + \mathbf{Q}_{k,k} \mathbf{v}_k[n] + \mathbf{Q}_{k,k+1} \mathbf{v}_{k+1}[n] + \mathbf{B}_k \boldsymbol{\eta}[l]$$

where  $\mathbf{y}_k[n] = [y_k[n], \dots, y_k[n - L_e + 1]]^T$  is an  $L_{eq} \times 1$  complex column vector,  $\mathbf{v}_k[n] = [v_k[n], \dots, v_k[n - N + 1]]^T$  an  $N \times 1$  column vector of OQAM symbols transmitted on the  $k$ -th subchannel and  $\mathbf{Q}_{i,j}$  denotes an  $L_{eq} \times N$  convolution matrix constructed from the cascade of:  $\uparrow M/2$ ,  $h_k[m]$ ,  $h[m]$ ,  $h_k[m]$  and  $\downarrow M/2$ .  $\boldsymbol{\eta}[l]$  is the  $L + (L_{eq} - 1)M/2 \times 1$  additive white Gaussian noise vector.  $\mathbf{B}_k$  is an  $L_{eq} \times L + (L_{eq} - 1)M/2$  convolution matrix constructed from the cascade of  $h_k[m]$  and  $\downarrow M/2$ .

In order to recover the transmitted symbols, the subchannel output  $y_k[n]$  is filtered by the feedforward filter  $w_k[n]$  and added to the negative of the output of the feedback filter  $f_k[n]$ . Let:

$$\bar{\mathbf{v}}_k[n] = [\mathbf{v}_{k-1}^T[n] \quad \mathbf{v}_k^T[n] \quad \mathbf{v}_{k+1}^T[n]]^T, \quad \text{and} \quad \mathbf{Q}_k = [\mathbf{Q}_{k,k-1} \quad \mathbf{Q}_{k,k} \quad \mathbf{Q}_{k,k+1}]$$

Subsequently, we have

$$\mathbf{y}_k[n] = \mathbf{Q}_k \bar{\mathbf{v}}_k[n] + \mathbf{B}_k \boldsymbol{\eta}[l]$$

Considering that all the decided and OQAM staggered symbols  $\hat{x}_k[n]$  at the output of the DFE are correct, the equalizer output can be written as:

$$\begin{aligned} \hat{a}_k[m] &= \text{Re}\{\mathbf{w}_k^H \mathbf{y}_k[n] - \mathbf{f}_k^H \hat{\mathbf{x}}_k[n]\} = \mathbf{w}_k^{(R),T} \mathbf{y}_k^{(R)}[n] + \mathbf{w}_k^{(I),T} \mathbf{y}_k^{(I)}[n] - f_k^{(R),T} \hat{\mathbf{x}}_k[n], \quad \text{for } k+n \text{ even,} \\ \hat{b}_k[m] &= \text{Im}\{\mathbf{w}_k^H \mathbf{y}_k[n] - \mathbf{f}_k^H \hat{\mathbf{x}}_k[n]\} = \mathbf{w}_k^{(R),T} \mathbf{y}_k^{(I)}[n] - \mathbf{w}_k^{(I),T} \mathbf{y}_k^{(R)}[n] - f_k^{(I),T} \hat{\mathbf{x}}_k[n], \quad \text{for } k+n \text{ odd,} \end{aligned}$$

where  $\mathbf{y}_k^{(R)}[n]$  and  $\mathbf{y}_k^{(I)}[n]$  can be expressed as follows

$$\begin{aligned} \mathbf{y}_k^{(R)}[n] &= \bar{\mathbf{Q}}_k^{(R)} \bar{\bar{\mathbf{v}}}_k[n] + \text{Re}\{\mathbf{B}_k \boldsymbol{\eta}[l]\}, \\ \mathbf{y}_k^{(I)}[n] &= \bar{\mathbf{Q}}_k^{(I)} \bar{\bar{\mathbf{v}}}_k[n] + \text{Im}\{\mathbf{B}_k \boldsymbol{\eta}[l]\}, \end{aligned}$$

where  $\bar{\mathbf{Q}}_k^{(R)}$  and  $\bar{\mathbf{Q}}_k^{(I)}$  are, respectively, the real and imaginary parts of  $\bar{\mathbf{Q}}_k$ .  $\bar{\mathbf{Q}}_k$  and  $\bar{\bar{\mathbf{v}}}_k[n]$  are obtained from  $\mathbf{Q}_k$  and  $\bar{\mathbf{v}}_k[n]$ , respectively by shifting the complex number  $j = \sqrt{-1}$  from the imaginary entries of  $\bar{\mathbf{v}}_k[n]$  into the corresponding columns of  $\mathbf{Q}_k$ . This is done before taking the real or imaginary parts. Finally, we get the compact expression:

$$\hat{d}_k[n] = \bar{\mathbf{w}}_k^T \bar{\mathbf{y}}_k[n] - \mathbf{f}_k^{(R),T} \bar{\mathbf{y}}_k[n]$$

$$\text{where } \bar{\mathbf{y}}_k[n] = \begin{bmatrix} \mathbf{y}_k^{(R)}[n] \\ \mathbf{y}_k^{(I)}[n] \end{bmatrix} \text{ and } \bar{\mathbf{w}}_k = \begin{bmatrix} \mathbf{w}_k^{(R)} \\ \mathbf{w}_k^{(I)} \end{bmatrix}.$$

In order to compute the coefficients of both feedforward and feedback filters we propose to minimize a classical MMSE criterion. It is given by:

$$J = E[(\hat{d}_k[n] - d_k[n])^2] = E[(\bar{\mathbf{w}}_k^T \bar{\mathbf{y}}_k[n] - \mathbf{f}_k^{(R),T} \bar{\mathbf{y}}_k[n] - d_k[n - \Delta])^2]$$

where  $\Delta$  is the equalizer delay and can be chosen properly.

Now by differentiating with respect to  $\bar{\mathbf{w}}_k$  and setting it equal to zero, we can easily find the following expression:

$$\begin{bmatrix} \bar{\mathbf{w}}_k \\ \mathbf{f}_k^{(R)} \end{bmatrix} = \begin{bmatrix} \bar{\mathbf{Q}}_k \bar{\mathbf{Q}}_k^T + \mathbf{R}_{\eta,k} & -\frac{\sigma_d}{\sqrt{2}} \bar{\mathbf{Q}}_{k,k} \mathbf{J}_\Delta \\ -\frac{\sigma_d}{\sqrt{2}} \mathbf{J}_\Delta^T \bar{\mathbf{Q}}_{k,k}^T & \mathbf{I}_{B+1} \end{bmatrix}^{-1} \begin{bmatrix} \frac{\sigma_d}{\sqrt{2}} \bar{\mathbf{Q}}_k \mathbf{e}_\Delta \\ 0_{B+1} \end{bmatrix}$$

where  $\bar{\mathbf{Q}}_k = \begin{bmatrix} \bar{\mathbf{Q}}_k^{(R)} \\ \bar{\mathbf{Q}}_k^{(I)} \end{bmatrix}$ ,  $\bar{\mathbf{Q}}_{k,k} = \begin{bmatrix} \bar{\mathbf{Q}}_{k,k}^{(R)} \\ \bar{\mathbf{Q}}_{k,k}^{(I)} \end{bmatrix}$ ,  $\mathbf{R}_{\bar{\mathbf{v}}} = E[\bar{\mathbf{v}}_{k,n} \bar{\mathbf{v}}_{k,n}^T] = \sigma_d^2 \mathbf{I}_{3N}$ ,  $\mathbf{e}_\Delta$  is the null vector with 1 in its  $\Delta$  entry

and  $\mathbf{R}_{\eta,k} = \begin{bmatrix} \mathbf{R}_{\eta,k}' & \mathbf{R}_{\eta,k}'' \\ -\mathbf{R}_{\eta,k}'' & \mathbf{R}_{\eta,k}' \end{bmatrix}$ , with :

$$\mathbf{R}_{\eta,k}' = 0.5 (\mathbf{B}_k^{(R)} \mathbf{R}_\eta \mathbf{B}_k^{(R),T} + \mathbf{B}_k^{(I)} \mathbf{R}_\eta \mathbf{B}_k^{(I),T})$$

$$\mathbf{R}_{\eta,k}'' = 0.5 (\mathbf{B}_k^{(R)} \mathbf{R}_\eta \mathbf{B}_k^{(I),T} - \mathbf{B}_k^{(I)} \mathbf{R}_\eta \mathbf{B}_k^{(R),T})$$

and  $\mathbf{R}_\eta = E[\boldsymbol{\eta}[l] \boldsymbol{\eta}[l]^T] = \sigma_\eta^2 \mathbf{I}$  for uncorrelated stationary noise, where  $\sigma_\eta^2$  is the noise power. Matrix  $\mathbf{J}_\Delta$  is defined as:

$$\mathbf{J}_\Delta = \begin{cases} \begin{bmatrix} \mathbf{0}_{(\Delta+1) \times (B+1)} & \mathbf{I}_{B+1} & \mathbf{0}_{(L-B-\Delta-1) \times (B+1)} \end{bmatrix}^T, & L - \Delta > B + 1, \\ \begin{bmatrix} \mathbf{0}_{(\Delta+1) \times (B+1)} & \mathbf{I}_{B+1} \\ \mathbf{0}_{(L-\Delta) \times (B+\Delta-L+1)} \end{bmatrix}^T, & L - \Delta < B + 1, \\ \begin{bmatrix} \mathbf{0}_{(\Delta+1) \times (B+1)} & \mathbf{I}_{B+1} \end{bmatrix}^T, & L - \Delta = B + 1. \end{cases}$$

Eventually,  $\mathbf{w}_k$  can be easily recovered from  $\bar{\mathbf{w}}_k$ . This provides the analytical solution for the DFE yielding the MMSE. This solution can also be approached in an adaptive way we will derive in section 4.2.

We have simulated the performance of the OQAM FBMC system applying the per-subcarrier DFE and the LE of [5] in a WiMAX framework. A sampling rate  $M/T = 11.2$  MHz and a transmission bandwidth of 10 MHz have been considered. The input symbols have been modulated using 16-QAM.

We have considered two versions of the subchannel bandwidth, i.e. two different total numbers of subchannels in the FBMC. First, following the standard, we have used  $M = 1024$  with a subchannel bandwidth of 10.94 kHz, where only 840 subchannels were occupied with input symbols, the others had zero input. Then we have reduced the total number of subchannels to  $M = 256$  with a subchannel bandwidth of 43.75 kHz, and occupied 210 subchannels. The data rate is the same for both configurations. But since the subchannels are wider for a lower  $M$ , the channel equalization is even more challenging. For that reason, we have also increased the length of the equalizers to evaluate its effectiveness. The motivation to use wider subchannels in an FBMC system is to benefit from a lower sensitivity to carrier frequency offset (CFO), and to Doppler effects, and lower peak-to-average power ratio (PAPR).

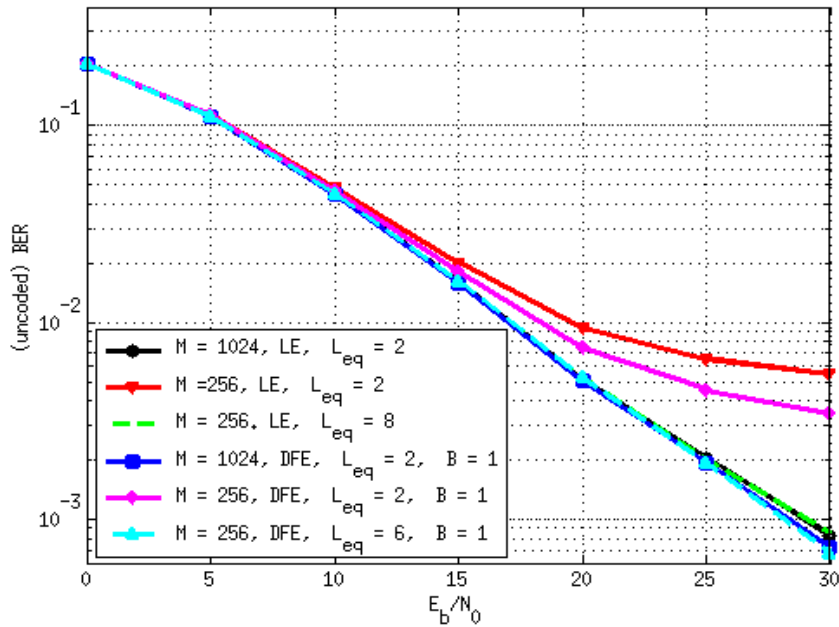


**Figure 3-6: Comparison between LE and DFE for different equalizer lengths and different number of subcarriers.**

As prototype filter we have employed a truncated version of a root raised cosine filter with  $K = 4$  and roll-off factor  $\rho = 0.5$ , as this kind of filter is nearly Nyquist (nearly ISI-free), and with that rolloff factor only immediately adjacent subchannels have a significant overlap. A lower  $K$  would imply a higher interference between nonadjacent subchannels. As channel model we have chosen the power delay profile of the Extended Typical Urban from 3GPP Long Term Evolution (LTE) in an static environment, i.e. without Doppler effects. Some simulation results in terms of uncoded bit error ratio (BER) as a function of  $E_b/N_0$  are depicted in Figure 3-6. In all the DFE simulations we have used  $B = 1$ , i.e. the feedback filter had length 2. We can note that, when  $M$  is reduced and  $L_{eq}$  and  $B$  are kept unchanged there is a loss in performance. However, the DFE performs considerably better than the LE in high  $E_b/N_0$  regimes. But if  $L_{eq}$  is increased, a better performance is achieved, since a longer

equalizer can compensate for higher frequency variations inside one subchannel coming along with the advantages listed before. It is worth mentioning that wider subcarriers are not desirable in CP-OFDM systems, as it would considerably reduce the spectral efficiency.

The simulation results have shown that the DFE has a similar or improved performance in comparison to the LE for static channels. They have also illustrated that the increase in the subchannel bandwidth can be effectively compensated by the use of longer equalizers, i.e. without any performance loss. From the results it can be concluded that the DFE is only worth being employed if the subcarrier bandwidth is wide enough to have high channel frequency selectivity inside of it. For the typical channel models used in WiMAX and the typical subcarrier bandwidth used there, the linear MMSE equalizer is enough to compensate for the frequency selectivity.

### 3.4 Frequency domain equalization

Time domain equalization techniques introduce an additional delay in the receiver, which leads to an increased latency of the FBMC systems. In some applications, such as online games or opportunistic communications, latency is critical. On the contrary, the frequency domain approach to equalization requires no additional delay.

The FBMC receiver can be implemented with an FFT whose size equals the prototype filter length. The block diagram is shown in Figure 3-7, for filter length  $L=KM$ , where  $K$  is the overlapping factor and  $M$  the number of sub-channels. The received sequence is denoted by  $r[n]$  and, considering the sub-channel with index  $i$ , the FFT outputs with indices  $iK-3, \dots, iK+3$  are weighted by the prototype frequency domain coefficients  $H_k$  and a summation yields the data symbols  $d_i(nM)$ .

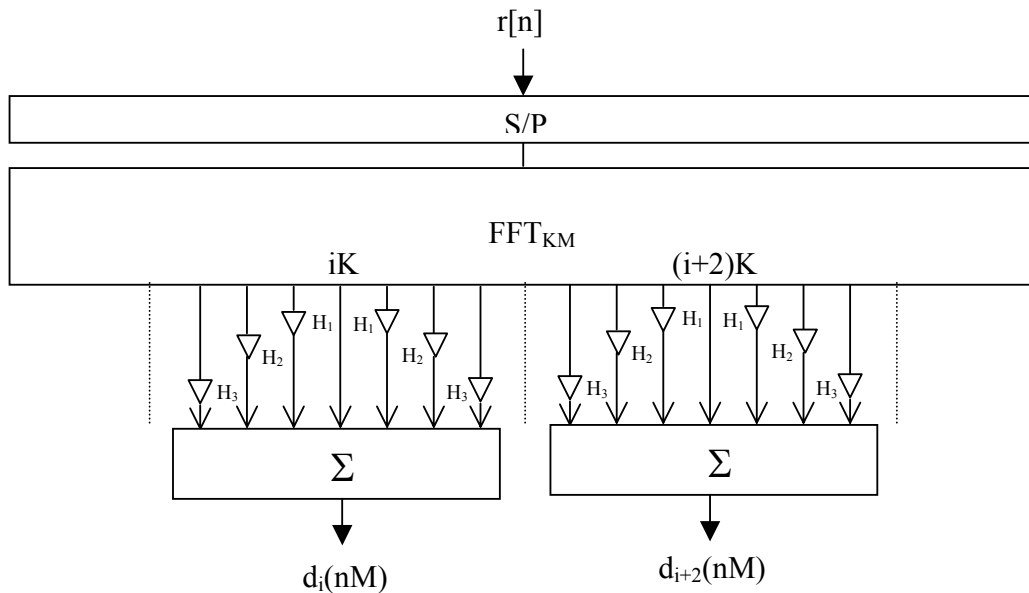


Figure 3-7: FFT-based FBMC receiver

The input of the FFT consists of 4 blocks of  $M$  samples which are shifted at the multicarrier symbol rate. It can be readily verified that the Nyquist criterion is satisfied for the sub-channels, as well as the orthogonality property of neighbouring sub-channels. In back to back connection, the delay of the system is the time it takes to fill the memory of the FFT in the receiver, namely  $KM$  samples or  $K$  multicarrier symbols.

Now, in the presence of the transmission channel, equalization has to be introduced. If the channel has been measured with the frequency spacing  $1/KM$ , assuming no noise, the equalizer coefficients are derived from the channel frequency response  $C(i)$  by

$$EQ(i) = \frac{1}{C(i)} \quad ; \quad 0 \leq i \leq KM - 1 \quad (3.16)$$

The equalizer is shown in Figure 3-8, for sub-channel “ $i$ ”.

With this equalizer, all the spectral components of the signal have been corrected and, if the channel is perfectly estimated, the signal is perfectly equalized. A key feature is that no additional delay is required, in contrast with time domain sub-channel equalization.

In the presence of channel noise, if the level of noise on each frequency component can be measured or estimated, the principle of maximum ratio combining can be applied to maximize the signal-to-noise ratio at the output of the sub-channels.

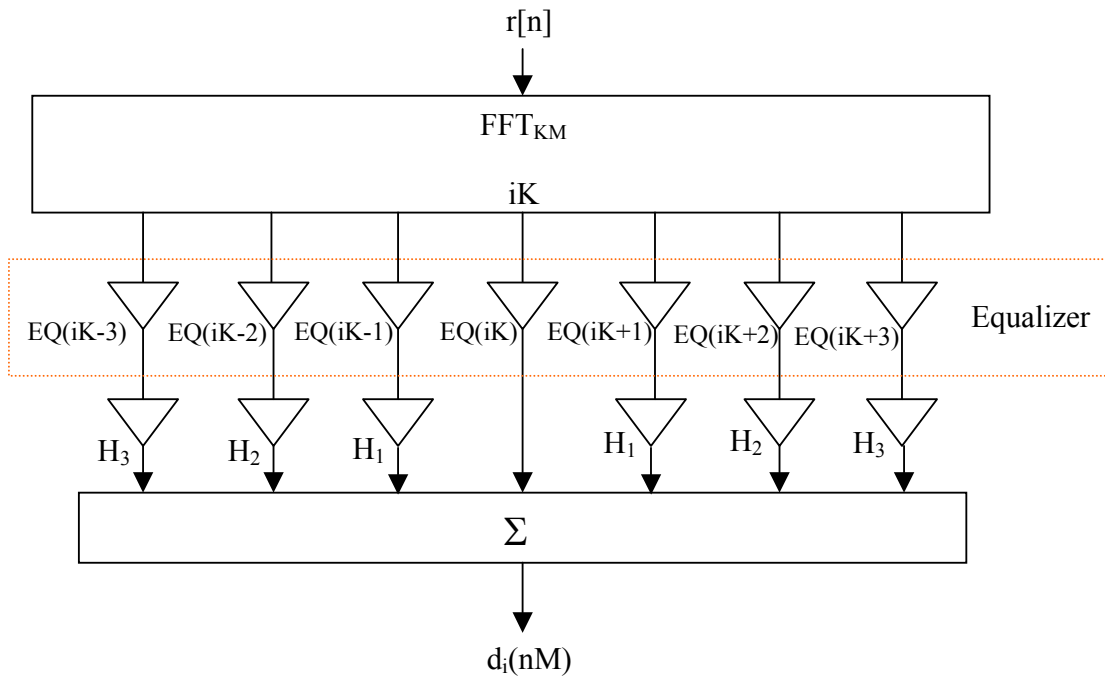


**Figure 3-8: Frequency domain equalizer for subchannel “ $i$ ”**

It is worth pointing out that the measurement of the transmission channel with spacing  $1/KM$  is obtained with the help of a pseudo-random input data sequence, because of the overlapping of the neighbouring sub-channels and the complementarity of the filter coefficients. For example, for  $K=4$ , if  $d_i = 1$  and  $d_{i+1} = j$ , after multiplication by the coefficients and summation, the samples at the input of the iFFT are

$$x_e(4i) = 1 ; x_e(4i+1) = H_1 + jH_3 ; x_e(4i+2) = (1+j)H_2 ; x_e(4i+3) = H_3 + jH_1$$

and they all have unit magnitude.

Finally, the frequency domain approach reveals the two conditions which are necessary to achieve perfect sub-channel equalization, in the absence of noise, namely measurement of the transmission channel with frequency spacing  $1/KM$  and number of equalizer coefficients equal to  $2K-1$ .

## 4 Channel estimation

Some channel estimation methods have already been presented in deliverable D3.1. We focus here on the issue of mobility and consider time varying channels. The performance of the pilot-based methods is re-evaluated below for different levels of mobility. Then, an adaptive MMSE DFE is derived to be able to track channel variations in the absence of pilots.

### 4.1 Pilot-based channel estimation

In this subsection we provide further insight into the performance of the PHYDYAS reference FBMC/OQAM system with synchronization and channel estimation based on scattered pilots. The system is as described above in Figure 2-11 and the scattered pilot estimation utilizes the auxiliary pilot technique described in D3.1 and defined by Equations (2.31) and (2.32).

#### 4.1.1 Simulation Setup and Results

The simulations presented in this section aim to understand the performance of the reference system when applied within a time-varying channel. The time variation of the channel is obtained by simulating a mobile user under different mobilities. In these simulations, the results are compared with the case of perfect channel state information (PCI). The latter is calculated for each FBMC/OQAM *subsymbol* (rate  $T/2$ ) by transforming the channel impulse response experienced by the high rate sample in the centre of the FBMC/OQAM subsymbol of interest. In case of high mobilities, the channel can vary within the duration of a FBMC/OQAM subsymbol, as can be seen in Figure 4-1. Therefore, even in the PCI simulation results, there will be degradation of the BER performance with increasing user mobility.

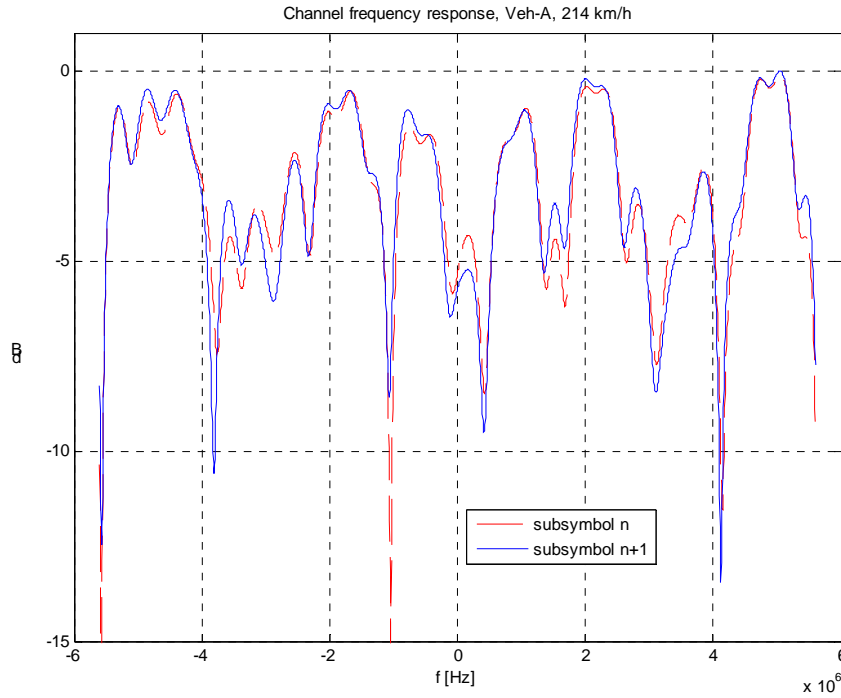


**Figure 4-1: Channel frequency response variation from one FBMC/OQAM subsymbol to the next in a Veh-A channel model and at 214 km/h.**

The simulation setup is similar to the setups applied so far: A filter bank of  $M = 1024$  subchannels using the standard PHYDYAS nearly perfect reconstruction prototype filter with overlapping factor  $K = 4$  transmits at 11.2 MHz sampling rate. Therefore, the subcarrier spacing is  $\Delta f = 10.94$  kHz. The signal is transmitted through a time-varying channel modeled according to the ITU-R Vehicular-A recommendations. The variation within a transmitted burst is due to the user mobility, and at each burst transmission, the channel is obtained from a different realization. From the synchronization point of view, we assume a steady state tracking mode, i.e., there is neither carrier frequency offset (CFO) nor fractional time delay (FTD) present. However, some of the simulations present the performance when the synchronization stages are tracking the timing and frequency offsets. For all estimation purposes, the auxiliary pilot scheme with pilots in the AMC-23 configuration as presented in D3.1, is used. The pilot/auxiliary pilot pair has a power boost of 4.54 dB with respect to the 16-QAM data transmitted. Synchronization and channel estimation takes place as described in deliverables D2.1 and D2.2, and the three tap complex FIR introduced in D3.1 equalizes the received signal. The performance of jointly estimating the FTD and the channel based on the iterative interference cancellation (IIC) approach presented above in this deliverable is also assessed.

Figure 4-2 shows the BER performance with respect to  $E_b/N_0$  when a burst of 4x2 AMC23 slots are transmitted. This means that 4 adjacent slots in frequency domain with 18 consecutive subcarriers each and 2 consecutive slots of 3 MC symbols each are sent per burst. The mobile velocity is parameterized in the graph, which shows results in the PCI case, and when synchronization and channel estimation is performed based on pilots, either with the conventional approach or with the novel IIC technique.

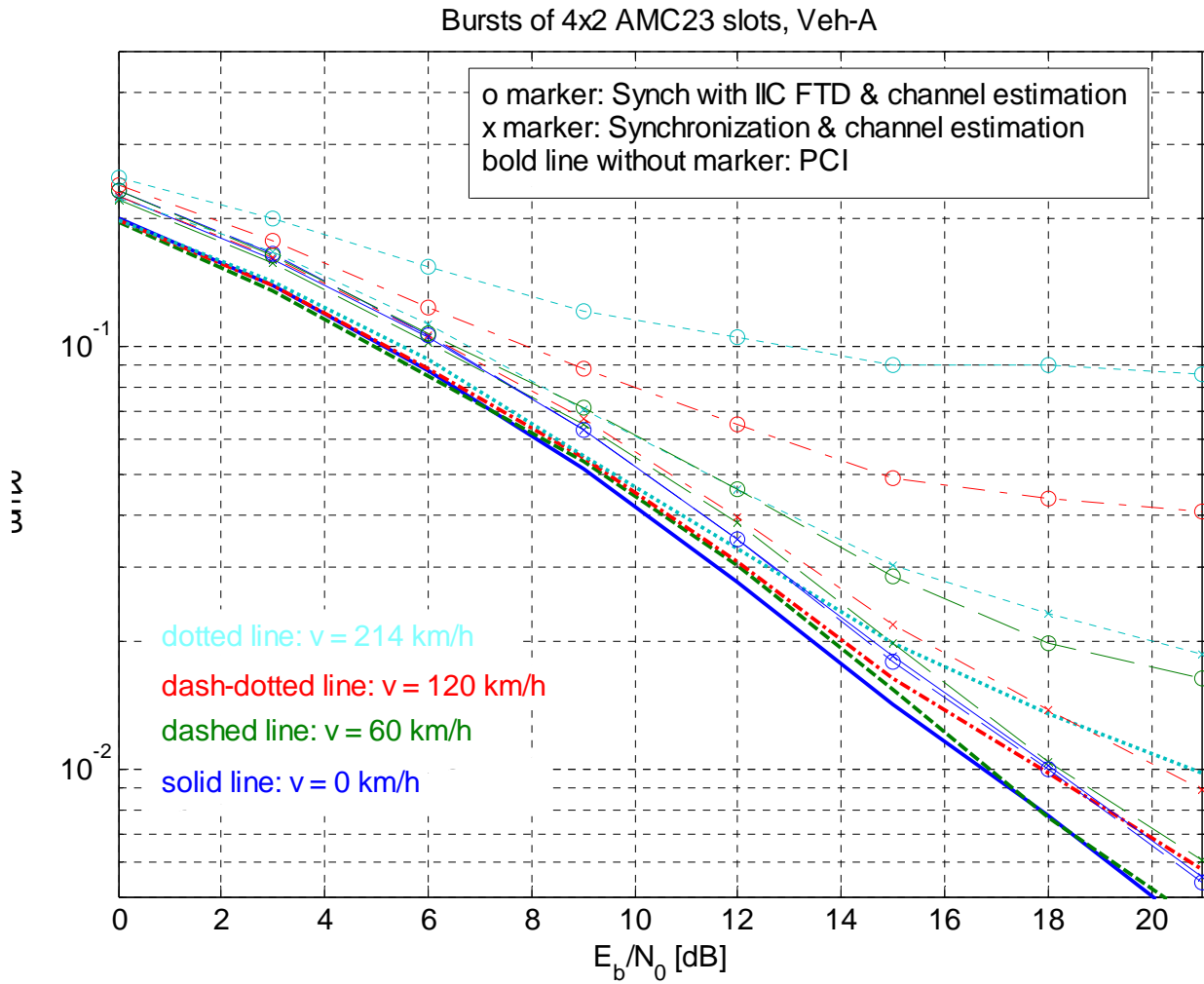


**Figure 4-2: BER performance vs.  $E_b/N_0$  with 16-QAM and different mobilities. Bursts of 4x2 AMC23 slots. PCI knowledge, synchronization and estimation and IIC based synchronization and estimation.**

The results presented in the figure show an estimation loss of approximately 1 dB with respect to PCI at low to medium mobilities. This difference experiences a fast degradation when the user increases his mobility. Although the IIC method performs as well as the classic FTD and channel estimation methods in the quasi-static case, its performance suffers severely already at city traffic velocities.

Figure 4-3 compares the performance of the CFO and FTD tracking with the case, in which instead of performing synchronization tracking, the CFO and FTD (both = 0) are assumed known at the receiver. It can be seen that only with German Autobahn sportscar mobility there is an appreciable difference in the performance. This indicates that in the synchronized case the tracking works very accurately up to high velocities.

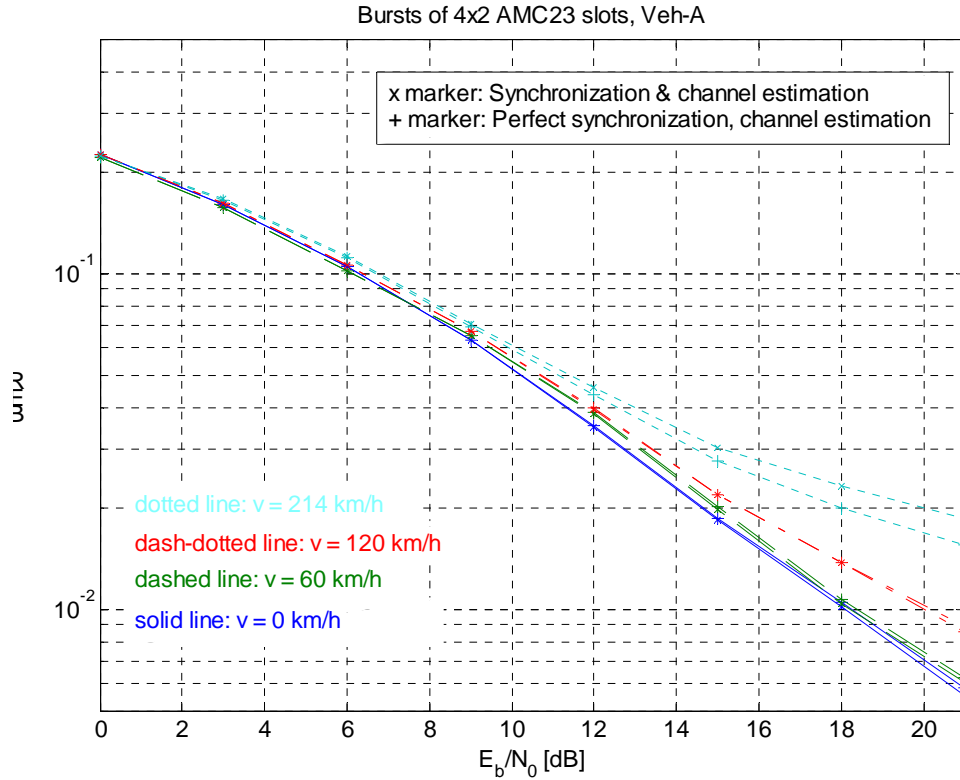


**Figure 4-3: BER performance vs.  $E_b/N_0$  with 16-QAM and different mobilities. Bursts of 4x2 AMC23 slots. Pilot-based synchronization and estimation, and perfect synchronization with pilot-based channel estimation.**

In Figure 4-4 we can evaluate similar results as in Figure 4-2 but for burst sizes 16x8. The performance of the IIC approach in the quasi-static case improves, compared to the smaller burst size results. However, with mobility there is even more degradation. This hints to averaging effects over the pilots in the IIC technique.

The comparison between the classical FTD, CFO and channel estimation method performance and the case in which FTD and CFO are known is not included here because the performances are even more similar than the ones for smaller burst sizes presented in Figure 4-3, even for the highest velocity.

The last BER results are shown in Figure 4-5, where the performances of the different burst sizes are compared. The improvement in the performance when using a bigger burst for transmission is pictured in a). In b), the already mentioned behavior of the IIC method can be better followed.

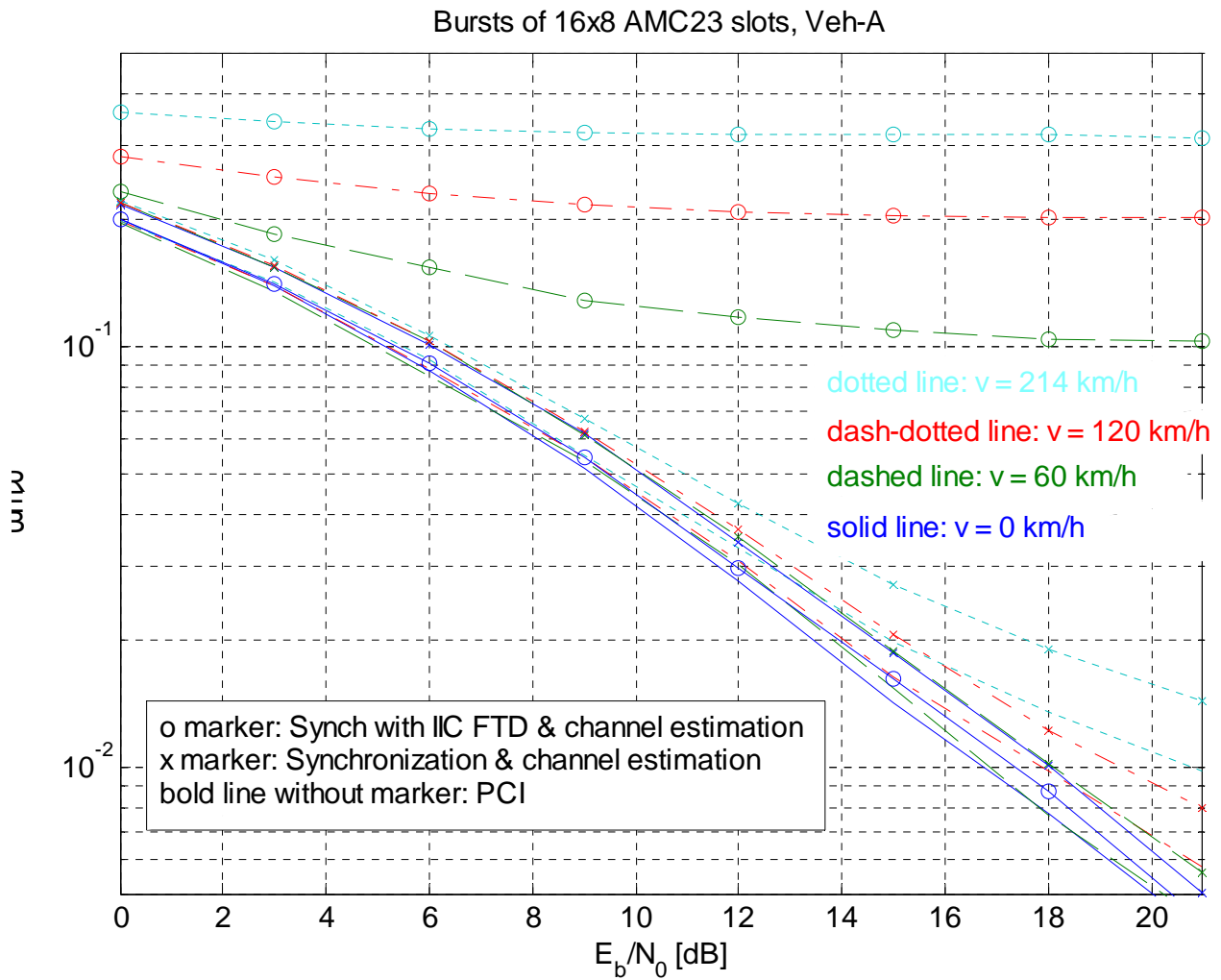


**Figure 4-4: BER performance vs.  $E_b/N_0$  with 16-QAM and different mobilities. Bursts of 16x8 AMC23 slots. PCI knowledge, synchronization and estimation and IIC based synchronization and estimation.**

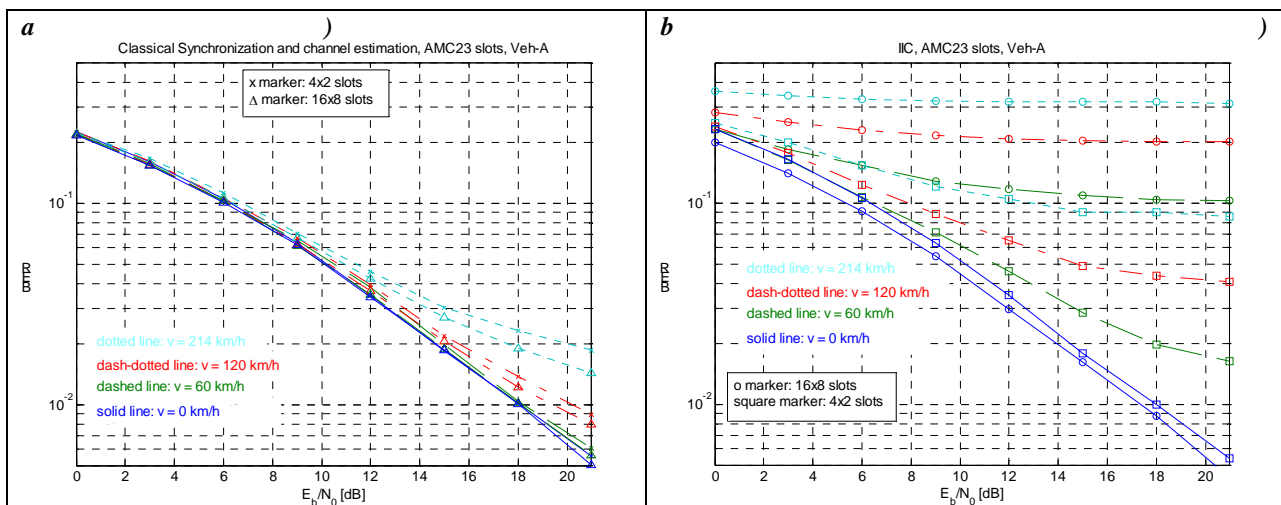


**Figure 4-5: BER performance vs.  $E_b/N_0$  with 16-QAM and different mobilities and bursts of 4x2 and 16x8 AMC23 slots. Conventional synchronization and channel estimation (a). IIC technique (b).**

Finally, we present synchronization performance results. First, the CFO estimation RMD error is plotted against  $E_b/N_0$  in Figure 4-6. Recall that the CFO estimation is common in both estimation approaches under study, namely the conventional and the IIC based approaches. The gain due to the availability of more pilots to estimate the CFO is evident at all velocities, but especially large in the quasi-static scenario. The small burst of 4x2 AMC23 slots complies with WiMAX CFO specifications of 2% of the subcarrier spacing above speeds of 120 km/h. The figure also conveys the notion that, with mobility, the variation of the channel rather than the noise level is limiting the CFO estimation performance.

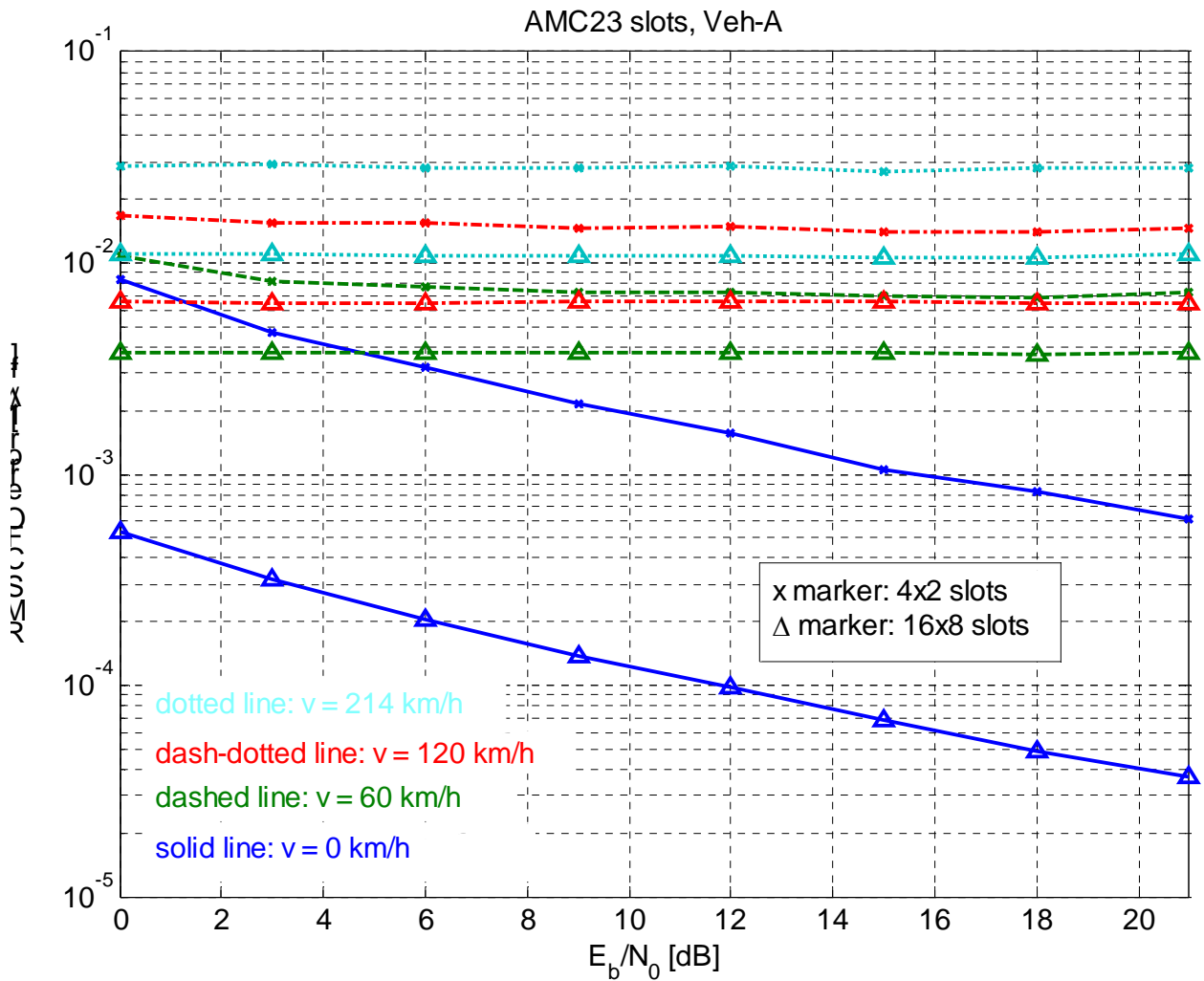


**Figure 4-6: RMS error in CFO estimation vs.  $E_b/N_0$ , for different velocities and bursts with 4x2 and 16x8 AMC23 slots. 16-QAM.**

Figure 4-7 shows analogous results from the FTD estimation error point of view. The conventional estimation approach performs quite independently of the noise level and the velocity. The independence from the velocity is because the channel becomes time-varying when the mobile station starts moving, but the estimation only uses pilots at different frequencies and within the same time instant for

estimating the FTD. This renders conventional FTD estimation quite immune to the time-variations of the channel. Transmitting larger bursts yields only marginal improvement. The estimation error floor is due to the fact that the estimate includes the de-facto delay introduced by the multipath channel, but the ideal case for calculating the error does not take this delay into account.

The IIC technique only approaches this error floor at relatively high  $E_b/N_0$  values, and only with low mobility and bigger burst size. The degradation of the FTD estimates with increasing speed grows faster when transmitting larger bursts.

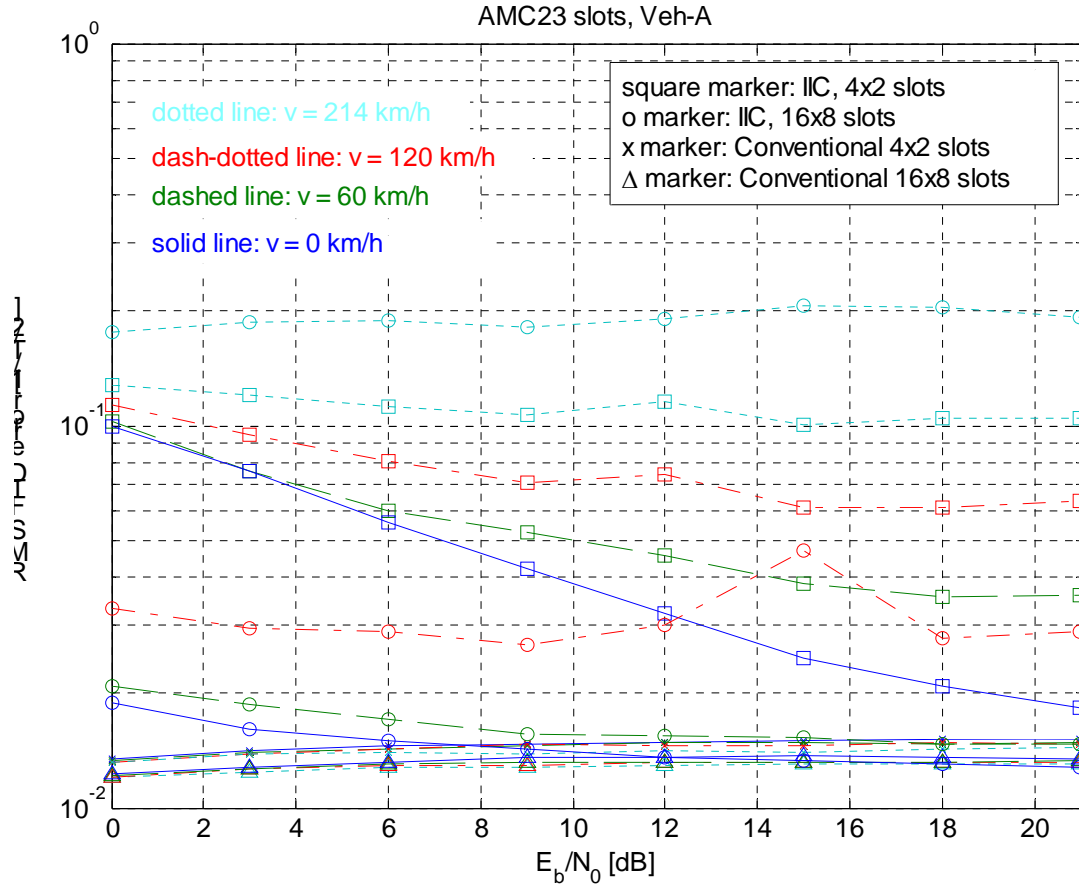


Figure 4-7: RMS error in FTD estimation vs.  $E_b/N_0$ , for different velocities and bursts with 4x2 and 16x8 AMC23 slots. 16-QAM.

#### 4.1.2 Conclusion

The results presented in this section give an idea of the performance of the PHYDYAS system of reference under mobility, assuming a tracking mode in which synchronization has been already achieved. At practical raw bit error rates, the degradation of the performance with the AMC23 pilot configuration becomes important when accelerating to speeds above 60 km/h. Also the effects of the mobile user's velocity on the synchronization tracking performance have been evaluated. The general conclusion is that, except with very high speeds, the estimation is more accurate with higher burst sizes, which transmit more pilots.

Regarding the novel joint FTD and channel estimation based on IIC, the results of this section reinforce the view given in the IIC section that this technique presents great advantages for coarser

synchronization tasks. However, when FTD and channel estimation are performed in the tracking mode, the less complex conventional methods are recommended.

## 4.2 Adaptive MMSE-DFE

We extend here the structure of the linear equalizer presented in D3.1 to the DFE structure. In this way the conventional DFE LMS adaptive filter has to be adapted to the orthogonal multiplexing of the subcarriers. After equalizing the received subcarrier signal  $y_k[n]$  with the LMS controlled feedforward filter  $\mathbf{w}_k[n]$  and by subtracting the output of the feedback filter  $\mathbf{f}_k[n]$  we get the following two equations for the estimation of the real and imaginary part of the input symbol according to Figure 4-10.

$$\begin{aligned}\Re[\mathbf{w}_k^H[n]\mathbf{y}_k[n] - \mathbf{f}_k^H[n]\hat{\mathbf{x}}_k[n]] &= \mathbf{w}_k^{R,T}[n]\mathbf{y}_k^R[n] + \mathbf{w}_k^{I,T}[n]\mathbf{y}_k^I[n] - \mathbf{f}_k^{R,T}[n]\hat{\mathbf{x}}_k[n] = \hat{a}_k[m], \quad \text{for } k+n \text{ even,} \\ \Im[\mathbf{w}_k^H[n]\mathbf{y}_k[n] - \mathbf{f}_k^H[n]\hat{\mathbf{x}}_k[n]] &= \mathbf{w}_k^{R,T}[n]\mathbf{y}_k^I[n] - \mathbf{w}_k^{I,T}[n]\mathbf{y}_k^R[n] - \mathbf{f}_k^{I,T}[n]\hat{\mathbf{x}}_k[n] = \hat{b}_k[m], \quad \text{for } k+n \text{ odd,}\end{aligned}$$

Where  $\mathbf{w}_k[n]$  and  $\mathbf{y}_k[n]$  are complex vectors of size  $B+1$ ,  $\mathbf{f}_k[n]$  and  $\hat{\mathbf{x}}_k[n]$  are vectors with pure real or pure imaginary components of length  $B+1$ . Signals  $\hat{a}_k[m]$  and  $\hat{b}_k[m]$  are estimations of the real and imaginary parts of the transmitted symbol  $d_k[m]$  show in Figure 4-8.

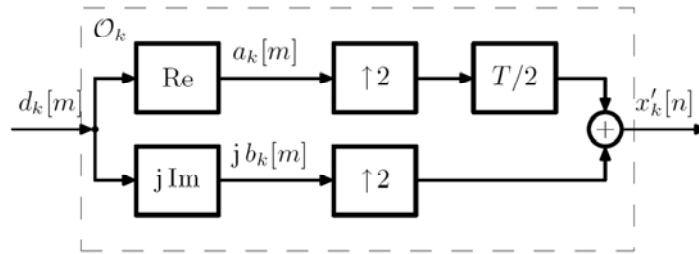


Figure 4-8: OQAM Staggering, k even

It is also important to mention that the OQAM structure necessitates that the real and imaginary part of Figure 4-8 and Figure 4-9 are interchanged from subcarrier to subcarrier.

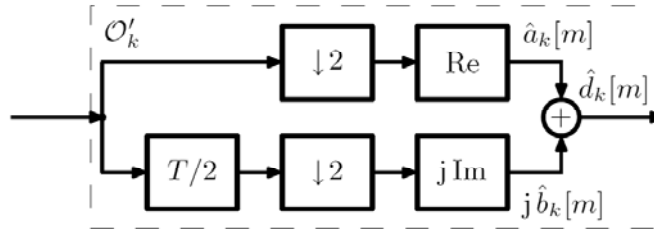


Figure 4-9: OQAM De-staggering, k even

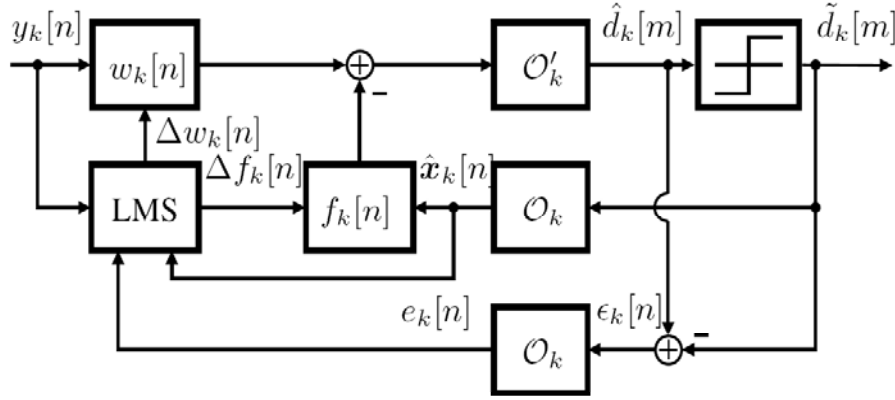


Figure 4-10: DFE OQAM-LMS (Decision-directed mode)

We use the same filter vectors  $\mathbf{w}_k[n]$  and  $\mathbf{f}_k[n]$  for both the real and imaginary part of  $x_k[n]$  as it can be shown to stay optimum in both cases under the assumption of additive white Gaussian noise and uncorrelated input symbols.

For updating the filter vectors  $\mathbf{w}_k[n]$  and  $\mathbf{f}_k[n]$  we have to determine the error signal  $\varepsilon_k[m]$  in Figure 4-10 by

$$\varepsilon_k[m] = \tilde{a}_k[2n] + j\tilde{b}_k[2n+1] - \hat{a}_k[2n] - j\hat{b}_k[2n+1] = Q[\hat{a}_k[2n] + j\hat{b}_k[2n+1]] - \hat{a}_k[2n] - j\hat{b}_k[2n+1]$$

where  $Q[\hat{a}_k[2n] + j\hat{b}_k[2n+1]]$  determines the nearest symbol of the corresponding modulation alphabet from  $\hat{d}_k[m]$  by a hard decision. Therefore, we are able to update the filter vector every half symbol duration  $T/2$  with either a pure real or a pure imaginary error signal. The error signal  $e_k[n]$  for the update process of the  $T/2$  spaced filter vector results to

$$e_k[n] = \begin{cases} \varepsilon_k^R[m], & m \in Z, \\ j\varepsilon_k^I[m], & m \in Z, \end{cases} \quad (4.1)$$

where the role of real and imaginary parts is interchanged again from subcarrier to subcarrier. In the QAM case we would update only every symbol duration  $T$  but with complex instead of pure real or pure imaginary values. The LMS adaptation is operated in the decision directed mode because the error is calculated based on the decisions of the estimated symbols  $\hat{d}_k[m]$ . The tap weight adaptation for the equalizer uses the error signal from (4.1) in the following way (cfr Figure 4-10.)

$$\mathbf{u}_k[n+1] = \mathbf{u}_k[n] + \Delta \mathbf{u}_k[n] = \mathbf{u}_k[n] + \mu \mathbf{z}_k[n] e_k^*[n],$$

where  $\mathbf{u}_k = [\mathbf{w}_k^T[n], \mathbf{f}_k^T[n]]^T$ ,  $\mathbf{z}_k = [\mathbf{y}_k^T[n], \hat{\mathbf{x}}_k^T[n]]^T$  and  $\mu$  is the step-size parameter of the LMS algorithm.

We have simulated the performance of the per-subchannel adaptive DFE in a WiMAX framework. We have considered a transmission bandwidth of 10 MHz and sampling frequency  $M/T = 11.2$  Mhz. The input symbols have been modulated using 16-QAM. We have considered two versions of the subchannel bandwidth, i.e. two different total numbers of subchannels in the FBMC. First, following the WiMAX standard, we have used  $M = 1024$  with a subchannel bandwidth of 10.94 kHz, but only 840 subchannels have been occupied with input signals, the others had zero input. Then we have reduced the total number of subchannels to  $M = 256$  with a subchannel bandwidth of 43.75 kHz and occupied 210 subchannels. The symbol rate remains the same for both configurations. Since the subchannels are wider for a lower  $M$ , the channel equalization is more challenging. For that reason, we have also increased the length of the equalizers to evaluate its effectiveness. The motivation of using wider subchannels in an FBMC system is to benefit from a lower sensitivity to carrier frequency offset (CFO) and to Doppler effects, and a lower peak-to-average power ratio (PAPR).

As prototype filter we have employed a truncated version of a root raised cosine filter with  $K=4$  and roll-off factor  $\rho=0.5$ , since this kind of filter is nearly Nyquist (nearly ISI free) and with that roll-off factor only immediately adjacent subchannels overlap significantly. A lower  $K$  would imply a higher interference between non-adjacent subchannels. As channel model we have chosen the Vehicular A Extended, a variation of the International Telecommunication Union (ITU) model used in WiMAX with a maximum delay spread of 10  $\mu$ s. We have considered a static and a mobile scenario (30 km/h).

The initial values of the equalizer coefficients at the beginning of each frame have been calculated analytically by using the results from Section 3.2 of this report.

Figure 4-11 depicts the simulations results in terms of uncoded bit error ratio (BER) as a function of  $E_b/N_0$  for a static scenario. For all the curves we have used  $L_{eq} = 3$ ,  $B = 1$  and both LMS and SMNLMS algorithms. The abbreviation “dec.-dir.” stands for decision-directed mode of operation and pilot means that the true transmitted symbols have been used for both error and input of the feedback filter, but the BER has been calculated with the detected symbol after the equalization. We can see that both equalizers perform very similar. The SM-NLMS behaves a little worse for high  $E_b/N_0$  regimes in the case of the dec.-dir. mode, because this algorithm realizes fewer updates of the coefficients than the

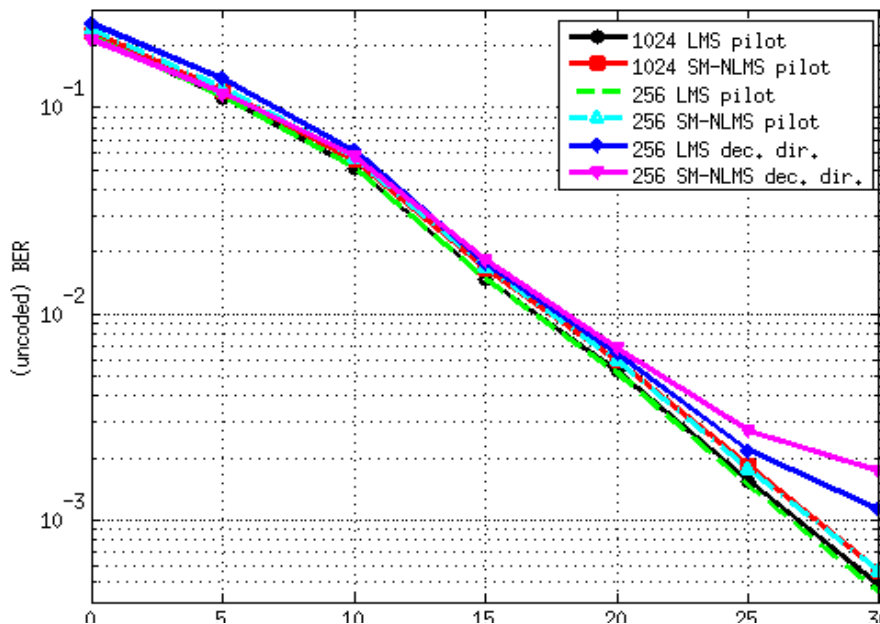
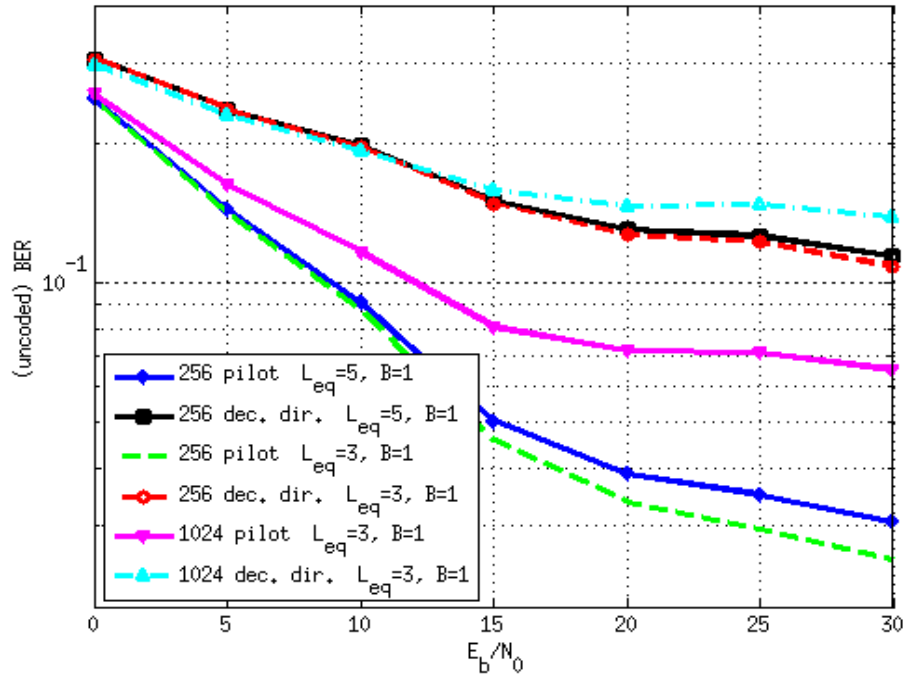


Figure 4-11: Comparison between LMS and SM-NLMS for different number of subcarriers in a static channel

standard LMS algorithm resulting in lower complexity.

Figure 4-12 depicts the simulation results for the SM-NLMS algorithm with different numbers of subcarriers in a mobile scenario. We can see that even if wider subchannels are used, the equalizer is still capable of tracking the channel variations. It is worth noting that a longer equalizer has not shown any advantage in the framework with the considered parameters.



**Figure 4-12: Comparison between different equalizer lengths using SM-NLMS with different number of subcarriers and for a speed of 30 km/h.**

Considering both decision and pilot directed adaptation an upper and a lower limit in the expected performance has been obtained for any scattered pilot structure.

Similarly to what was shown in section 3.3, we can conclude from the simulation results that the DFE should be chosen in preference to the linear equalizer only in cases where the channel selectivity inside one subcarrier is very high.

## 5 Joint Transmitter-receiver design

### 5.1 Subchannel and power allocation and rate adaptation for FBMC systems

Adaptive modulation is considered as a promising technique to increase the data rate that can be reliably transmitted over fading channels. For this reason some forms of adaptive modulation are being proposed and implemented in much recent wireless systems and next generation systems. Adaptive modulation provides many parameters that can be adjusted relative to the channel fading, including transmit power and data rate, instantaneous *BER*, and channel code rate. The optimization problem of the power allocation and the adaptive modulation and coding (AMC) scheme has been combined by different authors with more complex QoS requirements such as: the minimum or guaranteed rate (increasing the fairness), the maximum delay, the buffers state, etc. Under such general framework two possible schemes are usually considered.

First, in case the bit error rate (or packet error rate) is bounded but the maximum throughput is attained by allocating a certain power to each user with its corresponding MCS. This optimization problem was defined in [13] and is usually referred as *Rate Adaptation* (RA) process. The second optimization process is referred as *Margin Adaptation* (MA) where the optimum power and MCS is defined as that combination that allows the use of the minimum transmission power while at the same time guaranteeing the minimum QoS requirements (i.e. the BER bound).

Then, it is possible to generalize the (multiuser) link adaptation process considering either the RA objective function or the MA objective function. The outcomes of this adaptation process are the resource assigned to each user into the time, the frequency or the space domains as well as the amount of transmitted power per user and the optimum MCS. For an OFDM scheme, the resources can be efficiently assigned to different users without the need of guard band or time gaps (perfect synchronization among mobile stations and the base station is assumed). In fact the whole frequency and time domains are segmented into resource units (RU) that can be assigned arbitrarily to each user. Then, it falls off that the minimum RU is a symbol. Hence, the resource allocation algorithm is provided with the channel state information from all the users and the maximum transmission power, and it gives the optimum resource allocation mainly by considering the power and modulation and code scheme (MCS) applied to each RU.

In order to obtain the optimal power and rate adaptation for different modulation schemes, for each modulation technique we need an expression for its BER in AWGN that is easily inverted with respect to rate and power. As it well known, unfortunately, for most of nonbinary modulation techniques (e.g. MQAM, MPSK) exact expression for *BER* is hard to find. Often, the *BER* with Gray bit mapping at high SNR's is approximated as the symbol error rate (*SER*) divided by number of bits per symbol ( $\log_2 M$ ).

The equivalent subcarrier concept consists in allowing a group of subcarriers containing spread data symbols to be represented by a single equivalent subcarrier interpretation for use with bit and power loading. Let  $N$  be the number of subcarriers in the system (i.e. FFT order). For multiple access case every user will have only  $\frac{N}{M}$  assigned/active sub-carriers (in the particular case of only one user, we have  $N=\frac{N}{M}$ ). Let us consider in the following approach the case of an OFDM system.

Using the  $BER$  approximation for M-QAM developed in [16], we directly apply the expression with the concept of equivalent subcarrier [16][18]

$$BER_n \approx 0.2 \exp\left(\frac{-1.6 |H_{eff,n}|^2 P_n}{(2^{b_n} - 1) \sigma^2}\right) \quad (5.1)$$

Where  $BER_n$  is the approximation of the  $BER$ ,  $|H_{eff,n}|^2$  is the square magnitude of the effective channel function,  $P_n$  is the transmit power at the  $n$ -th subcarrier and  $b_n$  is the number of the bits in the  $n$ -th equivalent subcarrier, and  $\sigma^2$  the noise power. Using this expression as equality instead of an approximation, the power and the bit expression may be solved as [15],

$$P_n = \frac{-(2^{b_n} - 1) \sigma^2}{1.6 |H_{eff,n}|^2} \ln\left(\frac{BER_n}{0.2}\right) \text{ for } BER_n < 0.2 \quad (5.2)$$

$$\max b_n = \max \left\{ \log_2 \left( 1 - \frac{1.6 |H_{eff,n}|^2 P_n}{\sigma^2 \ln\left(\frac{BER_n}{0.2}\right)} \right) \right\} \quad (5.3)$$

$$\text{Subject to: } BER_n < 0.2 \quad (5.4)$$

$$\text{Subject to: } \sum_{n=1}^N P_n - P_T \leq 0 \quad (5.5)$$

where  $P_T$  is the total transmitted power. Having the effective channel value  $|H_{eff,n}|^2$  for each active user, the number of bits that can be loaded without exceeding a certain target  $BER$  can be estimated as

$$b_n = \left\lfloor \log_2 \left( 1 - \frac{1.6 |H_{eff,n}|^2 P_n}{\sigma^2 \ln\left(\frac{BER_n}{0.2}\right)} \right) \right\rfloor \quad (5.6)$$

The first step is the calculation of the effective channel values for the  $N$  subcarriers of each OFDM symbols that constitute the transmission frame (such parameters could be fixed during the simulation based on e.g. WiMAX standard specifications).

### 5.1.1 Calculating the $|H_{eff,n}|$ : OFDM case

We assume a single user case and denote the user's modulated data symbol at the  $n$ -th carrier by  $S_n$ . After the front-end OFDM demodulation, the  $n$ -th received frequency domain data symbol is

$$Y_n = S_n H_n + \eta_n \quad (5.7)$$

Where  $H_n$  is the sub-channel's sampled frequency response, and  $\eta_n$  is the AWGN component at the  $n$ -th subcarrier. After a zero-forcing equalizer the received subcarrier symbol becomes,

$$\tilde{S}_n = \frac{Y_n}{H_n} = S_n + \frac{\eta_n}{H_n} \quad (5.8)$$

From (5.8), the enhanced noise and interference terms after equalization in the  $n$ -th subcarrier is given by  $\frac{\eta_n}{H_n}$ . Assume that the noise variance, or power are identical in all the subcarriers and let it be  $\sigma^2$  and the noise variance of  $\eta_n$  is  $\sigma^2$  for  $n = \{1, \dots, N\}$ . Then the power enhanced noise term at the  $n$ -th subcarrier is  $\sigma^2 / |H_n|^2$ . If we denote by  $P_s = E\{S_n S_n^*\}$  the total power transmitted by a single carrier, the instantaneous signal to noise ratio is given by

$$SNR_n = \frac{P_s}{\sigma^2/|H_n|^2} \quad (5.9)$$

From (5.8), it may be seen that the effective channel power attenuation for the modulated symbol is given by

$$|H_{eff,n}|^2 = |H_n|^2 \quad (5.10)$$

$$SNR_n = \frac{P_s}{\sigma^2} |H_{eff,n}|^2 \quad (5.11)$$

Given the channel state information the base station transmitter can then use the value in (5.10) for the purpose of bit and power loading. Note that, as in almost every new generation systems the packet scheduler is in charge of formatting these packets to fit into one or more RU (resource unites) of the physical burst of the communication system. The modulation and coding scheme of the burst is fixed according to the effective SNR of the subchannel and the symbol where the burst is allocated. The effective SNR is a function of the different instantaneous SNR and is given by

$$SNR_{eff} = \phi^{-1} \left\{ \frac{1}{N} \sum_{n=1}^N \phi(SNR_n) \right\} \quad (5.12)$$

### 5.1.2 Calculating the $|H_{eff,n}|$ : FBMC case

Compared to conventional transmitted complex valued symbols at a given symbol rate, the FBMC transmits real symbols at twice this symbol rate and therefore similar spectral efficiency. In practice, it may provide a higher useful bit rate, since its operates without the addition of the guard interval, together with a pulse shaping that can be optimized according to given channel characteristics.

	-0.0001	0	0	0	-0.0001		
	-0.1250	0.2058i	0.2393	-0.2058i	-0.1250		
	0.0002	0.5644	1.0000	0.5644	0.0002		
	-0.1250	-0.2058i	0.2393	0.2058i	-0.1250		
	-0.0001	0	0	0	-0.0001		

Figure 5-1: PHYDYAS's bank weights reference

time sub-ch.	n-4	n-3	n-2	n-1	n	n+1	n+2	n+3	n+4
i-2	Re 0	Im 0.0006	Re -0.0001	Im 0	Re 0	Im 0	Re -0.0001	Im 0.0006	Re 0
i-1	Im 0.0054	Re j.0429	Im -0.1250	Re -j.2058	Im 0.2393	Re j.2058	Im -0.1250	Re -j.0429	Im 0.0054
i	Re 0	Im -0.0668	Re 0.0002	Im 0.5644	Re 1	Im 0.5644	Re 0.0002	Im -0.0668	Re 0
i+1	Im 0.0054	Re -j.0429	Im -0.1250	Re j.2058	Im 0.2393	Re -j.2058	Im -0.1250	Re j.0429	Im 0.0054
i+2	Re 0	Im 0.0006	Re -0.0001	Im 0	Re 0	Im 0	Re -0.0001	Im 0.0006	Re 0

Figure 5-2: Impulse response of the PHYDYAS's FBMC system (transmitter + receiver) and OQAM data

### 5.1.3 Demodulation and ZF equalization:

The demodulation of the received signal at position  $(n,m)$ , noise taken into account, provides a complex symbol  $y_{n,m}$

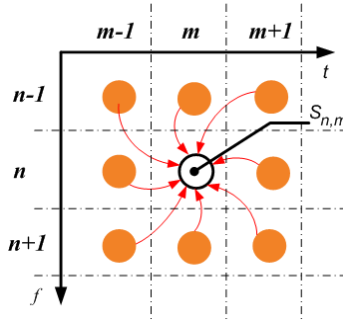


Figure 5-3: First time order neighbours in time-frequency representation for PHYDYAS FBMC system.

After computations, we get the following expression [19],

$$y_{n,m} = H_{n,m} S_{n,m} + j \sum_{(p,q) \neq (n,m)} H_{p,q} w_{p,q} S_{p,q} + \eta_{n,m} \quad (5.13)$$

where<sup>4</sup>  $j^2 = -1$ , the sub-index  $n$  represent the carrier position, and  $m$  is the symbol time sub-index, the values of  $w_{p,q}$  are the constant filter bank coefficients and equal to those depicted in Figure 5-1. We assume that the variance of the noise  $\eta_{n,m}$  is identical in all the subcarriers and is denoted by  $\sigma^2 \eta_{n,m}$ . Let us define a neighbourhood  $\Omega_{\Delta n, \Delta m}$  of a given point  $(n,m)$  such that:

$$\Omega_{\Delta n, \Delta m} = \{(p,q), |p| \leq \Delta n, |q| \leq \Delta m, H_{n+p, m+q} \approx H_{n,m}\} \quad (5.14)$$

<sup>4</sup> Note that the factor “ $j$ ” in (0.12) depends on the carrier position. If  $n$  is even the interference is an Imaginary component, and if  $n$  is odd the interference is a real component.

And let us also set  $\Omega_{\Delta n, \Delta m}^s = \Omega_{\Delta n, \Delta m} - (n, m)$ . At this step we have to notice that  $\Delta n$  and  $\Delta m$  are chosen according to the coherence time ( $T_c$ ) and the bandwidth ( $B_c$ ). It is worth mentioning that when  $B_c$  (resp.  $T_c$ ) decreases,  $\Delta n$  (resp.  $\Delta m$ ) also decreases. For well-dimensioned real systems,  $B_c$  encompasses a few subcarriers ( $\Delta n \geq 1$ ), and  $T_c$  is generally bigger than  $T_0$  ( $\Delta m \geq 1$ ). This allow us to rewrite (5.12) after ZF equalization as,

$$\begin{aligned} \frac{y_{n,m}}{H_{n,m}} &= S_{n,m} \\ &+ j \sum_{(p,q) \in \Omega_{\Delta n, \Delta m}^s} \frac{H_{n+p, m+q}}{H_{n,m}} w_{n+p, m+q} S_{n+p, m+q} \\ &+ j \sum_{(p,q) \notin \Omega_{\Delta n, \Delta m}^s} \frac{H_{n+p, m+q}}{H_{n,m}} w_{n+p, m+q} S_{n+p, m+q} + \frac{\eta_{n,m}}{H_{n,m}} \end{aligned} \quad (5.15)$$

Let us consider the case where we have a prototype function of the filter bank generation well localized in time and frequency. Consequently, we also have

$$\left| \sum_{(p,q) \notin \Omega_{\Delta n, \Delta m}^s} \frac{H_{n+p, m+q}}{H_{n,m}} w_{n+p, m+q} S_{n+p, m+q} \right| \ll \left| \sum_{(p,q) \in \Omega_{\Delta n, \Delta m}^s} \frac{H_{n+p, m+q}}{H_{n,m}} w_{n+p, m+q} S_{n+p, m+q} \right| \quad (5.16)$$

Then (5.13) can be rewritten as:

$$\frac{y_{n,m}}{H_{n,m}} \approx S_{n,m} + j \sum_{(p,q) \in \Omega_{\Delta n, \Delta m}^s} \frac{H_{n+p, m+q}}{H_{n,m}} w_{n+p, m+q} S_{n+p, m+q} + \frac{\eta_{n,m}}{H_{n,m}} \quad (5.17)$$

As  $(p, q) \in \Omega_{\Delta n, \Delta m}^s$  means that we can approximate the channel gain at  $(n+p, m+q)$  frequency-time position to that experienced in  $(n, m)$ . After a zero-forcing equalizer the received subcarrier symbol becomes,

$$\hat{S}_{n,m} = S_{n,m} + j \sum_{(p,q) \in \Omega_{\Delta n, \Delta m}^s} w_{n+p, m+q} S_{n+p, m+q} + \frac{\eta_{n,m}}{H_{n,m}} \quad (5.18)$$

$$\hat{S}_{n,m} = S_{n,m} + j I_{n,m} \quad (5.19)$$

From (5.16), the enhanced noise term after equalization in the  $n$ -th subcarrier and the  $m$ -th FBMC time symbol is given by

$$I_{n,m} = \sum_{(p,q) \in \Omega_{\Delta n, \Delta m}^s} w_{n+p, m+q} S_{n+p, m+q} + \frac{\eta_{n,m}}{H_{n,m}} \quad (5.20)$$

$$\mathbf{E}\{I_{n,m} I_{n,m}^*\} \approx \sum_{(p,q) \in \Omega_{\Delta n, \Delta m}^s} w_{n+p, m+q}^2 P_{n+p, m+q} + \frac{\sigma^2}{|H_{n,m}|^2} \quad (5.21)$$

If we let  $P_{n,m} = |S_{n,m}|^2$  the total power transmitted by a single carrier, and the instantaneous signal to noise ratio is given by

$$SNR_{n,m} = \frac{P_{n,m} |H_{n,m}|^2}{\sigma^2 \left( 1 + \frac{\sum_{(p,q) \in \Omega_{\Delta n, \Delta m}^s |H_{n,m}|^2 w_{n+p, m+q}^2 P_{n+p, m+q}}{\sigma^2} \right)} \quad (5.22)$$

$P_{n+p, m+q}$  is the power transmitted by the different symbols belonging to the values  $\Omega_{\Delta n, \Delta m}^s$  surrounding the symbol  $S_{n,m}$ . From (5.21), it may be seen that the effective channel power attenuation for the modulated symbol is given by

$$|H_{eff, n,m}|_{FBMC}^2 = \frac{|H_{n,m}|^2}{\left( 1 + \frac{\sum_{(p,q) \in \Omega_{\Delta n, \Delta m}^s |H_{n,m}|^2 w_{n+p, m+q}^2 P_{n+p, m+q}}{\sigma^2} \right)} \Rightarrow SNR_{eff, n,m} = \frac{P_{n,m}}{\sigma^2} |H_{eff, n,m}|_{FBMC}^2 \quad (5.23)$$

Note that, in the case of FBMC, the effective channel  $|H_{eff,FBMC}|^2$  for a given symbol may depend on the power  $\{P_{n+p,m+q}\}$  used for surrounding symbols due to the presence of the term  $\sum_{(p,q) \in \mathcal{Z}_{n,m}} w_{n+p,m+q}^2 P_{n+p,m+q}$ .

#### 5.1.4 Radio resource unit capacity

In case of a TDD approach, the communication frame is formed by  $N_s$  symbols and lasts for  $T_{frame}$  seconds. The number of downlink and uplink OFDM/FBMC symbols usually follows the ratio 2:1 or 3:1, however this parameter can be adjusted at the discretion of the base station according to the users demand.

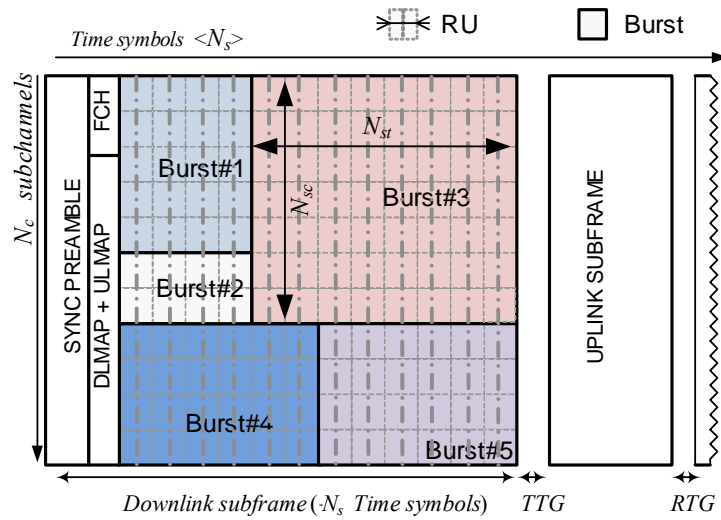


Figure 5-4: FBMC frame in TDD and the different burst structures based on IEEE 802.16e basis.

The total bandwidth  $BW$  is formed by a total of  $N_c$  subcarriers where only  $N_{used}$  are active subcarriers, the remaining ones are used as guard tones. The active sub-carriers include both the pilot subcarriers and the data subcarriers which will then be mapped over different subchannels according to the specific subcarrier permutation scheme. For the Full Usage of Subcarriers (FUSC) structure, pilot subcarriers are allocated first, and the remainder are grouped into subchannels where the data subcarriers are mapped. On the other hand, in the Partial Usage of Subcarriers (PUSC) and the adjacent subcarrier permutation (usually referred as Band AMC) structures, all the pilots and data subcarriers are mapped to the subchannels, and therefore each subchannel contains its own set of pilot subcarriers. For the FUSC and PUSC, the subcarriers assigned to each subchannel are distant in frequency, whereas for the Band AMC the subcarriers from one subchannel are adjacent. Note that FUSC and PUSC increase the frequency diversity and average the interference, whereas the Band AMC mapping mode is more convenient for loading and beamforming, where multiuser diversity is increased. As it is depicted in Figure 5-4 and similar to WiMAX standard, the minimum radio resource unit ( $RU$ ) allocated to any data stream within a frame has a two dimensional shape constructed by at least one subchannel and one OFDM symbol.

In general, we define a RU as a resource unit formed by a set of  $N_{sc} \times N_{st}$  subcarriers and FBMC/OFDM symbols respectively. Once the size of the RUs is defined we can obtain the total number of RUs per frame  $Q \times T$ , where  $Q = N_c / N_{sc}$  is the number subchannels and  $T = N_s / N_{st}$  defines the number of the time slots. Note that as it is fixed in [20], both the RU and the data region always follow a rectangular shape structure. In the IEEE 802.16 standard [20] the specific size of the RU varies according the permutation scheme, concretely for the Band AMC the RU may take the sizes  $9 \times 6$ ,  $18 \times 3$  or  $27 \times 2$  (subcarriers  $\times$  time symbols respectively), where  $1/9$  are dedicated to pilots. By analogy and considering that the OFDM symbol duration  $T = 2\tau_0$  ( $\tau_0$  is the FBMC symbol duration- see Figure 5-2) for the Band AMC the FBMC radio resource unit may take the sizes  $9 \times 12$ ,  $18 \times 6$  or  $27 \times 4$ .

The concept of the effective SNR in (5.12) and (5.23) has been introduced. The effective SNR aims to merge the SNR from the different subcarriers, i.e. in a subchannel or in a burst, thus the BER, Packet Error Rate or channel capacity can be obtained directly assuming the channel as AWGN and an equivalent SNR equal to the effective SNR. Assuming the power is distributed uniformly across all the subcarriers, the equivalent effective channel can be obtained by the geometric mean of the subcarriers gains, and the total capacity  $C_{RU}$  within each RU is given by

$$C_{RU} = \sum_{i=1}^{N_{st}/2} \Delta f N_{sc} \left[ \log_2 \left( 1 - \frac{1.6 H(\mathbf{Q}_{eff,g}^2) SNR(\mathbf{Q}_g)}{\ln\left(\frac{BER}{0.2}\right)} \right) \right] \quad (5.24)$$

where  $H(\mathbf{Q}_{eff,g}^2)$  is the geometric mean of the effective channels experienced during each duration  $i = 2\tau_0$  (which means that  $i = \{1, \dots, N_{st}/2\}$ ), and  $SNR(\mathbf{Q}_g)$  is the geometric mean of the SNR values over all the  $N_{sc}$  subchannels of the RU unit respectively.

### 5.1.5 Improved Joint RU Allocation and bit loading (JRAB) by Scheduling

Two competing aspects exist during the RU allocation and scheduling process, these are *i)* to guarantee the different service flows QoS constraints, and *ii)* to maximize the spectral efficiency. The packet scheduling functions described in subsection 4.3.1.2 in [21] try to maximize both the spectral efficiency (therefore the bit loading) and the delay based on the channel state aware information. Furthermore, according to the research carried by Shakkottai et. al. in [22] the prevalence of the channel over the distribution of the RUs (to maintain the QoS) or the opposite is difficult to assure. From system administrator perspective, this approach might be difficult to implement and furthermore it has been shown that when the physical layer is in charge of the bits allocation process to each active user the spectral efficiency is further increased [23]. For these reasons, proposed scheme in [23] tackled the problem from a different perspective. Since unavoidably the packets might be fragmented to fit into the physical layer burst. We assume that any packet can be arbitrarily fragmented as many times as necessary (obviously affecting the spectral efficiency due to the fragmentation headers). Then, under this assumption and having each packet delivered within a certain time interval (no matter which class of service it belongs to neither constant bit rate (CBR) or variable bit rate (VBR) [20]) we can obtain the minimum number of bits  $b_n^{(k)}$  that the system should assign to each active user during each frame and is given by

$$b_n^{(k)} = \begin{cases} T_{frame} \sum_{p=1}^P \frac{L_p^{(k)}}{\tau_{max}^{(k)} - \Delta\tau - \tau_p^{(k)}}, & \text{if } \forall p \rightarrow \tau_p^{(k)} < (\tau_{max}^{(k)} - \Delta\tau) \\ T_{frame} \sum_{p=1}^P \frac{L_p^{(k)}}{\tau_{max}^{(k)} - \Delta\tau - \tau_p^{(k)}} + T_{frame} \sum_p L_{up}, & \text{otherwise} \end{cases} \quad (5.25)$$

where  $T_{frame}$  is the frame period in seconds, and  $L_p^{(k)}$  the number of bits still queued from the  $p$ -th packet. Then, if  $b_n^{(k)}$  bits are allocated during each frame to each active user  $k$  and the  $n$ -th RU, the delay is certainly under its upper bound. Note that if any  $p'$  packet has waited more than  $(\tau_{max}^{(k)} - \Delta\tau)$  all the remaining bits from the packet are considered for transmission in the following frame. Then, the RU allocation and the bit loading problem following the *Rate Adaptation* can be solved the minimum rate  $R^{(k)}$  in (5.24) based on the allocated bits  $b_n^{(k)}$  as defined in (5.6). The  $b_n^{(k)}$  is also used to determine the priority assigned to each user in each Resource Unit (RU), hence for the  $k$ -th user in the  $n$ -th sub-channel the hereafter priority assignment is defined as in [21],

$$\varphi_n^{(k)} = \begin{cases} \min\left(\frac{b_n^{(k)}}{b_{max}}, 1\right) \frac{\varpi_n^{(k)}}{\varpi_{max}}, & \text{if } \forall p \rightarrow \tau_p^{(k)} < (\tau_{max}^{(k)} - \Delta\tau) \\ P_{urgency} \frac{\varpi_n^{(k)}}{\varpi_{max}}, & \text{otherwise} \end{cases} \quad (5.26)$$

where  $b_{max}$  is a normalization factor which is the maximum number of bits that can be transmitted within a frame using the highest MCS. Furthermore, when a packet from the  $k$ -th service flow/user is close to exceed its maximum delay, the term  $b_n^{(k)}/b_{max}$  in (5.26) is substituted by an urgency factor  $P_{urgency}$  which is a fixed constant such that  $P_{urgency} > (\varpi_{min}/\varpi_{max})^{-1}$ . As a result, the packets close to their maximum delay are put ahead in the allocation process in order to avoid the packet drops due to the excessive packet delay. The  $\varpi_n^{(k)}$  is the already introduced achievable throughput or the rate from the  $k$ -th user on the  $n$ -th RU which is obtained according the *effective SNR* and the available MCSs.

Table 1: Values for the *rtPS*, the *nrtPS*, the *UGS* and the *BE* services applied in simulations.

Class of Service	<i>rtPS</i>	<i>nrtPS</i>	<i>UGS</i>	<i>BE</i>	
<b>Application</b>	<i>Video call</i>	<i>Streaming</i>	<i>voice</i>	HTTP	FTP
<b>Average bit rate</b>	380Kbps	2Mbps	15Kbps	N/A	N/A
<b>Peak bit rate</b>	2Mbps	10Mbps	15Kbps	2Mbps	10Mbps
<b>Packet rate</b>	10 packets/s	10 packets/s	10 packets/s	Variable	Variable
<b>Max. delay</b>	50ms	300ms	75ms	N/A	N/A
<b>Max. BER</b>	$10^{-4}$	$10^{-4}$	$10^{-4}$	$10^{-6}$	$10^{-6}$
<b>Packet dropping ratio</b>	1%	0 – 1%	1%	0	0

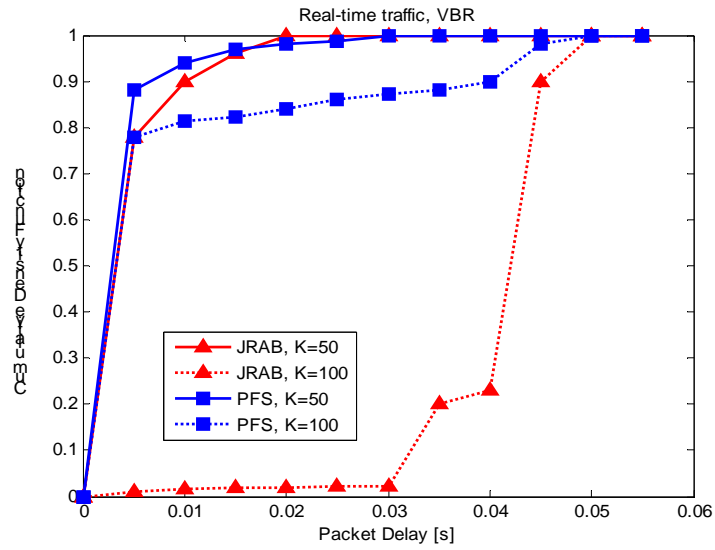
The system simulation parameters are depicted in Table 2.

Table 2: System simulation parameters

FBMC Air Interface and System Level configuration	
<b>Carrier Freq, Bandwidth</b>	3.5GHz, 20MHz
<b>Sampling Frequency</b>	22.857MSPS
<b>Subcarrier Permutation</b>	Band AMC
<b>FFT length</b>	2048
<b># of used subcarriers</b>	1728
<b># of subcarriers per subchannel</b>	18
<b># of FBMC time symbols per RU</b>	6
<b># of data symbols per RU</b>	48
<b>Modulation</b>	{4,16,64}-QAM
<b>Channel coding</b>	Punctured Convolutional with coding rates 1/2, 2/3
<b>Channel Model</b>	Pedestrian B
<b>MS velocity</b>	10Km/h
<b>Channel estimation and CQI</b>	Ideal
<b>Shadowing standard deviation</b>	5dB
<b>BS Tx power</b>	49dBm
<b>Thermal noise</b>	-174dBm
<b>Path loss, urban environment</b>	$139.57 + 28 \cdot \log_{10}(R)$ , R in Km.
<b>Other Link budget parameters</b>	BS height = 30m, MS height = 1.5m, MS Noise Figure = 5dB, Cables = 2dB, Cell Radius = 1000m
<b>Frame duration, <math>T_{frame}</math></b>	5ms
<b>DL/UL rate</b>	2:1

Figure 5-5 shows the cumulative density function of the packet delay for 50 and 100 active users. We focus first when  $K=50$ , as it is shown all the schemes achieve a delay lower than the maximum delay (50ms), in fact the 99<sup>th</sup> percentile<sup>5</sup> is achieved at 25ms for the *Joint RU Allocation and bit loading* (JRAB) procedure and the PFS. Furthermore, the packet loss rate performance for each scheme is near to zero for the JRAB, and  $1.6 \cdot 10^{-5}$  for the PFS. For the  $K=100$  case, we can observe that the PFS is the algorithm that achieved the lower packet delays whereas the JRAB sends the packets mainly when the urgency factor is applied. During the simulations, the guard time  $\Delta\tau$  was fixed equal to  $0.2 \cdot \tau_{max}^{(k)}$ , thus the urgency factor is activated here when  $\tau_p^{(k)} > (\tau_{max}^{(k)} - \Delta\tau) = 0.4\text{ms}$ . Now, for  $K=100$  the packet loss rate for each scheduling function and bit loading procedure is 0.0824 and 0.1375 for the JRAB and the PFS respectively. Therefore, although most of the packets are sent when they are near to expire with the JRAB, a lower packet loss rate is achieved.

<sup>5</sup> A percentile is the value of a variable below which a certain percent of observations fall. So the  $n^{\text{th}}$  percentile is the value (or score) below which  $n$  percent of the observations may be found.



**Figure 5-5: Cumulative density functions of the packet delay for the PFS, and JRAB algorithms with *rtPS* traffic having  $K=50$  and 100 active users.**

The performance of the JRAB in case of mixed traffic is shown in Figure 5-6. In this scenario  $K=50$  users are simulated, where 10 users require *non-real time test service*, 13 users require *real-time test service*, 10 users are browsing internet files (World Wide Web service), 5 are downloading files according to the File Transfer Protocol (FTP), and 12 users require UGS connections for applications such as Voice over IP. The maximum delay for each service is indicated in Table 1. The delay for the WWW and the FTP services has been assumed as  $\tau_{max}=60s$  and  $\tau_{max}=90s$  respectively. It is clearly shown in Figure 5-6 that each traffic type achieves a maximum packet delay lower than its defined maximum value. The 99th percentile for the delay sensitive applications is found at 100ms, 35ms and 20ms for the *nrtPS*, the *rtPS* and the UGS respectively, much lower than its fixed maximum values.

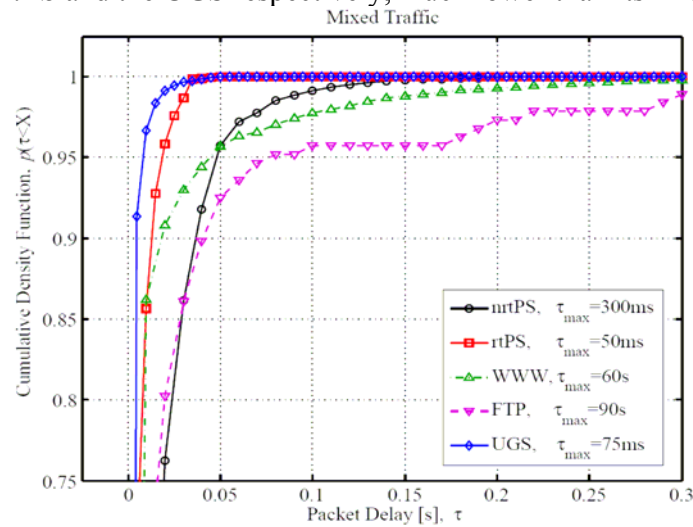


**Figure 5-6: Cumulative density functions of the packet delay for the JRAB algorithm with mixed traffic (*rtPS*, *nrtPS*, WWW, FTP and UGS) and  $K=50$  users.**

The analysis using the effective channel information at the RU level with Jointly with the bit loading gorithm has shown that could to guarantee the maximum delay for delay sensitive applications (*rtPS* and *nrtPS*) in a FBMC system despite the interferences experienced a each subcarrier (or subchannel), while at the same time it is possible to obtain a high spectral efficiency by exploiting the multiuser diversity on those unallocated resources.

## 6 Equalization and coding

### 6.1 Unitary precoding

In this section we investigate precoding for FBMC/OQAM systems. The main motivation behind this work is that, in multicarrier modulation based systems in general and in OFDM using cyclic prefix (CP-OFDM) in particular, multipath diversity is lost. Indeed, in CP-OFDM the frequency selective fading channel is converted into parallel flat fading channels. On the one hand, this allows simple equalization and enables using resource allocation techniques, but on the other hand, the multipath diversity is no longer available since, now, each stream is transmitted over a flat fading channel and if one (or more) subchannel undergoes a deep fade, reliable detection of the transmitted stream over this subchannel becomes difficult if not impossible. Intuitively the FBMC/OQAM systems, to some extent, may also be affected in the same way as OFDM. In FBMC systems the frequency selective fading channel is converted into parallel channels which are not completely flat fading channels, where each channel is affected by both inter-symbol interference (ISI) and inter-carrier interference (ICI). Therefore, some diversity remains and it depends on the degree of the frequency selectivity of the channel. In the case of highly frequency selective channels, each subchannel can be modelled as frequency selective and hence using multiple taps per subchannel equalizers allows taking advantage of the available diversity within each subchannel. In general, in well modelled FBMC/OQAM systems, ISI and ICI are negligible and hence each subchannel can be approximated by a flat fading channel and this way FBMC/OQAM behaves almost like CP-OFDM.

In the case of CP-OFDM many solutions have been proposed to deal with the problem of channel fades. One solution consists in using coding across the different subcarriers, e.g., convolutional codes or turbo codes. In addition to the redundancy added by this solution it may lead to a large decoding delay if interleaving is considered. Another solution is based on the use of precoders. Most of the proposed precoders in literature are linear. The idea behind precoding is the following: instead of sending each stream over only one subchannel, we send a linear combination (mixture) of these streams over each subchannel and hence if one subchannel undergoes a deep fade, the symbols can always be recovered from the signals received in the other subchannels. In what follows we will focus on unitary precoders for their simplicity and performance. In CP-OFDM, it is known that if the precoder is the truncated Fourier matrix the system becomes equivalent to the cyclic prefix single carrier modulation (CP-SCM) which is well known to provide additional frequency diversity while maintaining simple frequency domain equalization. It is important to state however, that these kind of precoders lose their utility when some channel information is available at the transmitter and when bit and power allocation mechanisms can be used as described in section 5. Similarly, the frequency diversity they provide can also be captured by coding across the subchannels. So this can be viewed as a solution to obtain some frequency diversity in a simple manner, when no coding is used across the frequencies, and when no channel information is available at the transmitter.

### 6.1.1 Precoded FBMC/OQAM

The precoded FBMC/OQAM system model is depicted in Figure 6-1. The main symbol stream is demultiplexed, by means of a serial to parallel converter, into  $M$  streams. The resulting streams are then precoded using a precoder  $\Phi$  of size  $M \times M$  where  $M$  denotes the number of subchannels in the FBMC/OQAM modulator. Note that the considered precoder does not add any redundancy and hence the rate remains unchanged. Next, as shown in Figure 6-1, the

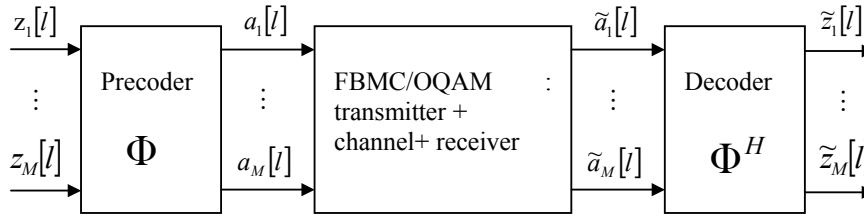


Figure 6-1: Precoded FBMC/OQAM system

precoder outputs are fed into the FBMC/OQAM modulator. For brevity and since the description of the FBMC/OQAM is not our aim here, we skip it and the interested reader can find a detailed description of the FBMC/OQAM system in Deliverable D3.1. Now let  $\mathbf{z}[l] = [z_1[l], z_2[l], \dots, z_M[l]]^T$  denote the input vector to the precoder  $\Phi$ . The output of the precoder can then be written as

$$\mathbf{a}[l] = \Phi \mathbf{z}[l]. \quad (6.1)$$

For simplicity reasons, the matrix  $\Phi$  is assumed to be constant and unitary. In general, precoders are designed by optimizing a certain criterion. In the case of OFDM many criteria have been used in order to compute the precoder. In [9],[10] the authors proposed a design based on the maximization of the diversity and coding gains by minimizing the pairwise error probability (PEP). In [11] the precoder is computed via the maximization of the mean cutoff rate. In practice however, because we want a simple system, we will restrict ourselves to simple unitary precoders as used in OFDM, without resorting to optimization. The choice of using unitary precoders is motivated by the fact that the unitary property maintains the outputs uncorrelated if the inputs are uncorrelated. This way, the per-subchannel equalizers can still be computed independently on each subchannel and independently of the precoder  $\Phi$ . A simple choice consists in taking the Hadamard matrix as precoder [12]

$$\Phi_2 = \begin{bmatrix} 1 & 1 \\ 1 & -1 \end{bmatrix}, \quad \Phi_M[n] = \begin{bmatrix} \Phi_{M/2} & \Phi_{M/2} \\ \Phi_{M/2} & -\Phi_{M/2} \end{bmatrix}$$

In order to make  $\Phi_M[n]$  unitary we normalize it by  $\frac{1}{\sqrt{M}}$ . Another precoder is the Vandermonde precoder [9],[10] given by

$$\Phi = \frac{1}{\kappa} \begin{bmatrix} 1 & \beta_1 & \cdots & \beta_1^{M-1} \\ 1 & \beta_2 & \cdots & \beta_2^{M-1} \\ \vdots & \vdots & \ddots & \vdots \\ 1 & \beta_M & \cdots & \beta_M^{M-1} \end{bmatrix}$$

where we take here  $\beta_i = \exp(-j2\pi i / M)$  and  $\kappa = \sqrt{M}$ , hence  $\Phi$  is nothing but the Fourier matrix of size  $M \times M$ . Note that other precoders may be used.

From (6.1) it is clear that each output of the precoder is a linear combination of its inputs. Each output of the precoder is sent through a different subchannel of the FBMC/OQAM modulator. This is equivalent to send every component of the vector  $\mathbf{a}[l]$  over a different subchannel. For brevity reasons and since a detailed description of the FBMC/OQAM with equalization is already given in deliverable D3.1, here we use directly the outputs of the equalizers. The per subchannel equalizers for the FBMC/OQAM system using unitary precoders can be computed exactly as in the case without precoding thanks to the unitary property. Let  $\tilde{\mathbf{a}}[l]$  be an  $M \times 1$  vector whose components are the outputs of the per subchannel equalizers. In order to retrieve the transmitted symbols we apply the inverse of the precoder, which is here  $\Phi^H$ , to  $\tilde{\mathbf{a}}[l]$ , i.e.

$$\tilde{\mathbf{z}}[l] = \Phi^H \tilde{\mathbf{a}}[l]$$

Finally, we obtain an estimation of the transmitted symbols  $\mathbf{z}[l]$  by taking a hard decision on  $\tilde{\mathbf{z}}[l]$ .

### 6.1.2 Discussion

In section 2, for simplicity reasons, we suggested an implementation of the precoder just at the input of the system and before the OQAM modulator. Note that an implementation after the OQAM modulator is possible but with some modifications regarding the characteristic of the OQAM signal. One can imagine two simple configurations. In the first one we consider a precoder for all subchannels at the OQAM modulator output. In this case, in order to maintain the fundamental idea of FBMC/OQAM, which is sending real and imaginary symbols both in frequency and time domains alternatively, the precoding matrix needs to be constructed accordingly. To this end, one proposition of unitary matrices is the following. Let

$$\mathbf{P}_2 = \begin{bmatrix} 1 & j \\ -j & -1 \end{bmatrix}, \quad \mathbf{P}_M = \begin{bmatrix} \mathbf{P}_{M/2} & \mathbf{P}_{M/2} \\ \mathbf{P}_{M/2} & -\mathbf{P}_{M/2} \end{bmatrix}$$

The unitary precoding matrix is given by

$$\Phi_M[n] = \frac{j^n}{\sqrt{M}} \begin{bmatrix} P_{M/2} & P_{M/2} \\ P_{M/2} & -P_{M/2} \end{bmatrix}$$

where we suppose that  $M$  is a power of 2, i.e.,  $M = 2^i$  where  $i$  is an arbitrary integer. Note that at the output of the per subchannel equalizers we apply  $\Phi_M[n]^H$ . Other constructions of the precoding matrix that satisfy the aforementioned constraint (keeping the principle of FBMC/OQAM) are possible. Another way of constructing a precoder is to precode odd and pair subchannels separately using a real unitary precoder, as for example the Hadamard matrix of size  $M/2$  for the  $M/2$  odd subchannels and the same matrix for the  $M/2$  even subchannels. It should be noted that using precoding after the OQAM modulator has higher complexity than using it before the OQAM modulator, this is due to the fact that the rate at the output of the OQAM modulator is twice of that at its input. The same remark is valid at the receiver side.

Another important point is that precoding can be carried out by optimal grouping of subchannels, this is crucial when subchannels are divided between several users. The solution proposed in [3], in the case of OFDM, may easily be translated to the FBMC/OQAM case. The authors in [3] proved that by grouping subchannels to groups of  $v+1$  subchannels, where  $v+1$  is the channel length, maximum diversity can be obtained.

### 6.1.3 Simulations

In this section we provide some numerical results where we assess the performance of the precoded FBMC/OQAM system by comparing it with the uncoded FBMC/OQAM, precoded OFDM and uncoded OFDM. We consider the following simulation parameters:  $M=256$  carriers, 16-QAM modulation, Phydias prototype filter with overlapping factor  $K=4$ . The guard interval for CP-OFDM is  $M/4$ . It is worth noting that the throughput of the FBMC system is higher than that of CP-OFDM, because the latter uses redundancy consisting of the CP. However, we normalized the information bit energy for both systems to be the same. In all simulations, unless otherwise specified, curves are obtained by averaging 200 trials.

In Figure 6-2 we compare the performance of CP-OFDM, FBMC/OQAM, with and without precoding, in terms of BER versus  $E_b/N_0$ . The considered channel model is Vehicular A. We observe clearly that, in the case of FBMC/OQAM 3-tap MMSE equalizer, precoding improves significantly the performance, notably for high SNR. However, for FBMC/OQAM using one tap equalizer the performance is slightly improved. This can be explained by the fact that using only one tap equalizer for the considered parameters does not permit to cancel intersymbol interference (ISI) and intercarrier interference (ICI) effectively.

In Figure 6-3 we investigate the effect of the frequency selectivity degree (length) of the channel on the performance for an  $E_b/N_0 = 20\text{dB}$ . For this purpose we consider  $M = 64$  carriers. We plot BER versus channel length. We observe that precoded FBMC/OQAM with 3-tap provides better performance for different channel lengths compared to non-precoded FBMC/OQAM. We also observe that the gain in performance decreases as the channel length increases. This can be explained by the fact that for longer channels equalizers with 3-tap do not perform well and hence in order to keep the gain high even for long channels we need to consider longer equalizers. In general, the choice of the equalizer length must take into account the channel length. For the one tap equalizer precoding improves the performance only for short channel. We also see that precoded CP-OFDM has better performance than non-precoded CP-OFDM as long as the channel length is shorter than the CP. Once the channel length becomes greater than the CP, the gain in performance starts decreasing and beyond a certain channel length, here 20-tap, it becomes even negative.

The simulation results show clearly that precoding makes FBMC/OQAM more robust against channel fades. In summary, the gains brought by this kind of precoder for FBMC/OQAM seem very similar to what is obtained in the case of OFDM.

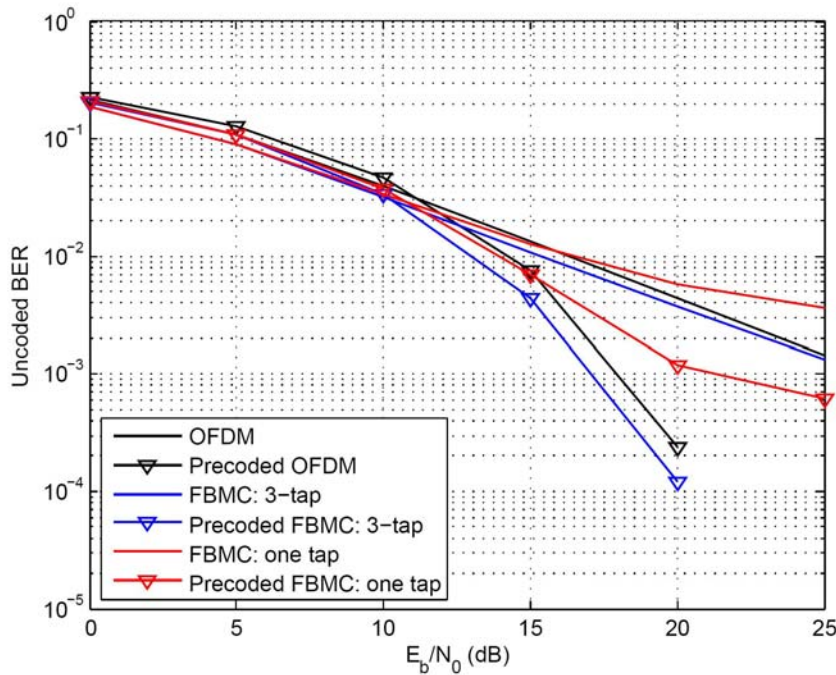


**Figure 6-2: Performance comparison for uncoded and precoded CP-OFDM and FBMC/OQAM systems. Bit error rate versus  $E_b/N_0$ .**

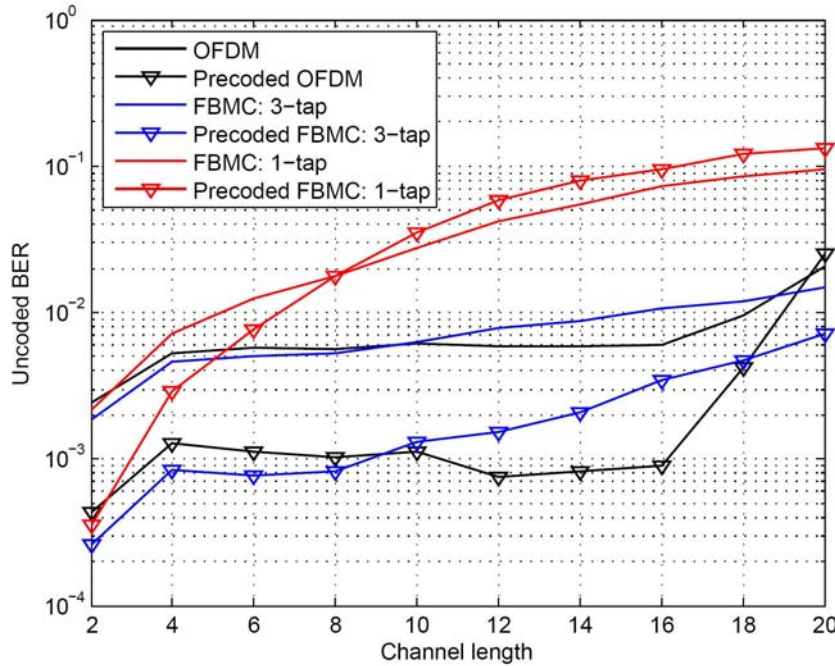


Figure 6-3: Effect of the channel length on the performance. BER versus channel length.  $E_b/N_0=20$  dB.

#### 6.1.4 Conclusion

In this report we have investigated the problem of precoding for FBMC/OQAM systems. We briefly described some precoders for FBMC/OQAM. We considered unitary precoders thanks to their simplicity and the fact that they do not add any redundancy so that the design of the equalizer remains unchanged. Simulation results have shown the large gain obtained by using precoding in FBMC/OQAM systems with multiple taps equalizers. However, for FBMC/OQAM systems with only one tap, the gain is small for mildly frequency channels and even negative for highly frequency selective channels. We can conclude that precoding makes FBMC/OQAM more robust against channels with fades.

## 6.2 Influence of noise correlation on decoding

Any filtering performed in a per-subcarrier fashion after the analysis FB will generate noise correlations. That is the case for the linear equalization when the equalizer has length higher than 1 as for example the solutions presented in D3.1. The noise correlations may affect the coded BER performance, because most of the channel coding algorithms developed so far consider the noise samples uncorrelated, although it is worth noting that the use of a bit interleaver may, at least partially, solve the issue.

There are three distinguishable cases of correlations. The intra-subcarrier is the correlation between the noise samples from one subcarrier but from different time indices. The adjacent inter-subcarrier is the correlation between noise samples of two immediately adjacent subcarriers. And finally the non-adjacent inter-subcarrier is the correlation between the noise samples of non-adjacent subcarriers.

In the case of an ideal scenario, that means a frequency flat channel and no necessity of an equalizer, all the correlations will be non-existent.

In situations where the channel has low frequency selectivity and a one-tap equalizer is considered sufficient, the intra-subcarrier is again non-existent. The adjacent inter-subcarrier will present some small correlation since the equalizer coefficients are different for different subcarriers. But in practical cases, this difference for immediately adjacent subcarriers will be very small, resulting in almost no correlation. The non-adjacent inter-subcarrier correlation will depend on the stop-band attenuation of the prototype filter. Since this attenuation is normally very high, the non-adjacent inter-subcarrier noise correlation will also be negligible.

For high frequency selective channels, where a linear multitap equalizer is necessary, high Intra-subcarrier and adjacent inter-subcarrier noise correlations are expected. The non-adjacent inter-subcarrier noise correlation is again prototype dependent and consequently very low.

To check the effects of noise correlations in the coded BER, we have considered a WiMAX simulation scenario. We have applied channel coding and decoding with and without interleaving. At the transmitter side we have used a convolutional encoder with native rate  $1/2$ , constraint length 7 and generator polynomials  $g_1(D) = 1 + D + D^2 + D^3 + D^6$  and  $g_2(D) = 1 + D^2 + D^3 + D^5 + D^6$ . The block interleaver has a length of  $2^b \times M_{used}$ . This encoder and the interleaver were taken from the IEEE standard 802.16-2004. At the receiver side we have employed the linear MMSE equalizer presented in D3.1 and a soft decoder that uses approximate log-likelihood ratios as soft information and the inputs to the Viterbi decoder were "unquantized".

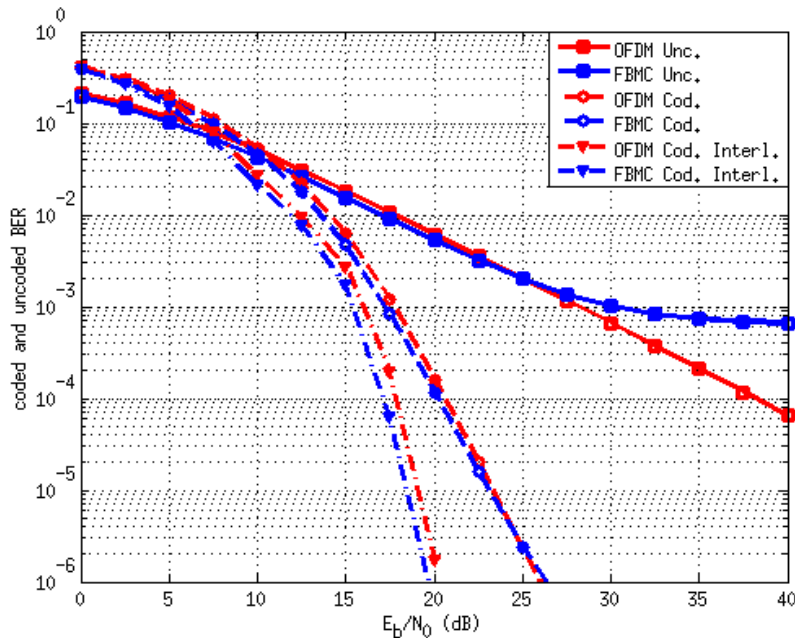


**Figure 6-4: Coded and uncoded BER for a VehB- ITU channel model.**

In Figure 6-4 some simulation results are depicted for both OFDM and FBMC systems considering the coded and uncoded, interleaved and non-interleaved setups. The modulation alphabet for all curves is 16-QAM, the total number of subcarriers is 1024 from which 768 were filled with data. The subcarrier

spacing is 10.9 kHz and the total bandwidth is 10MHz. The sampling period is 89.28 ns giving a cyclic prefix of length 91.42  $\mu$ s (1/4 of the symbol length) for the OFDM case. The linear equalizer used in the FBMC system has a length of 7. The channel model is the ITU Vehicular B with static coefficients.

From the results shown here we can conclude that for a typical WiMAX scenario where the channel has a high frequency selectivity, the noise correlations do not hurt the performance of the channel decoder.

## 7 Recommendations

Based on the results obtained in D3.1 and in this deliverable, the following recommendations can be expressed for the different elements of the transmitter/receiver chain:

**Channel estimation:** At initialization, the conventional OFDM preamble-based estimation methods can be employed with FBMC, for example with the help of the filter bank memory preloading technique. During data transmission, OQAM pilots, also called ‘pair of pilots’, can be used with the appropriate simple detection scheme. Alternatively, a specific approach, the so-called auxiliary pilot method, can be exploited, at initialization and during transmission. The impact is some processing and an additional delay at the emitter. Also, decision directed techniques, as in conventional modems, can be exploited. Some particular pilot structures have also been introduced and described in details, similar to those in WiMAX standards.

**Equalization:**

It has been shown that per-subchannel equalizers, operating at the fractional rate  $T/2$  are best suited to the FBMC context, because they allow for both the correction of the channel distortion and the compensation of the timing offset, which is essential in a number of applications, such as uplink in cellular networks or opportunistic communications. For the correction of the channel distortion, a single or just a few coefficients might be sufficient to reach a satisfactory level of performance. However, for the compensation of large timing offsets, more coefficients are needed, for example 5 or 7, which leads to an increase in complexity and an additional delay in the receiver, with the corresponding impact on the system latency. The additional delay can be avoided if a frequency domain implementation is employed. In order to minimize the computational complexity, the equalizer lengths can be adjusted individually for each user and subchannel depending on the channel conditions. If the system includes high-level synchronization mechanisms such that the timing and carrier frequency offsets are close to zero in steady-state tracking mode, and if the subcarrier spacing is small enough with respect to the channel coherence bandwidth, then single-tap equalizers could be used most of the time in continuous transmission. Yet, longer equalizers would help to achieve fast initialization with reduced complexity of overall synchronization scheme (concerning the ranging schemes, etc.), as well as adequate performance for asynchronous uplink transmission with low packet rate without need for accurate tracking of the synchronization parameters in idle mode.

For the design of the equalizer, a simple and fast method to derive the coefficient values from the channel measurements is the frequency sampling technique. It is well suited to odd numbers of coefficients and leads to an equalizer which introduces a delay equal to half the number of coefficients minus one. For higher performance, particularly in the presence of highly selective channels and high level of noise, it is recommended to use an MMSE equalizer. In that case, more time and processing is necessary to derive the coefficients and the delay is part of the optimization process. If adaption during the burst is necessary, periodic recalculation of the coefficients from the channel measurements can be performed or adaptive techniques can be implemented, for example with the LMS algorithm. Worth pointing out is the fact that adaptive techniques can lead to the suppression of the need for pilots inside the bursts.

**Coding:** It has been shown (section 6.2 of this deliverable) that no special action needs to be taken regarding the residual correlation between noise terms and its influence on the decoding process. It is advised to use coding across the frequencies to benefit from frequency diversity when possible. If not, linear unitary precoding can be used to recover this diversity (section 6.1 of this deliverable).

**Transmitter optimization:** When channel information is available at the transmitter, it is of course recommended to perform adaptive modulation and coding as well as optimizing the power allocation across subchannels. One method to implement this is described in section 5 of this deliverable.

In addition, software has been provided to the other WPs for the channel estimation and equalization methods recommended above.

## 8 Conclusion and achievements

The main achievements described in this deliverable can be summarized as follows.

- Two different joint synchronization and channel estimation schemes have been proposed. The first one (section 2.1) uses a short preamble and is based on a multi-tap channel model, which can be simplified to a single tap in order to estimate the dominant channel contribution. It provides a good CFO acquisition range but exhibits an error floor at high SNR. This error floor can however be further lowered by introducing an additional delay in the preamble. The second method (section 2.2) is based on the use of pilots and assumes a linear phase channel model. It is performing the joint estimation in an iterative manner. It provides a large FTD acquisition range but the performance degrades when the amount of pilots is too low (in case of high mobility or for small burst sizes). It appears to be efficient for providing a coarse estimate of both channel and FTD.
- Section 2.3 has investigated the effect of synchronization differences between different users in a multiuser uplink scenario. FBMC has been shown to be more robust to this effect than OFDM.
- Two additional equalization structures have been presented to cope with very selective channels in high SNR scenarios. The first one uses a two stage interference suppression mechanism that focuses on suppressing the interference from adjacent subchannels (section 3.2). The second one is the decision-feedback MMSE equalizer which focuses on lowering the intersymbol interference (section 3.3). Both require accurate channel estimates.
- A frequency-domain implementation of the equalization has been proposed in section 3.4 that reduces the overall latency.
- The performance of channel estimation based on pilot schemes has been further evaluated in the presence of time varying channels (section 4.1). The acceptable level of mobility for several possible pilot configurations has been assessed.
- In section 4.2, the adaptive MMSE DFE has been derived.
- The issue of adaptive modulation and adaptive resource allocation has been studied in section 5.
- A unitary precoder has been presented in section 6.1 to be able to capture frequency diversity when coding is not performed across the frequencies.
- The effect of residual correlation between equalizer outputs has been shown (section 6.2) to have a negligible impact on the decoding process.

The recommendations have been summarized in section 7 for the different elements of the receiver.

## 9 References

- [1] T. Schmidl, D. Cox, "Robust Frequency and Timing Synchronization for OFDM", *IEEE Trans. Comm.*, pp. 1613-1621, December 1997.
- [2] T. Fusco, A. Petrella and M. Tanda, "Joint symbol timing and CFO estimation for OFDM/OQAM systems in multipath channels," submitted for publication in the EURASIP Journal on Advances in Signal Processing, special issue on Filter Banks for Next-Generation Multicarrier Wireless Communications, June 2009.
- [3] Deliverable 3.1, "Equalization and demodulation in the receiver (single antenna)", ICT- 211887 PHYDYAS, July 2008.
- [4] A. Ikhlef and Jérôme Louveaux, "An enhanced MMSE per subchannel equalizer for highly frequency selective channels in FBMC/OQAM systems," In IEEE SPAWC09, Perugia, Italy, June 2009.
- [5] D. S. Waldhauser, L. G. Baltar, and J. A. Nossek, "MMSE subcarrier equalization for filter bank based multicarrier systems," in Proc. SPAWC-2008, Recife, Brazil, 6-9 July 2008.
- [6] L.G. Baltar, D. S. Waldhauser and J. A. Nossek, "MMSE Subchannel Decision Feedback Equalization for Filter Bank Based Multicarrier Systems," in *Circuits and Systems, 2009. ISCAS 2009. IEEE International Symposium on*, 24-27 May 2009.
- [7] D. S. Waldhauser, L.G. Baltar, and J. A. Nossek, "Adaptive equalization for filter bank based multicarrier systems," in *Circuits and Systems, 2008. ISCAS 2008. IEEE International Symposium on*, 18-21 May 2008.
- [8] D. S. Waldhauser, L.G. Baltar, and J. A. Nossek, "Adaptive Decision Feedback Equalization for Filter Bank Based Multicarrier," in *Circuits and Systems, 2009. ISCAS 2009. IEEE International Symposium on*, 24-27 May 2009.
- [9] Z. Wang and G. B. Giannakis, "Linearly precoded or coded OFDM against wireless channel fades?," in *Proc. Third IEEE Workshop Signal Process. Adv. Wireless Commun.*, Taoyuan, Taiwan, Mar. 2001.
- [10] Z. Liu, Y. Xin, and G. B. Giannakis, "Linear constellation precoding for OFDM with maximum multipath diversity and coding gains," *IEEE Trans. Commun.*, vol. 51, pp. 416-427, Mar. 2003.
- [11] Y. Rong, S. Shahbazpanahi, and A. B. Gershman, "Robust linear receivers for space-time block coded multiaccess MIMO systems with imperfect channel state information," *IEEE Trans. Signal Processing*, vol. 53, pp. 3081-3090, Aug. 2005.
- [12] S. M. Phoong, K. Y. Chang, and Y. P. Lin, "Antipodal paraunitary precoding for OFDM application", Proc. IEEE International Symposium on Circuits And Systems, Vancouver, Canada, May 2004.
- [13] X. Liu, E. K. P. Chong, N. B. Shroff, "A Framework for Opportunistic Scheduling in Wireless Networks," *Comp. Net. J.*, 2002
- [14] A. Czylik, "Adaptive OFDM for Wideband Radio Channels" IEEE Global Communications Conference (IEEE GLOBECOM'96), Vol 1, pp.713-718, Nov 18-22, 1996. London, UK.
- [15] S. Vishwanath, S. A. Jafar, A. Goldsmith, "Adaptive Resource allocation in Composite Fading Environments," IEEE Global Communications Conference (IEEE GLOBECOM 2001), Vol2, pp-1312-1316. San Antonio, Texas. USA. Nov 25-29, 2001.
- [16] Seong Taek Chung, Andrea J. Goldsmith, "Degrees of Freedom in Adaptive Modulation: A Unified View", IEEE Transactions on Communications, Vol. 49, N° 9, pp. 1561-1571, September 2001.

- [17] Clive Tang, Victor J. Stolpman, “*Multiple User Adaptive Modulation Scheme for MC-CDMA*,” in Proc. IEEE Global Communications Conference (IEEE Globecom’04), pp. 3823-3827. Dallas, Texas-USA. 29 Nov to 3 Dec 2004.
- [18] I. Gutierrez, F. Bader, J. L. Pijoan, “*Radio Resource Allocation in MC-CDMA Under QoS Requirements*”. Book title: Multi-Carrier Spread Spectrum 2007. Chapter 5: Adaptive Transmission, pp. 207-216. Editors: S. Plass, A. Dammann, S. Kaiser and K. Fazel, Ed. Springer © 2007. ISBN: 978-1-4020-6128-8. Netherlands.
- [19] C. L   , J.-P. Javaudin, R. Legouable, A. Skrzypczak, and P. Siohan, “*Channel estimation methods for preamble-based OFDM/OQAM modulations*”, in Proc. European Wireless (EW’07). Paris, France. April 2007.
- [20] IEEE 802.16e-2005, “*IEEE standard for local and Metropolitan Networks. Part 16: Air Interface for Fixed and Mobile Broadband Wireless Access Systems, amendment 2: Physical and Medium Control Layers for Combined Fixed and Mobile Operation in Licensed Bands and Corrigendum I*”. Feb 2006.
- [21] Deliverable 6.1: “*Duplexing and multiple access techniques, software description*,” January 2009. European project ICT–211887 PHYDYAS, <http://www.ict-phydyas.org>.
- [22] S. Shakkottai and A. Stolyar, “*Scheduling for Multiple flows Sharing a Time-Varying Channel: The Exponential Rule*”, American Mathematical Society Translations, Vol. 207, 2002.
- [23] I. Guti  rrez, F. Bader, J.L. Pijoan, “*New Prioritization Function for Packet Data Scheduling in OFDMA Systems*”, IEEE Radio and Wireless Symposium 2009 (IEEE RWS’09), San Diego, USA, Jan. 2009.